Supplementary Information

for

Supramolecular Tunnelling Junctions with Robust High Rectification Based on Assembly Effects

Max Roemer‡, Xiaoping Chen‡, Li Yuan, Lejia Wang, Xiaojiang Yu, Pierre-André Cazade, Cameron Nickle, Romena Akter, Enrique Del Barco, Damien Thompson and Christian A. Nijhuis**

*Corresponding authors: damien.thompson@ul.ie (D.T.), c.a.nijhuis@utwente.nl (C.A.N.)

Table of Contents

1. Syntheses

General

Reactions were performed under argon atmospheres, using standard Schlenk techniques. Tetrahydrofuran was distilled from sodium/benzophenone, dichloromethane was distilled from calcium chloride, triethylamine and N,N-dimethylformamide were distilled from calcium hydride. Diethylmalonate was distilled under argon. Ferrocene, *n*-butyllithium (2.5 M in hexanes), 10-bromodecanoic acid, 11-bromoundecanoic acid, ethynylferrocene and MePhos (2-Dicyclohexylphosphino-2′-methylbiphenyl) were purchased from Sigma-Aldrich. Tri-*n*-butyltin chloride was purchased from Alfa-Aesar. 9-Bromononanoic acid and 15-bromopentadecanoic acid were purchased from PI-chemicals. Commercially obtained substances were used without further purification, unless otherwise stated. 1,1'-diiodo-ferrocene[1], 1-iodo-1'-(tri-*n*-butyltin)ferrocene[2, 3] and 1-iodo-1'-(11-bromoundecanoyl)-ferrocene[3] were prepared according to the literature. 13-Bromotridecanoic- and 14-bromotetradecanoic acid were prepared as described below. ^{1}H and ^{13}C NMR spectra were recorded on Bruker Avance 300 MHz (AV300) and Bruker Avance 500 MHz (AV500) spectrometers using chloroform-*d* as solvent. The spectra were referenced using residual solvent signals.[4] Melting points were determined by differential scanning calometry on a Mettler Toledo DSC 1 STARe system. Mass spectra and high resolution mass spectra (ESI) were recorded on a Bruker micrOTOF-QII mass spectrometer.

We prepared the series of target molecules in several steps from 1,1'-diiodoferrocene as outlined in Scheme S1.

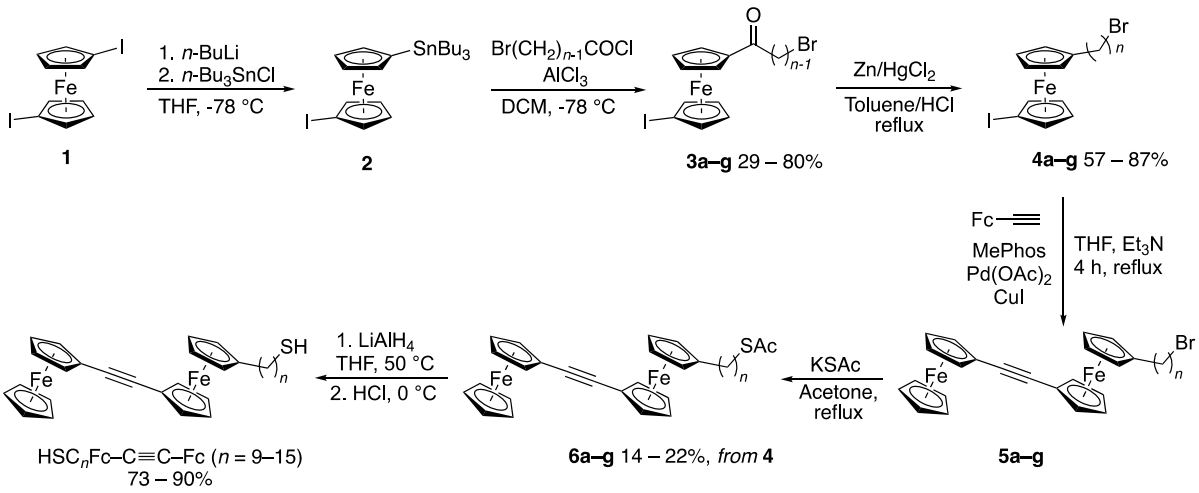

Scheme S1. Syntheses of the HSC$_n$Fc–C≡C–Fc (n_c = 9–15) series.

1,1'-diiodoferrocene (**1**) was converted into 1-iodo-1'-(tri-*n*-butyltin)ferrocene (**2**) according to the literature.[2, 3] Tin mediated Friedel-Crafts acylation of compound **2** yields the alkanyol functionalised iodoferrocenes of type **3**.[3, 5] We have previously reported the synthesis of **3g** (*n* = 15)[5] and **3c** (*n* = 11)[3]. The other homologues were prepared by the reported procedure.

The respective long-chain alkanoic acid bearing a terminal Br was converted into the acid chloride by reaction with oxalyldichloride in dichloromethane. An acylium species was generated by addition of $AlCl_3$ in dichloromethane, which was added slowly to a solution of **2** in dichloromethane at -78 °C. Aqueous work-up and column chromatography on silica afforded each product as orange solid.

Syntheses of 13-Bromotridecanoic- and 14-Bromotetradecanoic acid

Due to the limited commercial availability, we synthesised 14-bromotetradecanoic- and 13-bromotridecanoic acid. For this we applied a modified literature procedure, starting from diethylmalonate.[6] We deprotonated diethylmalonate with sodium ethoxide, prepared from sodium and ethanol. The generated carbanion is suitable for a nucleophilic substitution reaction with dibromoalkanes to form the corresponding addition products (**I1** and **I2**). After purification, we converted those into the carboxylic acids by reaction with HBr (Scheme S2).

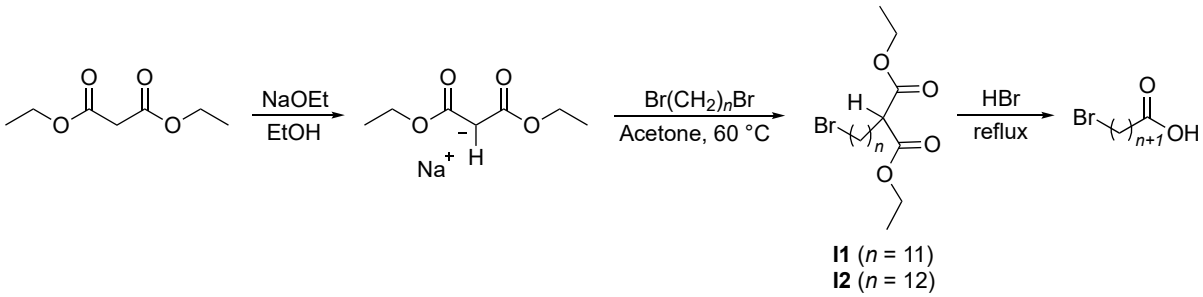

Scheme S2. Preparation of and 14-bromotetradecanoic acid and 13-bromotridecanoic acid.

13-Bromotridecanoic acid: A 250 mL flask was filled with finely cut sodium (0.40 g, 1.7 mmol), which was washed prior with hexane and blown to dryness using a stream of N_2. Ethanol (75 mL) was added, and the mixture was stirred at room temperature until the sodium dissolved. Diethylmalonate (2.50 g, 15.6 mmol) was added, and the temperature was raised to 60 °C. Stirring was continued for one hour. 1,11-dibromoundecane (4.90 g, 15.6 mmol) was added and the mixture of refluxed for 30 min upon which a precipitation of NaBr formed. The mixture was allowed to cool down to room temperature, ethyl acetate (100 mL) was added and an extraction with brine (100 mL) was carried out. The supernatant layer was collected and dried over sodium sulfate. Short way distillation at a temperature of 180 °C (~1.0×10^{-2} mbar) afforded 2.09 g of **I1**, containing minor amounts 1,11-dibromoundecane, as colourless oil. ^{1}H NMR (300 MHz): δ 4.17 (q, ^3J = 7 Hz, 4H), 3.38 (t, $J_{H–H}$ = 7 Hz, 2H), 3.28 (t, $J_{H–H}$ = 7 Hz, 1H), 1.84 (m, 4H), 1.39 (m, 2H), 1.26 – 1.22 (m, 20H) ppm. ^{13}C NMR (75 MHz, $CDCl_3$): δ 169.7, 61.3, 52.2, 34.1, 32.9, 29.52, 29.48, 29.4, 29.3, 28.8, 28.3, 27.4, 14.2 ppm. MS (ESI): 393 $[M + H]^+$. HRMS (ESI): calcd for $C_{18}H_{34}BrO_4$ 393.1635; found: 393.1634.

We converted **I1** to 13-bromotridecanoic acid by refluxing in concentrated HBr (5 mL; 47 %) for 3 h using a short-way distillation set-up at atmospheric pressure which allowed the constant removal of ethylbromide, which forms as side product, from the reaction mixture. Once the reaction was completed we allowed the mixture to cool down to room temperature.

Extraction with dichloromethane (50 mL), drying over sodium sulfate, solvent evaporation and flash filtration through a plug of silica using ethyl acetate / hexane (3:1) as solvent afforded the carboxylic acid in the form of a white crystalline material after solvent evaporation (838 mg, 2.7 mmol; 17 % over two steps). ^{1}H NMR (300 MHz): δ 3.40 (t, $J_{H–H}$ = 7 Hz, 2H), 2.34 (t, $J_{H–H}$ = 7 Hz, 2H), 1.85 (m, 2H), 1.62 (m, 2H), 1.41 (m, 2H), 1.27 (brd) ppm. ^{13}C NMR (75 MHz, $CDCl_3$): δ 180.7, 34.2, 34.1, 33.0, 29.63, 29.60, 29.53, 29.50, 29.3, 29.2, 28.9, 28.3, 24.8 ppm. MS (ESI): 291 $[M – H]^-$. HRMS (ESI): calcd for $C_{13}H_{24}BrO_2$: 291.0965; found: 291.0972.

14-Bromotetradecanoic acid: We prepared the compound in analogy to the above described procedure by using 1,12-dibromododecane (10.24 g, 3.1 mmol), sodium (0.78 g, 3.4 mmol) and diethylmalonate (5.00 g, 3.1 mmol) as starting materials. Short way distillation at a temperature of 180 °C (~1×10^{-2} mbar) afforded 4.30 g of the intermediate **I2**, containing unreacted 1,12-dibromododecane, ~ 40%, as colourless oil. ^{1}H NMR (300 MHz, $CDCl_3$): δ 4.14 (q, $J_{H–H}$ = 7 Hz, 4H), 3.35 (t, $J_{H–H}$ = 7 Hz, 2H), 3.25 (t, $J_{H–H}$ = 7 Hz, 1H), 1.80 (m, 4H), 1.37 (m, 2H), 1.24 – 1.19 (m, 20H) ppm. MS (ESI): 407 $[M]^+$. HRMS (ESI): calcd for $C_{19}H_{36}BrO_4$ 407.1791; found: 407.1795.

We converted **I2** to 14-bromotetradecanoic acid by the above described procedure, affording the title compound as white crystalline material (1.38 g, 4.5 mmol, 14% from diethylmalonate). ^{1}H NMR (300 MHz): δ 3.40 (t, ^{3}J = 7 Hz, 2H), 2.34 (t, ^{3}J = 7 Hz, 2H), 1.85 (m, 2H), 1.63 (m, 2H), 1.42 (m, 2H), 1.26 (brd, 16H) ppm. ^{13}C NMR (75 MHz, $CDCl_3$): δ 180.3, 34.2, 34.1, 33.0, 29.69, 29.65, 29.56, 29.5, 29.4, 29.2, 28.9, 28.3, 24.8 ppm. MS (ESI): 329 $[M + Na]^+$. HRMS (ESI): calcd for $C_{13}H_{24}BrO_2Na$: 329.1087; found: 329.1081.

Syntheses of the Ferrocene Derivatives

The series of alkanoyl functionalised iodoferrocenes were prepared by tin mediated Friedel-Crafts acylation of **2** (Scheme S3).

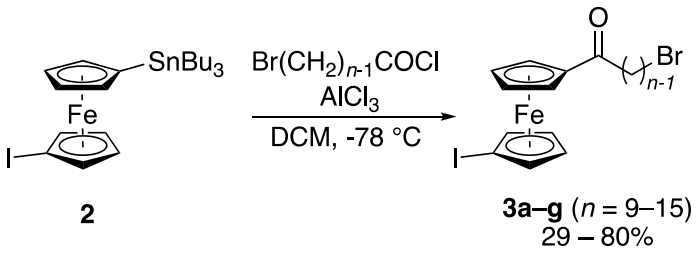

2 **3a–g** (*n* = 9–15) 29 – 80%

Scheme S3. Tin mediated Friedel-Crafts reaction of **2**, affording the alkanoyl functionalised iodoferrocenes.

1-Iodo-1'-(9-bromononanoyl)ferrocene (3a): We charged a Schlenk flask with 9-

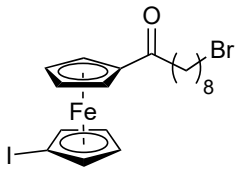

bromononanoic acid (1.03 g, 6.0 mmol), dichloromethane (50 mL) and oxalyldichloride (1.5 mL, 18.0 mmol; 3 eq.). The mixture was stirred at room temperature and one drop of DMF was added after which a vigorous gas evolution started. After 30 min, the solvent and excess of oxalyldichloride was removed *in vaccuo.* The substance was re-dissolved in dichloromethane (80 mL), aluminium trichloride (879 mg, 6.6 mmol; 1.1 eq.) was added and the mixture was stirred for 10 min. Another Schlenk flask was charged with compound **2** (3.0 g, 5.0 mmol) and dichloromethane (150 mL). The flask was cooled to – 78 °C. Under stirring, the acid chloride/$AlCl_3$ solution was added dropwise over one hour. The reaction mixture turned deep purple upon addition. After completed addition, the cooling bath was removed and the mixture was allowed to warm up to room temperature. The crude mixture was extracted with water (150 mL), the organic layer was dried over sodium sulfate and the solvents were removed under reduced pressure. The product was purified by column chromatography over silica, using hexane/ethylacetate (95:5) as eluent. Solvent evaporation and drying under vacuum afforded the title product as orange solid (2.10 g, 4.0 mmol, 79%). ^{1}H NMR (500 MHz, $CDCl_3$): δ

4.72 (pst, 2H), 4.47 (pst, 2H), 4.39 (pst, 2H), 4.17 (pst, 2H), 3.40 (t, $J_{H–H}$= 7 Hz, 2H), 2.72 (t, $J_{H–H}$ = 7 Hz, 2H), 1.85 (m, 2H), 1.70 (m, 2 H), 1.43 (m, 2H), 1.35 (m, 8H) ppm. ^{13}C NMR (126 MHz, $CDCl_3$): δ 204.0, 80.8, 76.2, 75.2, 72.2, 70.7, 40.2, 39.9, 34.1, 32.9, 29.44, 29.40, 28.7, 28.2, 24.4 ppm. *m/z* 553 $[M + Na]^+$, HRMS (ESI): calcd for $C_{19}H_{25}BrFeIO$: 530.9479, found: 530.9472.

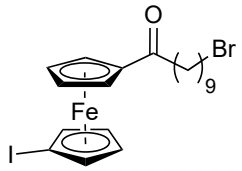

1-Iodo-1'-(10-bromodecanoyl)ferrocene (3b): Analogous procedure as for preparation of **3a**; Reaction of 10-bromodecanoic acid (1.05 g, 4.2 mmol) and compound **2** (2.1 g, 3.5 mmol) gave after work-up and purifcation the title product as orange solid (1.53 g, 2.8 mmol, 80%).^{1}H NMR (500 MHz, $CDCl_3$): δ4.66 (pst, 2H), 4.41 (pst, 2H), 4.32 (pst, 2H), 4.11 (pst, 2H), 3.33 (t, $J_{H–H}$ = 7 Hz, 2H), 2.66 (t, $J_{H–H}$ = 7 Hz, 2H), 1.77 (m, 2H), 1.63 (m, 2 H), 1.37 – 1.25 (m, 10H) ppm.

^{13}C NMR (75 MHz, $CDCl_3$): δ 203.6, 75.9, 75.0, 72.0, 70.5, 39.9, 39.8, 34.0, 32.7, 29.3, 29.2, 28.6, 28.0, 24.2 ppm. MS (ESI): *m/z* 545 $[M + H]^+$, HRMS (ESI): calcd for $C_{20}H_{27}BrFeI$: 544.9635, found: 544.9634.

1-Iodo-1'-(12-bromododecanoyl)ferrocene (3c): Analogous procedure as for preparation of

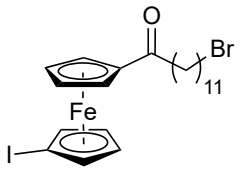

3a; Reaction of 12-bromododecanoic acid (1.39 g, 5.0 mmol) and compound **2** (3.0 g, 5.0 mmol) gave after work-up and purification the title product as orange solid (1.99 g, 3.5 mmol, 69%). ^{1}H NMR (500 MHz, $CDCl_3$): 4.69 (pst, 2H), 4.43 (pst, 2H), 4.35 (pst, 2H), 4.13 (pst, 2H), 3.34 (t, $J_{H–H}$ = 7 Hz, 2H), 2.68 (t, $J_{H–H}$ = 7 Hz, 2H), 1.80 (m, 2H), 1.66 (m, 2H), 1.40-1.24 (m, 14H) ppm. ^{13}C NMR (126 MHz, $CDCl_3$): δ 203.7, 80.7, 76.0, 75.0, 72.1, 70.5, 40.1, 39.8, 34.0, 32.8, 29.6,

29.5, 29.44, 29.40, 29.37, 28.7, 28.1, 24.3 ppm. *m/z* 595 $[M + H + Na]^+$, HRMS (ESI): calcd for $C_{22}H_{31}BrFeIO$: 572.9948, found: 572.9946.

1-Iodo-1'-(13-bromodtridecanoyl)ferrocene (3d): Analogous procedure as for preparation of **3a**; Reaction of 13-bromotridecanoic acid (0.84 g, 2.8 mmol) and compound **2** (1.70 g, 2.8 mmol) gave after work-up and purification the title product as orange solid (0.98 g, 1.7 mmol, 59%). ^{1}H NMR (300 MHz, $CDCl_3$): δ 4.72 (pst, 2H), 4.46 (pst, 2H), 4.38 (pst, 2H), 4.16 (pst, 2H), 3.38 (t, $J_{H–H}$ = 7 Hz, 2H), 2.71 (t, $J_{H–H}$ = 7 Hz, 2H), 1.83 (m, 2H), 1.69 (m, 2H), 1.42 – 1.26 (brd, 16H) ppm. ^{13}C NMR (75 MHz, $CDCl_3$): δ 204.0, 80.8, 76.1, 75.2, 72.2, 70.7, 40.2, 39.9, 34.1, 32.9, 29.6, 29.6, 29.5, 28.8, 28.2, 24.5 ppm. MS (ESI): *m/z* 587 $[M + H]^+$, HRMS (ESI): calcd for $C_{23}H_{33}BrFeIO$: 587.0105, found: 587.0100.

1-Iodo-1'-(14-bromotetradecanoyl)ferrocene (3e): Analogous procedure as for preparation of **3a**; Reaction of 14-bromotetradecanoic acid (0.91 g, 3.1 mmol) and compound **2** (1.85 g, 3.1 mmol) gave after work-up and purification the title product as orange solid (0.54 g, 0.9 mmol, 29%). ^{1}H NMR (500 MHz, $CDCl_3$): δ 4.72 (m, 2H), 4.46 (m, 2H), 4.38 (m, 2H), 4.16 (m, 2H), 3.38 (t, $J_{H–H}$ = 7 Hz, 2H), 2.71 (t, $J_{H–H}$ = 7 Hz, 2H), 1.83 (m, 2H), 1.69 (m, 2H), 1.41 – 1.26 (brd, 18H) ppm. ^{13}C NMR (126 MHz, $CDCl_3$): δ 204.0, 80.8, 76.1, 75.2, 72.2, 70.6, 40.2, 39.9, 34.1, 32.9, 29.7, 29.6, 29.5, 28.8, 28.2, 24.4 ppm. MS (ESI): *m/z* 601 $[M + H]^+$, HRMS (ESI): calcd for $C_{24}H_{35}BrFeIO$: 601.0261; found: 601.0269.

We reduced the 1-iodo-1'-bromoalkanoylferrocenes **3** to the respective 1-iodo-1'-(1-bromoalkyl)ferrocenes **4** by a Clemmensen reduction procedure (Scheme S4).

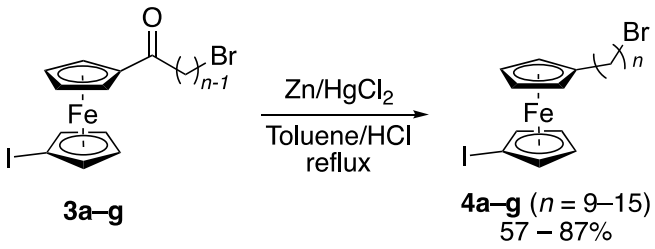

Scheme S4. Clemmensen reduction of 1-iodo-1'-alkanoyl ferrocenes to 1-iodo-1'-alkyl ferrocenes.

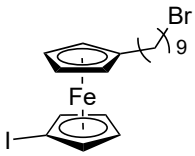

1-Iodo-1'-(9-bromononanyl)ferrocene (4a): We charged a round bottom flask with zinc granules (2.50 g, 38.2 mmol) and $HgCl_2$ (0.25 g, 0.9 mmol). HCl (10 mL) and water (5 mL) were added and the Hg-Zn amalgam was allowed to form over 5 min under gentle shaking of the flask. The acidic solution was removed and the amalgam was washed twice with water (10 mL). Concentrated HCl (30 mL) and water (20 mL) were added, followed by compound **3a** (1.00 g, 2.0 mmol), dissolved in toluene (50 mL). The reaction mixture was refluxed for 2 h upon which the colour changed from red-orange to yellow. The mixture was allowed to cool down to room temperature, phases were separated, and the organic layer was dried over sodium sulfate. Solvent removal afforded a yellow oil, which was purified by flash-chromatography over silica eluting with hexane. Solvent removal under reduced pressure afforded the title compound as yellow oil (0.75 g, 1.5 mmol, 77%). ^{1}H NMR (300 MHz): δ 4.31 (pst, 2H), 4.11 – 4.08 (m, 4H), 4.02 (pst, 2H), 3.41 (t, $J_{H–H}$ = 7 Hz, 2H), 2.35 (t, $J_{H–H}$ = 8 Hz, 2H), 1.86 (m, 2H), 1.54 – 1.41 (m, 4H), 1.32 (brd, 8H) ppm. ^{13}C NMR (75 MHz, $CDCl_3$): δ 91.1, 75.1, 71.3, 70.3, 69.4, 40.8, 34.1, 32.9, 31.1, 29.6, 29.5, 28.9, 28.8, 28.2 ppm. MS(ESI): *m/z* 516 $[M]^+$, HRMS (ESI): calcd for $C_{19}H_{26}BrFeI$: 515.9608; found: 515.9606.

1-Iodo-1'-(10-bromodecanyl)ferrocene (4b): Analogous procedure as for preparation of **4a**;

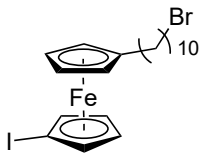

Reaction of **3b** (1.53 g, 2.8 mmol) with the Zn-Hg amalgam gave after work-up and purification the title product as yellow oil (1.04 g, 2.0 mmol, 80%). ^{1}H NMR (300 MHz): δ 4.33 (pst, 2H), 4.12 – 4.09 (m, 4H), 4.04 (pst, 2H), 3.41 (t, J_{H-H} = 7 Hz, 2H), 2.37 (t, J_{H-H} = 8 Hz, 2H), 1.87 (m, 2H), 1.54 (m, 2H), 1.45 (m, 2H), 1.33 (brd, 10H) ppm. ^{13}C NMR (75 MHz, $CDCl_3$): δ 90.9, 74.9, 71.2, 70.2, 69.3, 40.8, 33.9, 32.8, 31.0, 29.5, 29.45, 29.42, 29.39, 28.8, 28.7, 28.1 ppm. MS(ESI): *m/z* 530 $[M]^+$, HRMS (ESI): calcd for $C_{20}H_{28}BrFeI$: 529.9765; found: 529.9759.

1-Iodo-1'-(11-bromoundecanyl)ferrocene (4c): Analogous procedure as for preparation of

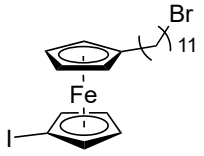

4a; Reaction of **3c** (1.13 g, 2.0 mmol) with the Zn-Hg amalgam gave after work-up and purification the title product as yellow oil (0.88 g, 1.6 mmol, 79%). ^{1}H NMR (500 MHz, $CDCl_3$): δ 4.30 (m, 2H), 4.09 – 4.08 (m, 4H), 4.02 (m, 2H), 3.41 (t, J_{H-H} = 7 Hz, 2H), 2.35 (t, J_{H-H} = 8 Hz, 2H), 1.86 (m, 2H), 1.51 (m, 2H), 1.42 (m, 2H), 1.29 (brd, 12H) ppm. ^{13}C NMR (126 MHz, $CDCl_3$): δ 91.2, 75.1, 71.4, 70.3, 69.4, 40.8, 34.1, 33.0, 31.2, 29.67, 29.66, 29.62, 29.59, 29.5, 28.9, 28.9, 28.3 ppm. MS (ESI): *m/z* 544 $[M]^+$, HRMS (APCI): calcd for $C_{21}H_{30}BrFeI$: 543.9916 , found: 543.9927.

1-Iodo-1'-(12-dodecanyl)ferrocene (4d): Analogous procedure as for preparation of **4a**;

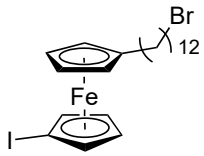

Reaction of **3d** (1.40 g, 2.4 mmol) with the Zn-Hg amalgam gave after work-up and purification the title product as yellow oil (1.19 g, 2.1 mmol, 87%). ^{1}H NMR (500 MHz, $CDCl_3$): δ 4.30 (m, 2H), 4.09 – 4.08 (m, 4H), 4.02 (pst, 2H), 3.41 (t, J_{H-H} = 7 Hz, 2H), 2.34 (t, J_{H-H} = 8 Hz, 2H), 1.86 (m, 2H), 1.51 (m, 2H), 1.43 (m, 2H), 1.28 (brd, 14H) ppm. ^{13}C NMR (126 MHz, $CDCl_3$): δ 91.3, 75.1, 71.4,

70.3, 69.4, 40.8, 34.2, 33.0, 31.2, 29.7, 29.65, 29.62, 29.55, 29.0, 28.9, 28.3 ppm. MS (ESI): *m/z* 558 $[M]^+$, HRMS (ESI): calcd for $C_{22}H_{32}BrFeI$: 558.0078; found: 558.0080.

1-Iodo-1'-(13-tridecanyl)ferrocene (4e): Analogous procedure as for preparation of **4a**;

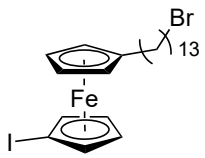

Reaction of **3e** (0.80 g, 1.4 mmol) with the Zn-Hg amalgam gave after work-up and purification the title product as yellow oil (0.63 g, 1.1 mmol, 81%). ^{1}H NMR (500 MHz, $CDCl_3$): δ 4.32 (pst, 2H), 4.12 – 4.09 (m, 4H), 4.04 (pst, 2H), 3.42 (t, $J_{H–H}$ = 7 Hz, 2H), 2.37 (t, $J_{H–H}$ = 8 Hz, 2Hk), 1.87 (m, 2H), 1.51 (m, 2H), 1.45 (m, 2H), 1.31 (brd, 16H) ppm.^{13}C NMR (75 MHz, $CDCl_3$): δ 91.1, 75.0, 71.3, 70.3, 69.4, 40.8, 34.0, 32.9, 31.1, 29.69, 29.67, 29.64, 29.59, 29.57, 29.5, 28.9, 28.8, 28.2 ppm. MS (ESI): *m/z* 572 $[M]^+$, HRMS (ESI): calcd for $C_{23}H_{34}BrFeI$: 572.0234; found: 572.0233.

1-Iodo-1'-(14-tetradecanyl)ferrocene (4f): Analogous procedure as for

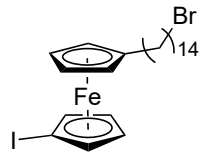

preparation of **4a**; Reaction of **3f** (0.50 g, 0.8 mmol) with the Zn-Hg amalgam gave after work-up and purification the title product as yellow oil (0.35 g, 0.6 mmol, 71%). ^{1}H NMR (500 MHz, $CDCl_3$): δ 4.31 (m, 2H), 4.10 – 4.09 (m, 4H), 4.03 (m, 2H), 3.41 (t, $J_{H–H}$ = 7 Hz, 2H), 2.36 (t, $J_{H–H}$= 8 Hz, 2H), 1.87 (m, 2H), 1.52 (m, 2H), 1.44 (m, 2H), 1.29 (brd, 18H) ppm. ^{13}C NMR (126 MHz, $CDCl_3$): δ 91.2, 75.1, 71.3, 70.3, 69.4, 40.8, 34.1, 32.9, 31.1, 29.74, 29.70, 29.68, 29.64, 29.61, 29.5, 28.9, 28.9, 28.3 ppm. MS (ESI): *m/z* 462 $[M – I + H]^+$, HRMS (ESI): calcd for $C_{24}H_{36}BrFeI$: 586.0384; found: 586.0391.

In the next step we applied a Sonogashira coupling reaction with ethynylferrocene to attach another ferrocene unit via triple bond, using a catalyst system of MePhos/$Pd(OAc)_2$ in THF with Et_3N as base (Scheme S4).

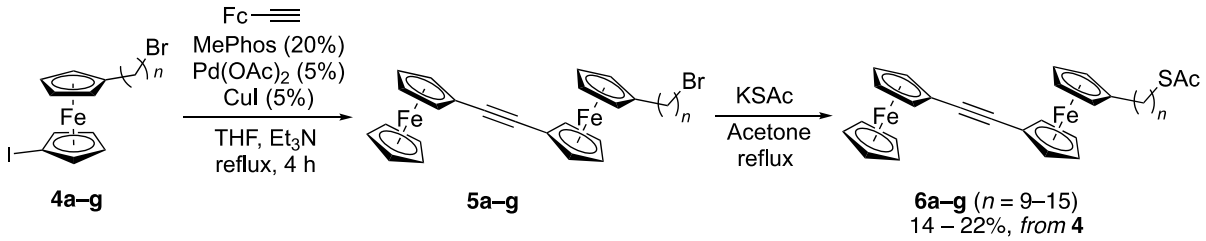

Scheme S5. Sonogashira coupling of 1-iodo-1'-(1-bromoalkyl)ferrocenes and ethynylferrocene followed by conversion of terminal Br into a thioacetate by reaction with potassium thioacetate to afford the binuclear head group bearing a protected alkane thiol.

The reaction afforded for all homologues mixtures of starting materials, products and homo-coupling products of ethynylferrocene. Additionally, we observed an exchange of the terminal bromine function versus iodine to an extent of ~ 10 – 20 % (estimated according to integration of the methylene resonances of RCH_2Br and RCH_2I in the ^{1}H NMR spectra). Separation of the homocoupling product by column chromatography from the product was successful for the homologues with lower numbers of *n* (e.g. 9 – 11) whereas it turned out to be difficult for $n > 11$ as the R_f-values of the product are very similar to the ones of the homocoupling product. Furthermore, separation of RCH_2Br and RCH_2I was not achieved, consequently we purified and characterised the intermediates only in the next step, i.e. after conversion of the terminal Br-moiety into the thioacetate.

AcS(CH$_2$)$_9$Fc–C≡C–Fc (6a): A Schlenk flask was charged with compound **4a** (0.40 g, 0.8 mmol), ethynylferrocene (0.24 g, 1.2 mmol), MePhos (56 mg, 0.18 mmol; 20 mol %), $Pd(OAc)_2$ (9 mg, 0.04 mmol; 5 mol %), CuI (7 mg, 0.04 mmol; 5 mol %), THF (20 mL) and Et_3N (2 mL). The reaction mixture was refluxed for 4h and allowed to cool down to room temperature. Silica gel (~ 5 g) was added the solvents were evaporated *in vaccuo*. The solid was subject to flash chromatography on silica, using hexane/DCM (9:1) as

eluent. Solvent evaporation afforded a dark red oil, which solidified upon standing. The solid was taken up in acetone (40 mL) and potassium thioacetate (177 mg, 1.5 mmol) was added. The mixture was refluxed for 2 h and allowed to cool down to room temperature. Solvent evaporation afforded a crude solid, which was purified by flash chromatography on silica using hexane/dichloromethane (6:3). Solvent evaporation and drying under vacuum afforded the product as an orange solid (73 mg, 0.01 mmol; 16% over 2 steps).

^{1}H NMR (500 MHz, $CDCl_3$): δ 4.44 (pst, 2H), 4.35 (m, 2H), 4.23, (s, 5H), 4.20 (pst, 2H), 4.15 (pst, 2H), 4.10 (m, 2H), 4.08 (m, 2H), 2.86 (t, $J_{H–H}$ = 7 Hz, 2H), 2.38(t, $J_{H–H}$ = 8 Hz, 2H), 2.32 (s, 3H) 1.56 – 1.52 (m, 4H), 1.34 – 1.26 (m, 10H) ppm. ^{13}C NMR (126 MHz, $CDCl_3$): δ 196.2, 90.5, 84.2, 84.0, 71.8, 71.3, 70.0, 69.1, 68.6, 66.7, 66.5, 31.2, 30.8, 29.7, 29.62, 29.60, 29.57, 29.3, 29.2, 28.9, 28.7 ppm. MS (ESI): *m/z* 595 $[M]^+$, HRMS (ESI): calcd for $C_{33}H_{39}Fe_2OS$: 595.1416; found: 595.1417.

$AcS(CH_2)_{10}Fc–C≡C–Fc$ (6b): Analogous procedure as for preparation of **6a**. Reaction of

compound **4b** (0.50 g, 0.9 mmol) with ethynylferrocene (0.30 g, 1.4 mmol), promoted by MePhos (67 mg, 0.19 mmol), $Pd(OAc)_2$ (11 mg, 0.05 mmol), CuI (9 mg, 0.05 mmol) in THF/Et_3N gave a crude solid after work-up, which was reacted in subsequent sequence with an excess of potassium thioacetate in acetone to give after purification the product as an orange solid (73 mg, 0.12 mmol; 13% over 2 steps).

^{1}H NMR (500 MHz, $CDCl_3$): δ 4.44 (pst, 2H), 4.35 (m, 2H), 4.23, (s, 5H), 4.20 (pst, 2H), 4.15 (pst, 2H), 4.10 (m, 2H), 4.08 (m, 2H), 2.86 (t, $J_{H–H}$ = 7 Hz, 2H), 2.38 (t, $J_{H–H}$ = 8 Hz), 2.32 (s, 3H) 1.59 – 1.50 (m, 4H), 1.36 – 1.26 (m, 12H) ppm. ^{13}C NMR (126 MHz, $CDCl_3$) δ: 196.2, 90.5, 84.2, 84.0, 71.9, 71.3, 70.0, 69.1, 68.6, 66.7, 66.6, 31.2, 30.8, 29.8, 29.66, 29.62,

29.59, 29.3, 29.2, 28.9, 28.7 ppm. MS (ESI): *m/z* 609 $[M]^+$, HRMS (ESI): calcd for $C_{34}H_{41}Fe_2OS$: 609.1572; found: 609.1588.

$AcS(CH_2)_{11}Fc–C\equiv C–Fc$ (6c): Analogous procedure as for preparation of **6a**. Reaction of

compound **4c** (0.50 g, 0.9 mmol) with ethynylferrocene (0.29 g, 1.4 mmol), promoted by MePhos (67 mg, 0.18 mmol), $Pd(OAc)_2$ (10 mg, 0.05 mmol), CuI (9 mg, 0.05 mmol) in THF/Et_3N gave a crude solid after work-up, which was reacted in subsequent sequence with an excess of potassium thioacetate in acetone to give after purification the product as an orange solid (93 mg, 0.15 mmol; 16% over 2 steps). ^1H NMR (300 MHz, $CDCl_3$): δ 4.44 (pst, 2H), 4.36 (m, 2H), 4.23, (s, 5H), 4.20 (pst, 2H), 4.16 (m, 2H), 4.11 (m, 4H), 2.87 (t, $J_{H–H}$ =7 Hz, 2H), 2.38 (t, $J_{H–H}$ =8 Hz), 2.32 (s, 3H) 1.59-1.52 (m, 4H), 1.27 (m, 14H) ppm. ^{13}C NMR (75 MHz, $CDCl_3$): δ 196.2, 90.6, 84.2, 84.0, 71.9, 71.3, 70.1, 70.0, 69.1, 68.6, 66.8, 66.5, 31.2, 30.8, 29.8, 29.73, 29.69, 29.6, 29.3, 29.2, 29.0, 28.7 ppm. MS (ESI): *m/z* 622 $[M]^+$, HRMS (ESI): calcd for $C_{35}H_{43}Fe_2OS$: 623.1729; found: 623.1719.

$AcS(CH_2)_{12}Fc–C\equiv C–Fc$ (6d): Analogous procedure as for preparation of **6a**. Reaction of

compound **4d** (0.60 g, 1.1 mmol) with ethynylferrocene (0.34 g, 1.6 mmol), promoted by MePhos (78 mg, 0.22 mmol), $Pd(OAc)_2$ (12 mg, 0.05 mmol), CuI (9 mg, 0.05 mmol) in THF/Et_3N gave a crude solid after work-up, which was reacted in subsequent sequence with an excess of potassium thioacetate in acetone to give after purification the product as an orange solid (95 mg, 0.15 mmol; 14% over 2 steps). ^1H NMR (500 MHz, $CDCl_3$): δ 4.45 (pst, 2H), 4.36 (pst, 2H), 4.23, (s, 5H), 4.20 (pst, 2H), 4.15 (pst, 2H), 4.11 – 4.08 (m, 4H), 2.87 (t, $J_{H–H}$, 2H), 2.39 (t, $J_{H–H}$ = 8 Hz), 2.32 (s, 3H) 1.59 – 1.52 (m, 4H), 1.34 – 1.26 (m, 16H) ppm. ^{13}C NMR (126 MHz,

$CDCl_3$): δ 196.1, 90.5, 84.2, 84.0, 71.8, 71.3, 70.0, 69.0, 68.5, 66.7, 66.5, 31.2, 30.8, 29.8, 29.74, 29.69, 29.62, 29.59, 29.3, 29.2, 28.9, 28.7 ppm. MS (ESI): *m/z* 636 $[M]^+$, HRMS (ESI): calcd for $C_{36}H_{44}Fe_2OS$: 636.1812; found: 636.1794.

$AcS(CH_2)_{13}Fc–C\equiv C–Fc$ (6e): Analogous procedure as for preparation of **6a**. Reaction of

compound **4e** (0.60 g, 1.0 mmol) with ethynylferrocene (0.44 g, 2.1 mmol), promoted by MePhos (153 mg, 0.42 mmol), $Pd(OAc)_2$ (24 mg, 0.05 mmol), CuI (10 mg, 0.05 mmol) in THF/Et_3N gave a crude solid after work-up, which was reacted in subsequent sequence with an excess of potassium thioacetate in acetone to give after purification the product as an orange solid (152 mg, 0.23 mmol; 22% over 2 steps). ^{1}H NMR (500 MHz, $CDCl_3$): δ 4.44 (m, 2H), 4.36 (m, 2H), 4.23, (s, 5H), 4.20 (m, 2H), 4.16 (m, 2H), 4.11 – 4.09 (m, 4H), 2.87 (t, $J_{H–H}$ = 7 Hz, 2H), 2.38 (t, $J_{H–H}$ = 8 Hz), 2.32 (s, 3H) 1.59 – 1.51 (m, 4H), 1.37 – 1.26 (m, 18H) ppm. ^{13}C NMR (126 MHz, $CDCl_3$): δ 196.1, 90.6, 84.2, 84.0, 71.9, 71.3, 70.1, 70.0, 69.1, 68.6, 66.8, 66.6, 31.7, 31.2, 30.8, 29.78, 29.76, 29.72, 29.70, 29.63, 29.60, 29.3, 29.2, 29.0, 28.7 ppm. MS (ESI): *m/z* 651 $[M + H]^+$, HRMS (ESI): calcd for $C_{37}H_{47}Fe_2OS$: 651.2042; found: 651.2047.

$AcS(CH_2)_{14}Fc–C\equiv C–Fc$ (6f): Analogous procedure as for preparation of **6a**. Reaction of

compound **4f** (0.24 g, 0.4 mmol) with ethynylferrocene (0.18 g, 0.9 mmol), promoted by MePhos (62 mg, 0.17 mmol), $Pd(OAc)_2$ (10 mg, 0.04 mmol), CuI (4 mg, 0.02 mmol) in THF/Et_3N gave a crude solid after work-up, which was reacted in subsequent sequence with an excess of potassium thioacetate in acetone to give after purification the product as an orange solid (56 mg, 0.08 mmol; 20% over 2 steps). ^{1}H NMR (500 MHz, $CDCl_3$): δ 4.44 (pst, 2H), 4.39 (m, 2H), 4.23 (s, 5H), 4.20 (pst, 2H), 4.19 (m, 2H), 4.13 (m, 4H), 2.87 (t, $J_{H–H}$ = 7 Hz, 2H), 2.37 (t, $J_{H–H}$ = 8

Hz), 2.32 (s, 3H) 1.59 – 1.51 (m, 4H), 1.35 – 1.26 (m, 18H) ppm. ^{13}C NMR (75 MHz, $CDCl_3$): δ 196.1, 91.0, 84.3, 84.0, 72.0, 71.3, 70.3, 70.1, 69.3, 69.3, 68.6, 67.2, 66.6, 31.2, 30.8, 29.79, 29.76, 29.72, 29.69, 29.6, 29.3, 29.2, 28.9, 28.7 ppm. MS (ESI): *m/z* 665 $[M + H]^+$, HRMS (ESI): calcd for $C_{38}H_{49}Fe_2OS$: 665.2199; found: 665.2194.

We deprotected the thioacetates by using an excess of lithium aluminium hydride in THF, followed by addition of HCl (Scheme S6).

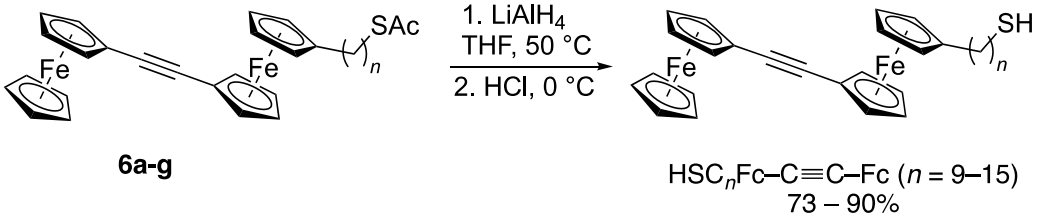

Scheme S6. Deprotection of the binuclear thioacetates by reaction with lithium aluminium hydride to yield the target thiols $HSC_nFc–C≡C–Fc$.

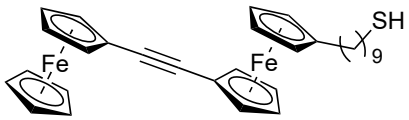

$HS(CH_2)_9Fc–C≡C–Fc$: We charged a Schlenk tube with **6a** (73 mg, 0.12 mmol) and THF (7 mL). Under stirring, lithium aluminium hydride (47 mg, 1.2 mmol) was added. The mixture was heated to 50 °C for 1 h and subsequently cooled to 0 °C using an ice bath. Degassed hydrochloric acid was added dropwise (0.1 M, 5 mL) followed by degassed hexane (15 mL). The supernatant hexane layer was separated with a pipette and dried over Na_2SO_4. Solvent evaporation afforded an orange solid, which was subject to flash chromatography on silica using hexane/DCM (4:1) as eluent. The first fraction contained the product, solvent evaporation afforded an orange oil (51 mg, 0.09 mmol, 73 %) which solidified upon standing. M.p.: 67 ℃.^{1}H NMR (500 MHz, $CDCl_3$): δ 4.44 (pst, 2H), 4.35 (m, 2H), 4.23, (s, 5H), 4.20 (pst, 2H), 4.15 (pst, 2H), 4.10 (m, 2H), 4.09 (m, 2H), 2.52 (dt, $J_{H–H}$ = 8 Hz, $J_{H–H}$ = 7 Hz, 2H), 2.38 (t, $J_{H–H}$ = 8 Hz, 2H) 1.64 – 1.51 (m, 4H), 1.39 – 1.26 (m, 10H), 1.33 (t, $J_{H–H}$ =8 Hz, 1H, S*H*). ^{13}C NMR (126 MHz, $CDCl_3$): δ 90.5, 84.2, 84.0, 71.9, 71.3, 70.1, 69.1, 68.6, 66.7, 66.6,

34.2, 31.2, 29.8, 29.6, 29.2, 28.7, 28.5, 24.8 ppm. MS(ESI): *m/z* 553 $[M]^+$, HRMS (ESI): calcd for $C_{31}H_{37}Fe_2OS$: 553.1310; found: 553.1317.

$HS(CH_2)_{10}Fc–C\equiv C–Fc$: Compound **6b** (73 mg. 0.12 mmol) and lithium aluminium hydride

(45 mg, 1.2 mmol) gave after reaction in THF, work-up and purification the title compound as orange solid (56 mg, 0.10 mmol, 82%). M.p.: 78 °C. ^{1}H NMR (500 MHz, $CDCl_3$): δ 4.44 (pst, 2H), 4.35 (m, 2H), 4.27, (s, 5H), 4.20 (pst, 2H), 4.15 (pst, 2H), 4.10 (m, 2H), 4.09 (m, 2H), 2.52 (dt, $J_{H–H}$ = 8 Hz, $J_{H–H}$ = 7 Hz, 2H, C*H*$_2$SH), 2.38 (t, $J_{H–H}$ = 8 Hz), 1.60 (m, 2H), 1.60 (m, 2H), 1.55 – 1.50 (m, 2H), 1.38 – 1.26 (m, 12H), 1.33 (t, $J_{H–H}$ = 8 Hz, 1H, S*H*). ^{13}C NMR (126 MHz, $CDCl_3$): δ 90.6, 84.2, 71.9, 71.3, 70.1, 69.1, 68.6, 66.7, 66.6, 34.2, 31.2, 29.8, 29.70, 29.66, 29.2, 28.7, 28.5, 24.8 ppm. MS (ESI): *m/z* 567 $[M]^+$. HRMS (ESI): calcd for $C_{32}H_{39}Fe_2S$: 567.1467, found: 567.1475.

$HS(CH_2)_{11}Fc–C\equiv C–Fc$: Compound **6c** (50 mg. 0.08 mmol) and lithium aluminium hydride

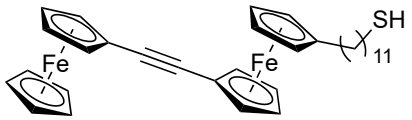

(29 mg, 0.76 mmol) gave after reaction in THF, work-up and purification the title compound as orange solid (35 mg, 0.06 mmol, 78%). M.p.: 62 °C. ^{1}H NMR (500 MHz, $CDCl_3$): δ 4.44 (pst, 2H), 4.36 (m, 2H), 4.23 (s, 5H), 4.20 (pst, 2H), 4.16 (pst, 2H), 4.11 (m, 2H), 4.09 (m, 2H), 2.53 (dt, $J_{H–H}$ = 7 Hz, $J_{H–H}$ = 7 Hz, 2H, C*H*$_2$SH), 2.38 (t, $J_{H–H}$ = 8 Hz) 1.61 (m, 2H), 1.54 (m, 2H), 1.39 – 1.27 (m, 12H), 1.36 (t, *J* = 8 Hz, 1H, S*H*) ppm. ^{13}C NMR (126 MHz, $CDCl_3$): δ 90.6, 84.2, 84.0, 71.9, 71.3, 70.1, 70.1, 69.1, 68.6, 66.8, 66.6, 34.2, 31.2, 29.8, 29.74, 29.71, 29.65, 29.2, 28.7, 28.5, 24.8 ppm. MS (ESI): *m/z* 580 $[M]^+$. HRMS (ESI): calcd for $C_{33}H_{41}Fe_2S$: 581.1623, found: 581.1621.

HS(CH$_2$)$_{12}$Fc–C≡C–Fc: Compound **6d** (77 mg. 0.12 mmol) and lithium aluminium hydride

(46 mg, 1.21 mmol) gave after reaction in THF, work-up and purification the title compound as orange solid (65 mg, 0.11 mmol, 90%). M.p.: 81 °C.^{1}H NMR (500 MHz, $CDCl_3$): δ 4.45 (pst, 2H), 4.36 (m, 2H), 4.23, (s, 5H), 4.21 (pst, 2H), 4.16 (pst, 2H), 4.11 – 4.09 (m, 4H), 2.53 (dt, $J_{H–H}$ = 7 Hz, $J_{H–H}$ = 7 Hz, 2H), 2.39 (t, $J_{H–H}$ = 8 Hz, 2H), 1.66 – 1.49 (m, 4H), 1.40 – 1.27 (m, 14H) ppm., 1.34 (t, J = 8 Hz, 1H, S*H*). ^{13}C NMR (75 MHz, $CDCl_3$): δ 90.5, 84.2, 84.0, 71.9, 71.3, 70.0, 69.1, 68.6, 66.7, 66.5, 34.2, 31.2, 29.8, 29.76, 29.72, 29.6, 29.2, 28.7, 28.5, 24.8 ppm. MS (ESI): *m/z* 595 $[M + H]^+$. HRMS (ESI): calcd for $C_{34}H_{42}Fe_2S$: 594.1711, found: 594.1702.

HS(CH$_2$)$_{13}$Fc–C≡C–Fc: Compound **6e** (50 mg. 0.08 mmol) and lithium aluminium hydride

(29 mg, 0.76 mmol) gave after reaction in THF, work-up and purification the title compound as orange solid (41 mg, 0.07 mmol, 86%). M.p.: 74 °C. ^{1}H NMR (300 MHz, $CDCl_3$): δ 4.44 (pst, 2H), 4.37 (m, 2H), 4.23, (s, 5H), 4.20 (pst, 2H), 4.17 (m, 2H), 4.12 – 4.10 (m, 4H), 2.52 (dt, $J_{H–H}$ =7 Hz, $J_{H–H}$ = 7 Hz, 2H), 2.38 (t, $J_{H–H}$ = 8 Hz), 1.61 (m, 2H), 1.53 (m, 2H), 1.39 – 1.27 (m, 12H), 1.33 (t, J =8 Hz, 1H, S*H*) ppm. ^{13}C NMR (126 MHz, $CDCl_3$): δ 90.8, 84.3, 84.0, 71.9, 71.3, 70.2, 70.1, 69.2, 69.2, 68.6, 66.9, 66.6, 34.2, 31.2, 29.8, 29.8, 29.74, 29.67, 29.2, 28.7, 28.5, 24.8 ppm. MS (ESI): *m/z* 609 $[M + H]^+$, HRMS (ESI): calcd for $C_{35}H_{45}Fe_2S$: 609.1936, found: 609.1928.

HS(CH$_2$)$_{14}$Fc–C≡C–Fc: Compound **6f** (56 mg. 0.08 mmol) and lithium aluminium hydride

(32 mg, 0.84 mmol) gave after reaction in THF, work-up and purification the title compound as orange solid (45 mg, 0.07 mmol, 86%). M.p.: 79 °C.^{1}H NMR (300 MHz, $CDCl_3$): δ 4.44 (pst, 2H), 4.36 (m, 2H),

4.23 (s, 5H), 4.20 (pst, 2H), 4.15 (m, 2H), 4.11 – 4.09 (m, 4H), 2.52 (dt, $J_{H–H}$ = 7 Hz, $J_{H–H}$ = 7 Hz, 2H), 2.38 (t, $J_{H–H}$ = 8 Hz), 1.65 – 1.49 (m, 4H), 1.39 – 1.26 (m, 12H), 1.33 (t, *J* =8 Hz, 1H, S*H*) ppm. ^{13}C NMR (75 MHz, $CDCl_3$): δ 90.7, 84.2, 84.0, 71.9, 71.3, 70.1, 70.1, 69.1, 68.6, 66.8, 66.6, 34.2, 31.2, 29.8, 29.75, 29.68, 29.2, 28.7, 28.5, 24.8 ppm. MS (ESI): *m/z* 623 $[M + H]^+$, HRMS (ESI): calcd for $C_{36}H_{47}Fe_2S$: 623.2093, found: 623.2096.

2. ^{1}H- and ^{13}C NMR Spectra and HRMS Data for the $HS(CH_2)_nFc–C\equiv C–Fc$ Series

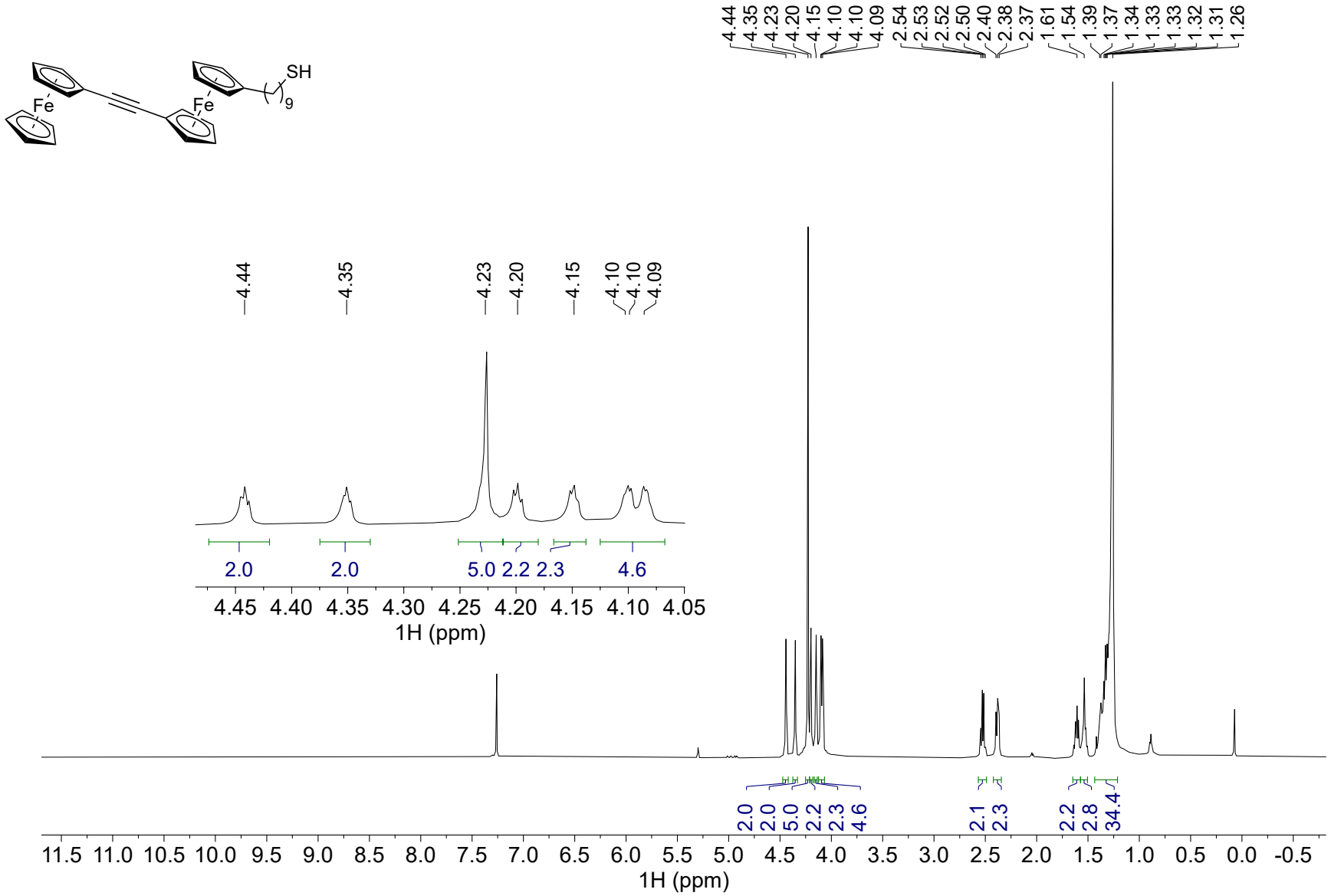

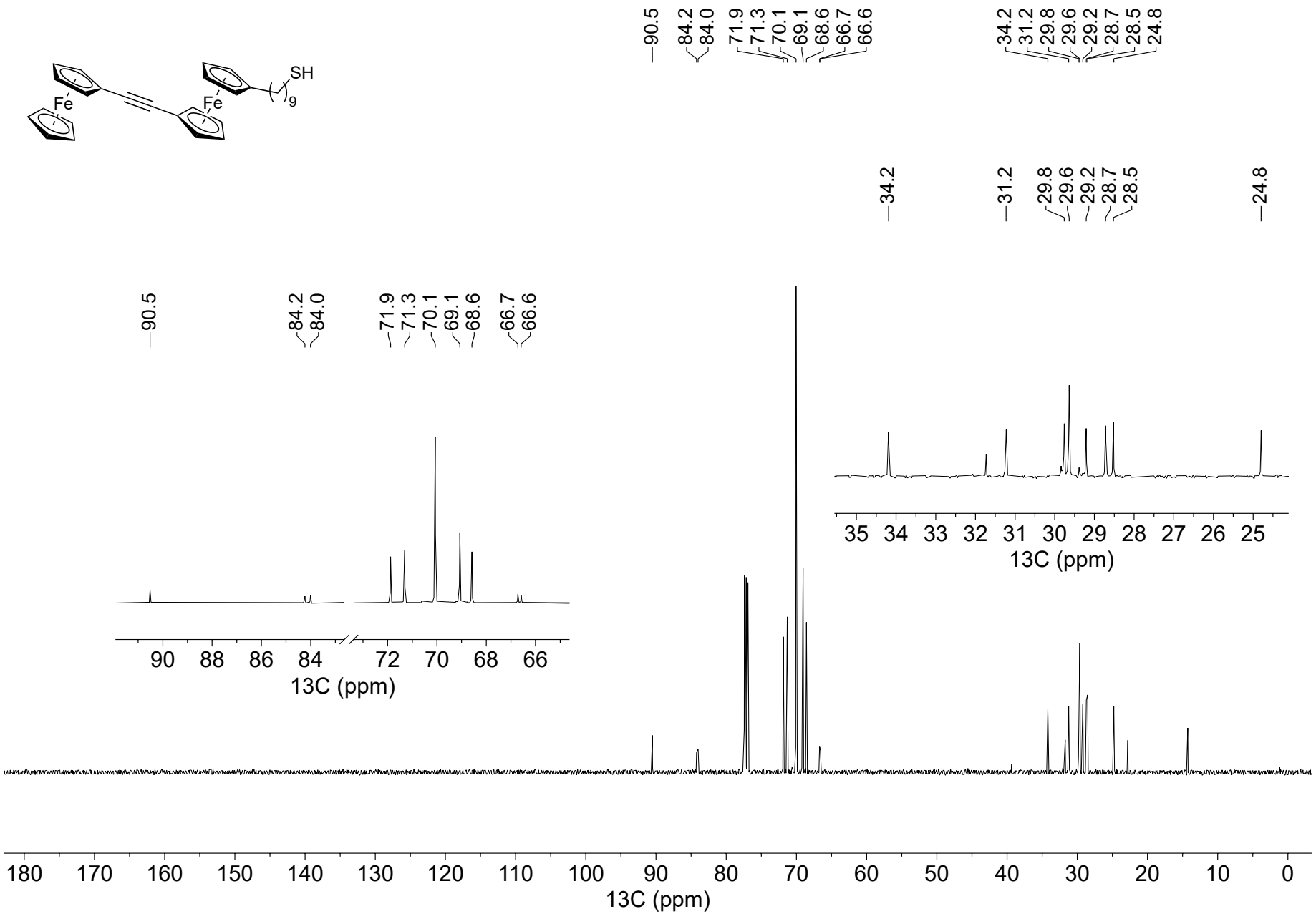
SH
9
Fe
Fe
90.5
84.2
84.0
71.9
71.3
70.1
69.1
68.6
66.7
66.6
34.2
31.2
29.8
29.6
29.2
28.7
28.5
24.8
13C (ppm)
13C (ppm)
13C (ppm)

Acquisition Parameter

Source Type	ESI	Ion Polarity	Positive	Set Nebulizer	3.0 Bar
Focus	Not active	Set Capillary	4500 V	Set Dry Heater	200 °C
Scan Begin	50 m/z	Set End Plate Offset	-500 V	Set Dry Gas	6.0 l/min
Scan End	1800 m/z	Set Collision Cell RF	200.0 Vpp	Set Divert Valve	Waste

Meas. m/z	#	Formula	m/z	err [ppm]	rdb	e⁻ Conf	N-Rule
553.1317	1	C 31 H 37 Fe 2 S	553.1310	-1.2	13.5	even	ok

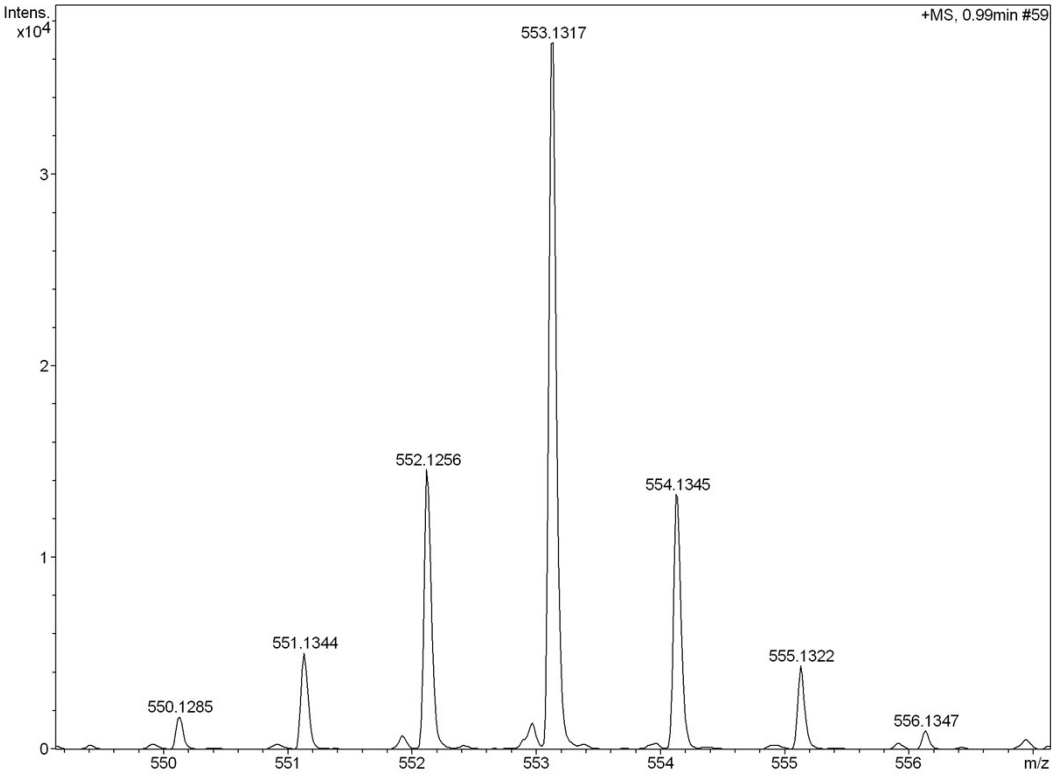

W

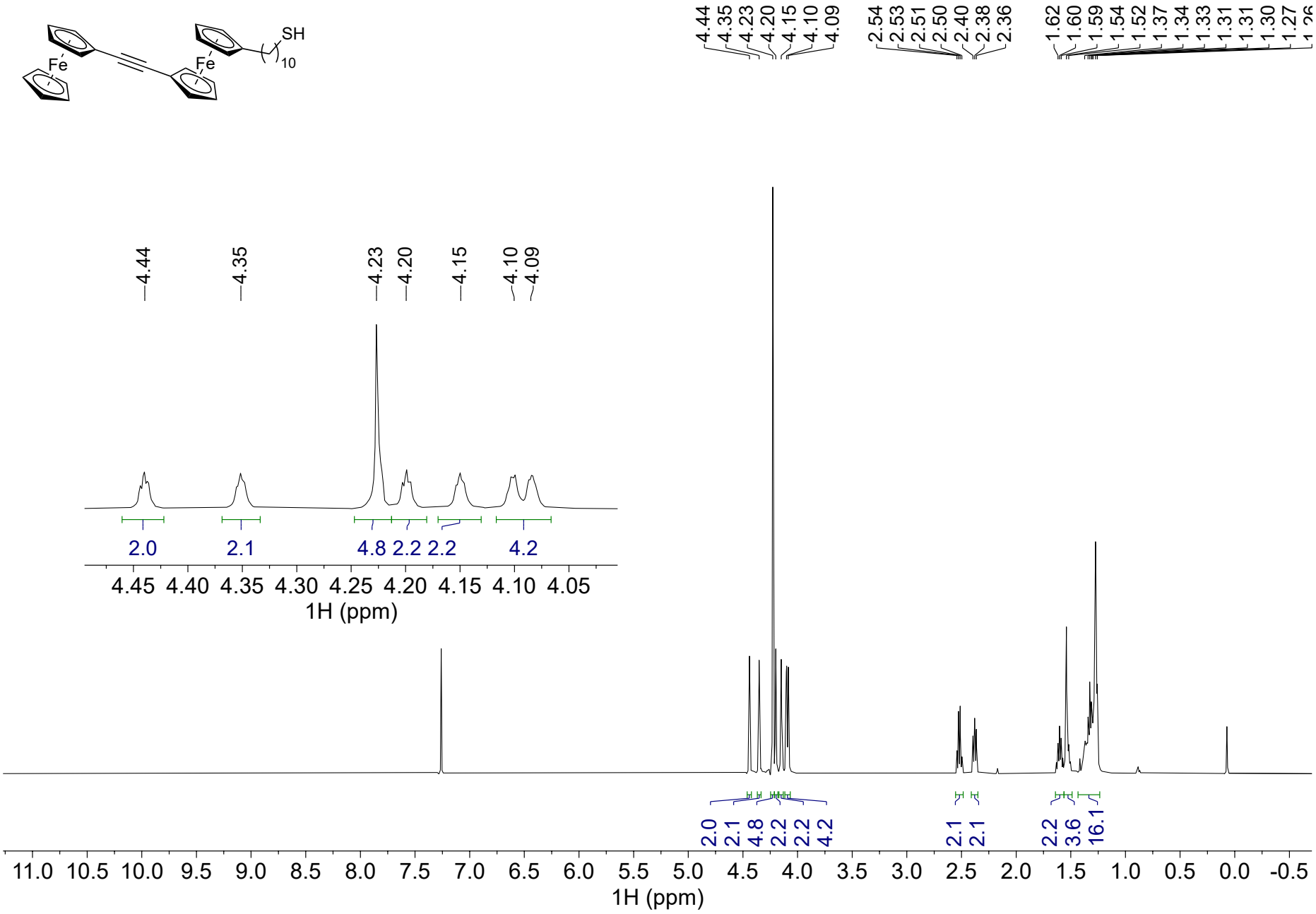
Fe
Fe
SH
10
4.44
4.35
4.23
4.20
4.15
4.10
4.09
2.54
2.53
2.51
2.50
2.40
2.38
2.36
1.62
1.60
1.59
1.54
1.52
1.37
1.34
1.33
1.31
1.31
1.30
1.27
2.0
2.1
4.8
2.2
2.2
4.2
2.1
2.1
2.2
3.6
16.1
11.0 10.5 10.0 9.5 9.0 8.5 8.0 7.5 7.0 6.5 6.0 5.5 5.0 4.5 4.0 3.5 3.0 2.5 2.0 1.5 1.0 0.5 0.0 -0.5
1H (ppm)
4.45 4.40 4.35 4.30 4.25 4.20 4.15 4.10 4.05
1H (ppm)

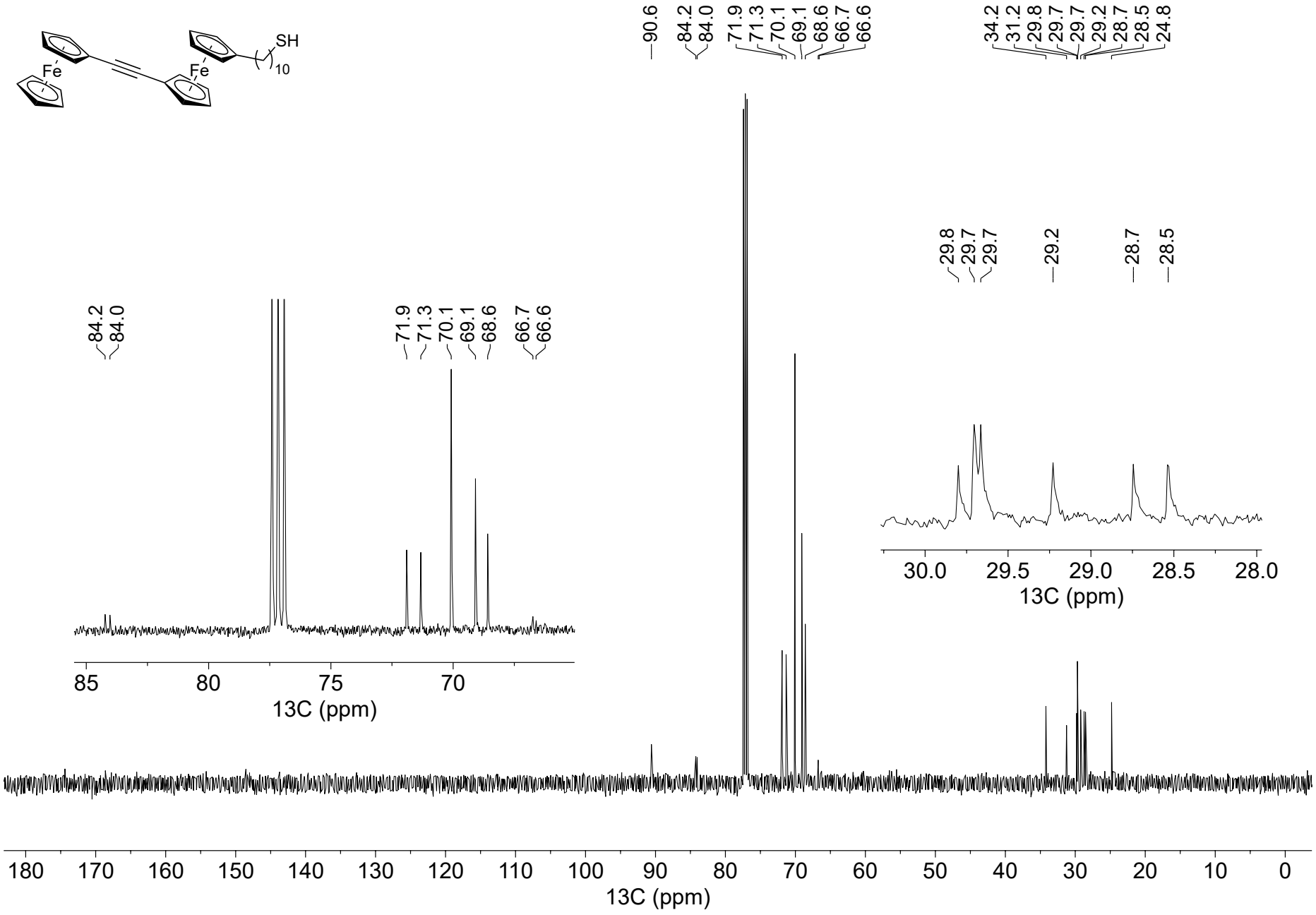
Fe
Fe
SH
10
90.6
84.2
84.0
71.9
71.3
70.1
69.1
68.6
66.7
66.6
34.2
31.2
29.8
29.7
29.7
29.2
28.7
28.5
24.8
84.2
84.0
71.9
71.3
70.1
69.1
68.6
66.7
66.6
85
80
75
70
13C (ppm)
29.8
29.7
29.7
29.2
28.7
28.5
30.0
29.5
29.0
28.5
28.0
13C (ppm)
180
170
160
150
140
130
120
110
100
90
80
70
60
50
40
30
20
10
0
13C (ppm)

Acquisition Parameter

Source Type	ESI	Ion Polarity	Positive	Set Nebulizer	3.0 Bar
Focus	Not active	Set Capillary	4500 V	Set Dry Heater	200 °C
Scan Begin	50 m/z	Set End Plate Offset	-500 V	Set Dry Gas	6.0 l/min
Scan End	1800 m/z	Set Collision Cell RF	200.0 Vpp	Set Divert Valve	Waste

Meas. m/z	#	Formula	m/z	err [ppm]	rdb	e⁻ Conf	N-Rule
567.1475	1	C 32 H 39 Fe 2 S	567.1467	-1.4	13.5	even	ok

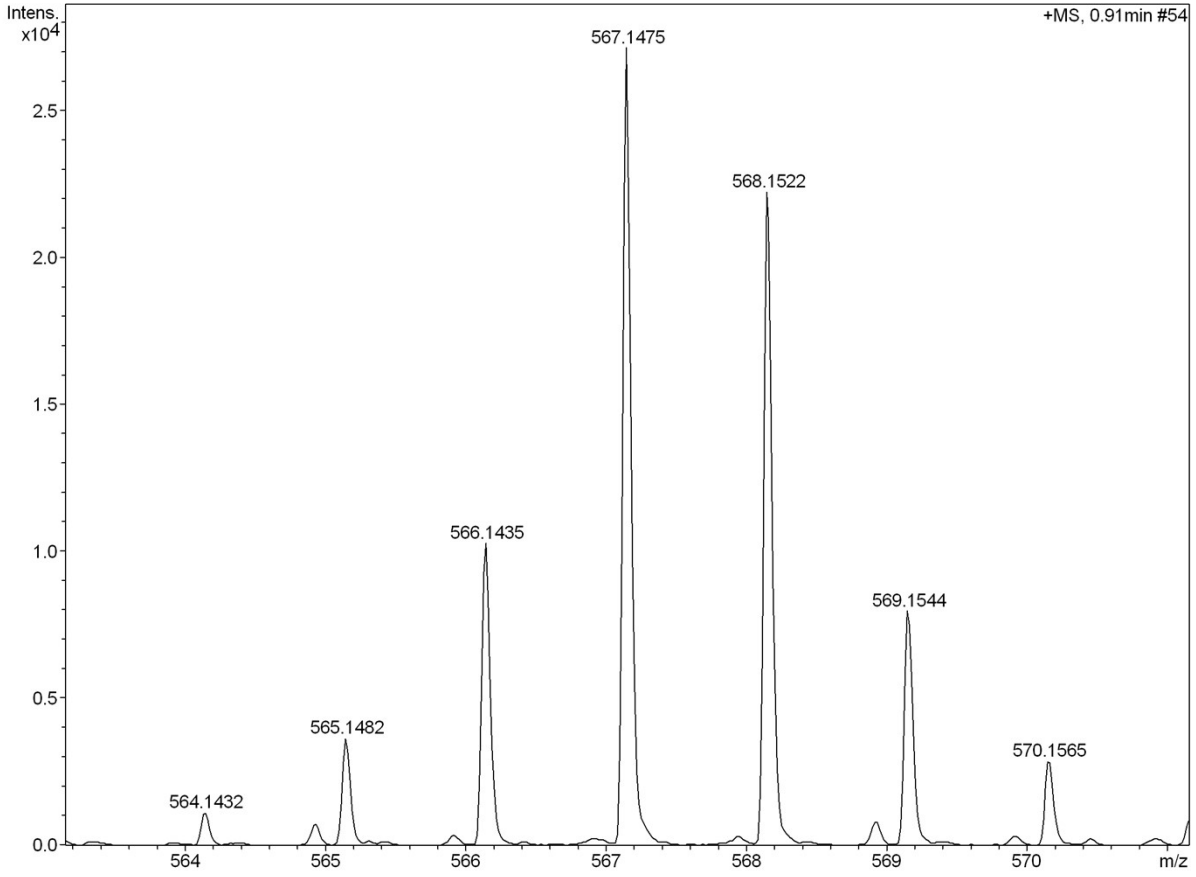

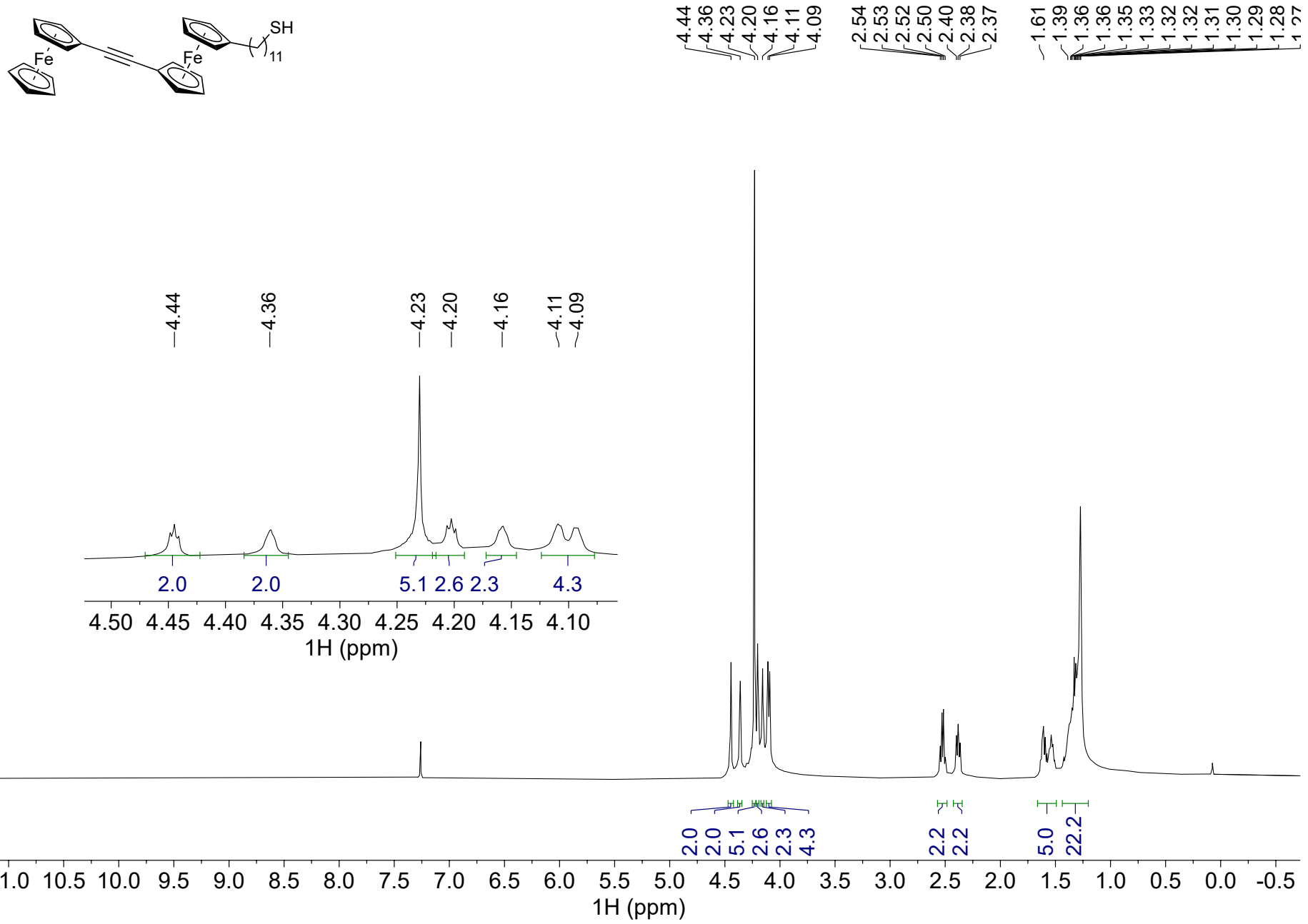
Fe
Fe
SH
11
4.44
4.36
4.23
4.20
4.16
4.11
4.09
2.54
2.53
2.52
2.50
2.40
2.38
2.37
1.61
1.39
1.36
1.36
1.35
1.33
1.32
1.32
1.31
1.30
1.29
1.28
2.0
2.0
5.1
2.6
2.3
4.3
2.2
2.2
5.0
22.2
11.0 10.5 10.0 9.5 9.0 8.5 8.0 7.5 7.0 6.5 6.0 5.5 5.0 4.5 4.0 3.5 3.0 2.5 2.0 1.5 1.0 0.5 0.0 -0.5
1H (ppm)
2.0
2.0
5.1 2.6 2.3
4.3
4.50 4.45 4.40 4.35 4.30 4.25 4.20 4.15 4.10
1H (ppm)

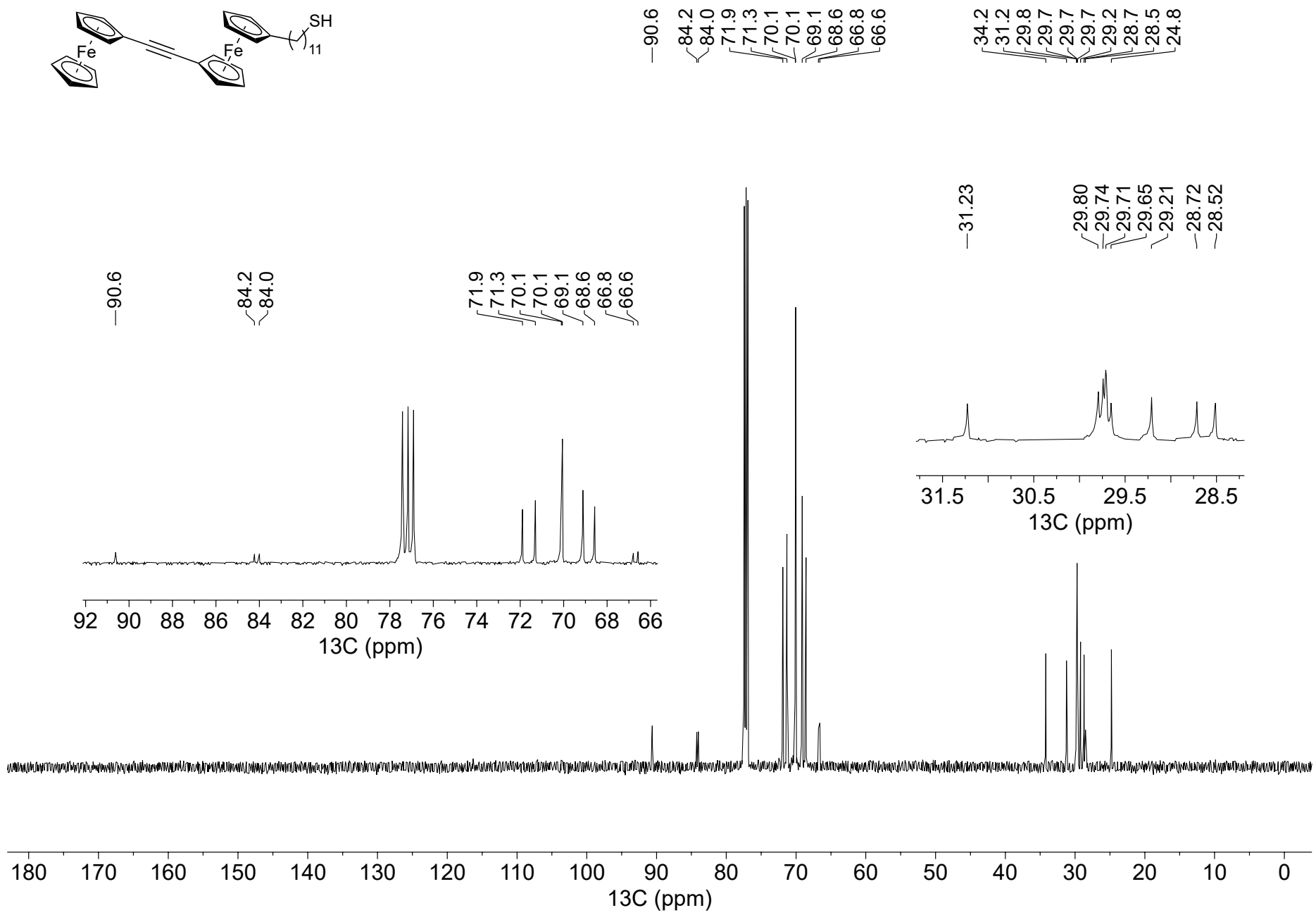
Fe
Fe
SH
11
90.6
84.2
84.0
71.9
71.3
70.1
70.1
69.1
68.6
66.8
66.6
34.2
31.2
29.8
29.7
29.7
29.7
29.2
28.7
28.5
24.8
31.23
29.80
29.74
29.71
29.65
29.21
28.72
28.52
13C (ppm)
13C (ppm)
13C (ppm)

Acquisition Parameter

Source Type	ESI	Ion Polarity	Positive	Set Nebulizer	2.0 Bar
Focus	Active	Set Capillary	4500 V	Set Dry Heater	200 °C
Scan Begin	50 m/z	Set End Plate Offset	-500 V	Set Dry Gas	6.0 l/min
Scan End	3000 m/z	Set Collision Cell RF	120.0 Vpp	Set Divert Valve	Waste

Meas. m/z	#	Formula	m/z	err [ppm]	rdb	e⁻ Conf	N-Rule
581.1621	1	C 33 H 41 Fe 2 S	581.1623	0.4	13.5	even	ok

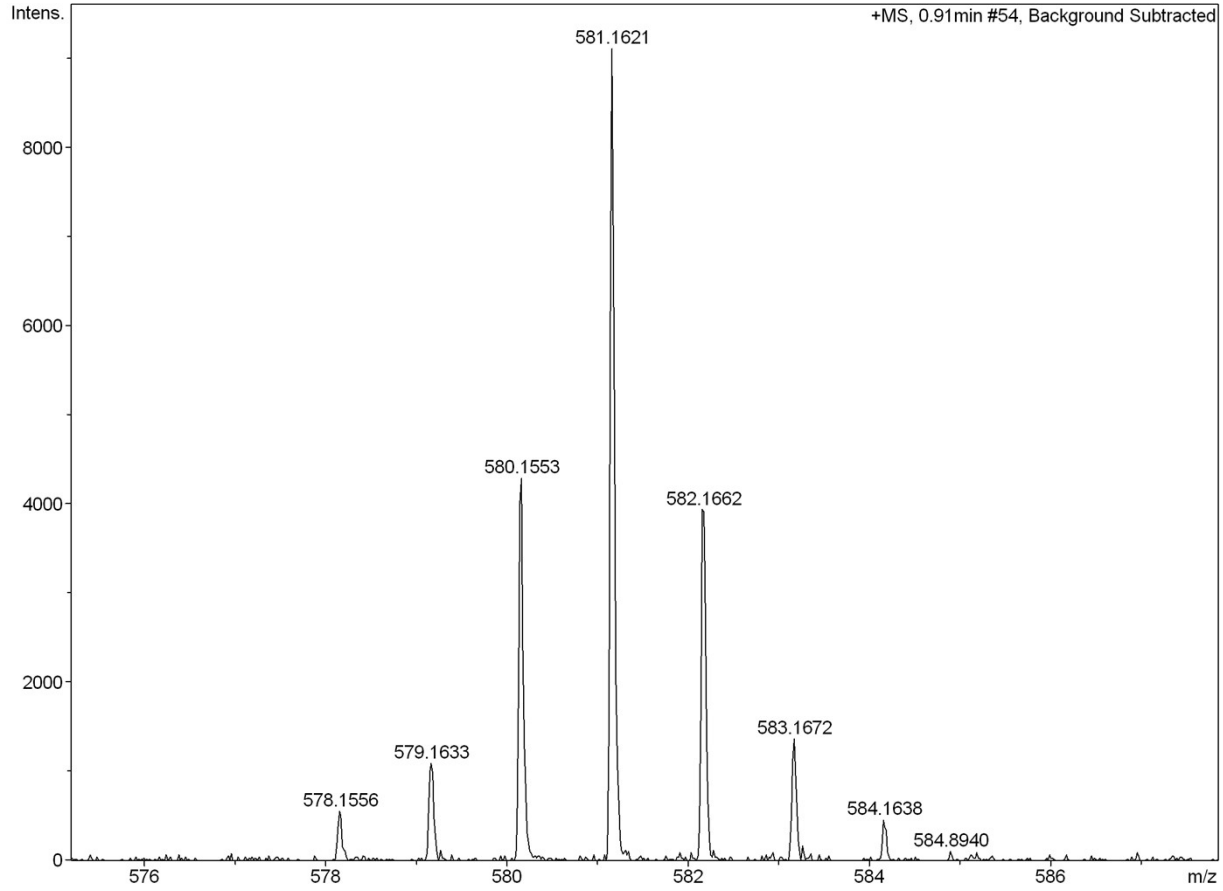

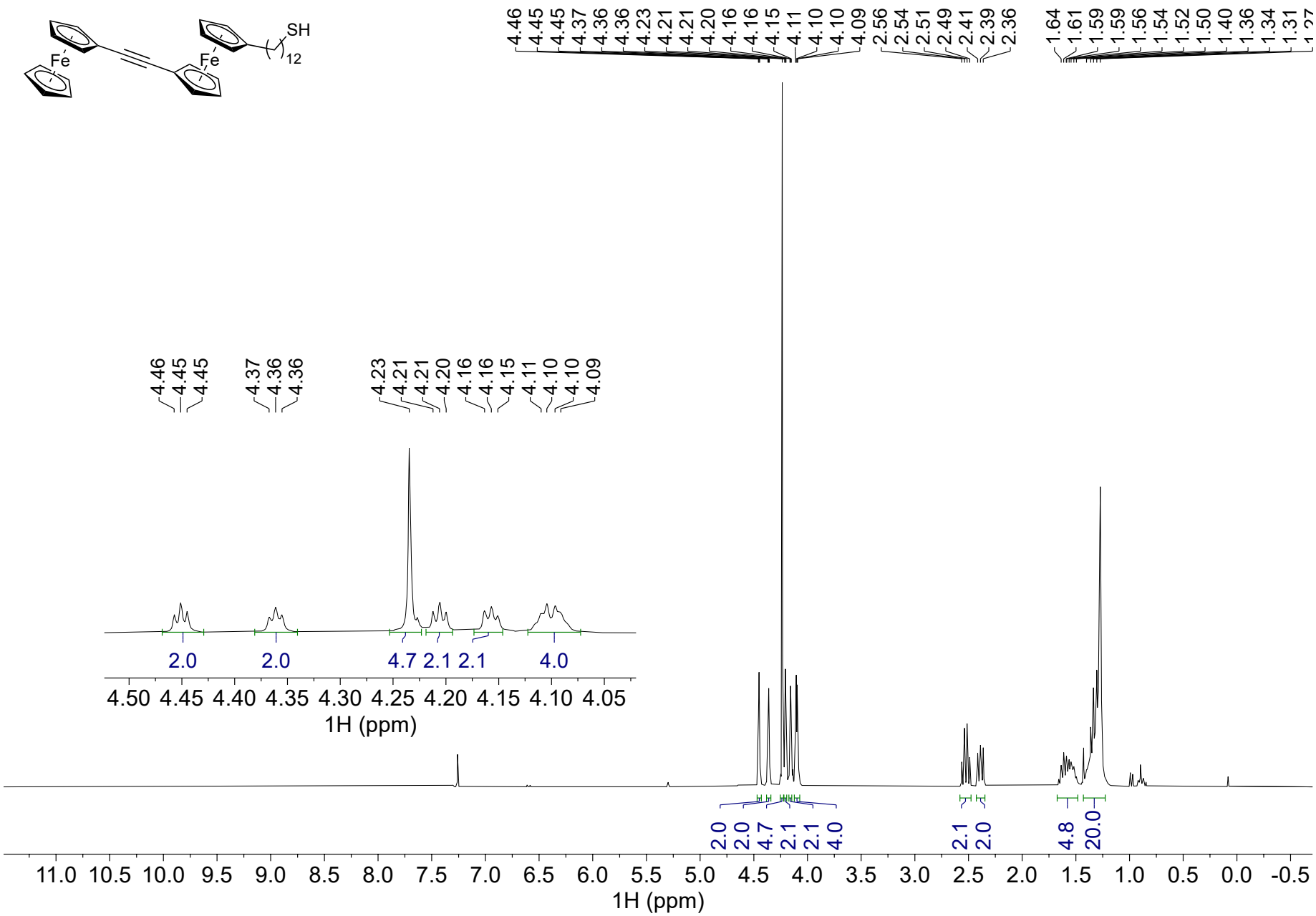
SH
12
Fe
Fe
4.46 4.45 4.45 4.37 4.36 4.36 4.23 4.21 4.21 4.20 4.16 4.16 4.15 4.11 4.10 4.10 4.09 2.56 2.54 2.51 2.49 2.41 2.39 2.36 1.64 1.61 1.59 1.59 1.56 1.54 1.52 1.50 1.40 1.36 1.34 1.31
2.0 2.0 4.7 2.1 2.1 4.0 2.1 2.0 4.8 20.0
11.0 10.5 10.0 9.5 9.0 8.5 8.0 7.5 7.0 6.5 6.0 5.5 5.0 4.5 4.0 3.5 3.0 2.5 2.0 1.5 1.0 0.5 0.0 -0.5
1H (ppm)
4.46 4.45 4.45 4.37 4.36 4.36 4.23 4.21 4.21 4.20 4.16 4.16 4.15 4.11 4.10 4.10 4.09
2.0 2.0 4.7 2.1 2.1 4.0
4.50 4.45 4.40 4.35 4.30 4.25 4.20 4.15 4.10 4.05
1H (ppm)

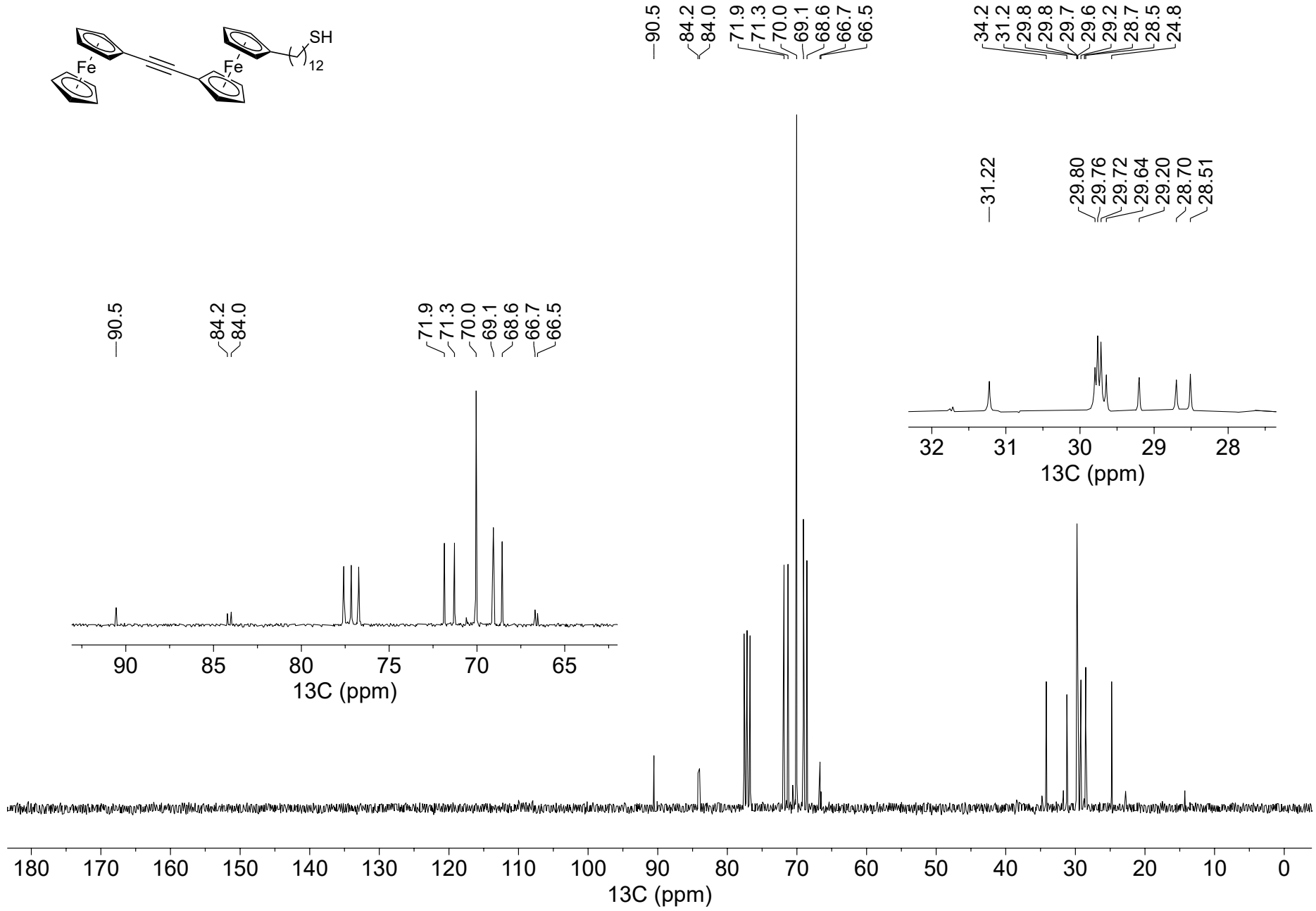
Fe
Fe
SH
12
90.5
84.2
84.0
71.9
71.3
70.0
69.1
68.6
66.7
66.5
34.2
31.2
29.8
29.8
29.7
29.6
29.2
28.7
28.5
24.8
31.22
29.80
29.76
29.72
29.64
29.20
28.70
28.51
32
31
30
29
28
13C (ppm)
90
85
80
75
70
65
13C (ppm)
180
170
160
150
140
130
120
110
100
90
80
70
60
50
40
30
20
10
0
13C (ppm)

Acquisition Parameter

Source Type	ESI	Ion Polarity	Positive	Set Nebulizer	2.0 Bar
Focus	Not active	Set Capillary	4500 V	Set Dry Heater	200 °C
Scan Begin	50 m/z	Set End Plate Offset	-500 V	Set Dry Gas	6.0 l/min
Scan End	2500 m/z	Set Collision Cell RF	300.0 Vpp	Set Divert Valve	Waste

Meas. m/z	#	Formula	m/z	err [ppm]	rdb	e^- Conf	N-Rule
594.1711	1	C 34 H 42 Fe 2 S	594.1702	-1.6	14.0	odd	ok

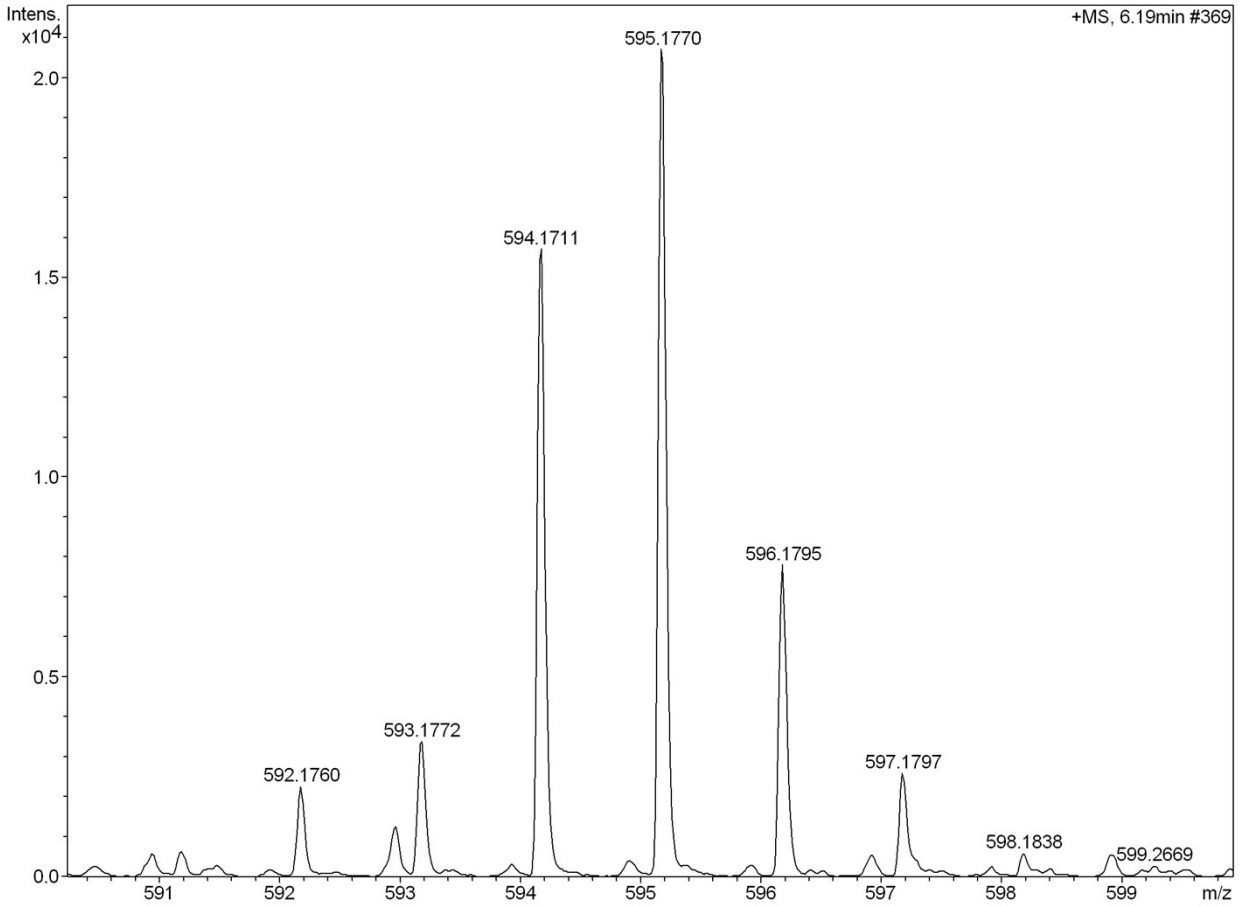

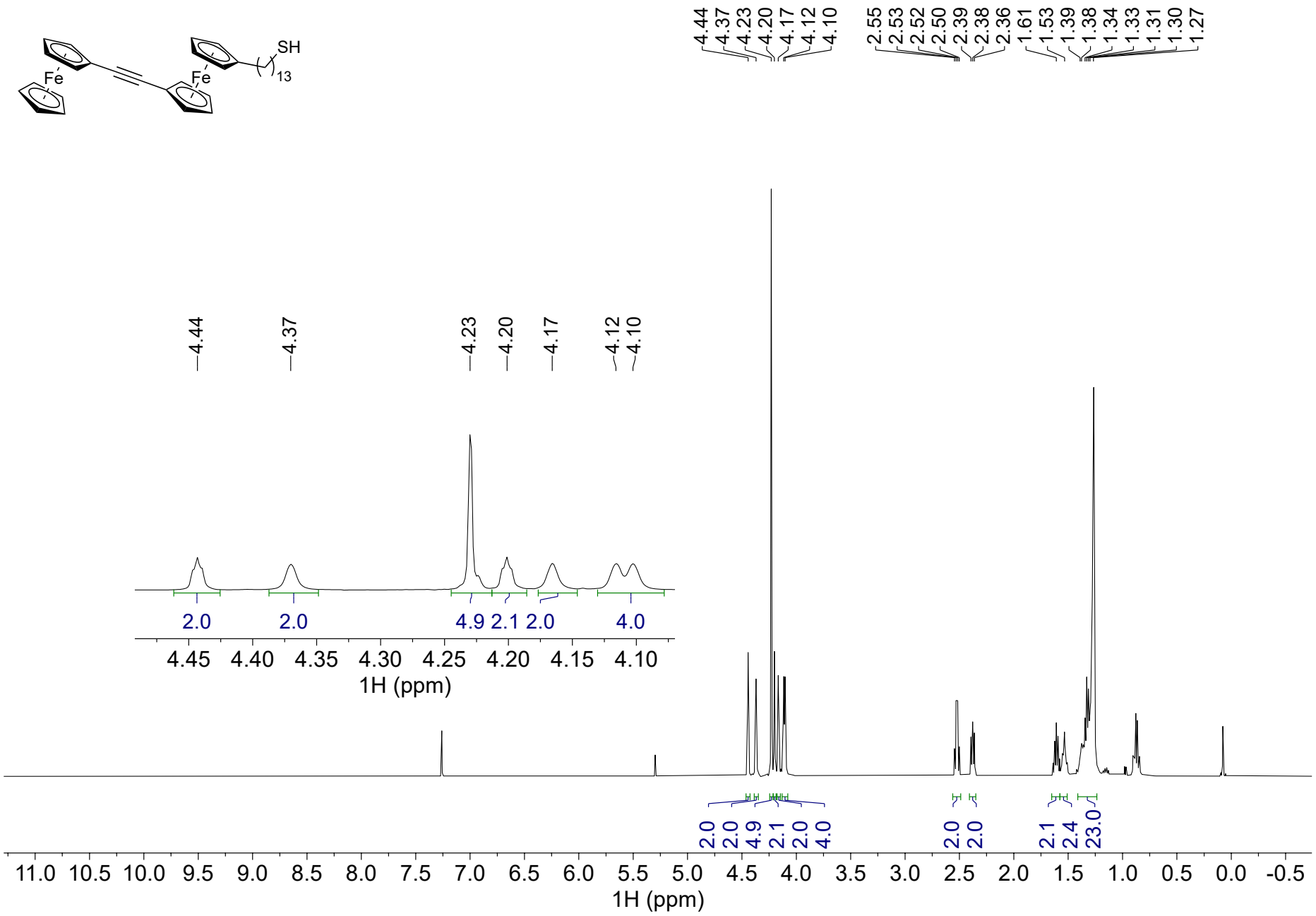
SH
13
Fe
Fe
4.44
4.37
4.23
4.20
4.17
4.12
4.10
2.55
2.53
2.52
2.50
2.39
2.38
2.36
1.61
1.53
1.39
1.38
1.34
1.33
1.31
1.30
1.27
2.0
2.0
4.9
2.1
2.0
4.0
2.0
2.0
2.1
2.4
23.0
11.0 10.5 10.0 9.5 9.0 8.5 8.0 7.5 7.0 6.5 6.0 5.5 5.0 4.5 4.0 3.5 3.0 2.5 2.0 1.5 1.0 0.5 0.0 -0.5
1H (ppm)
4.45 4.40 4.35 4.30 4.25 4.20 4.15 4.10
1H (ppm)

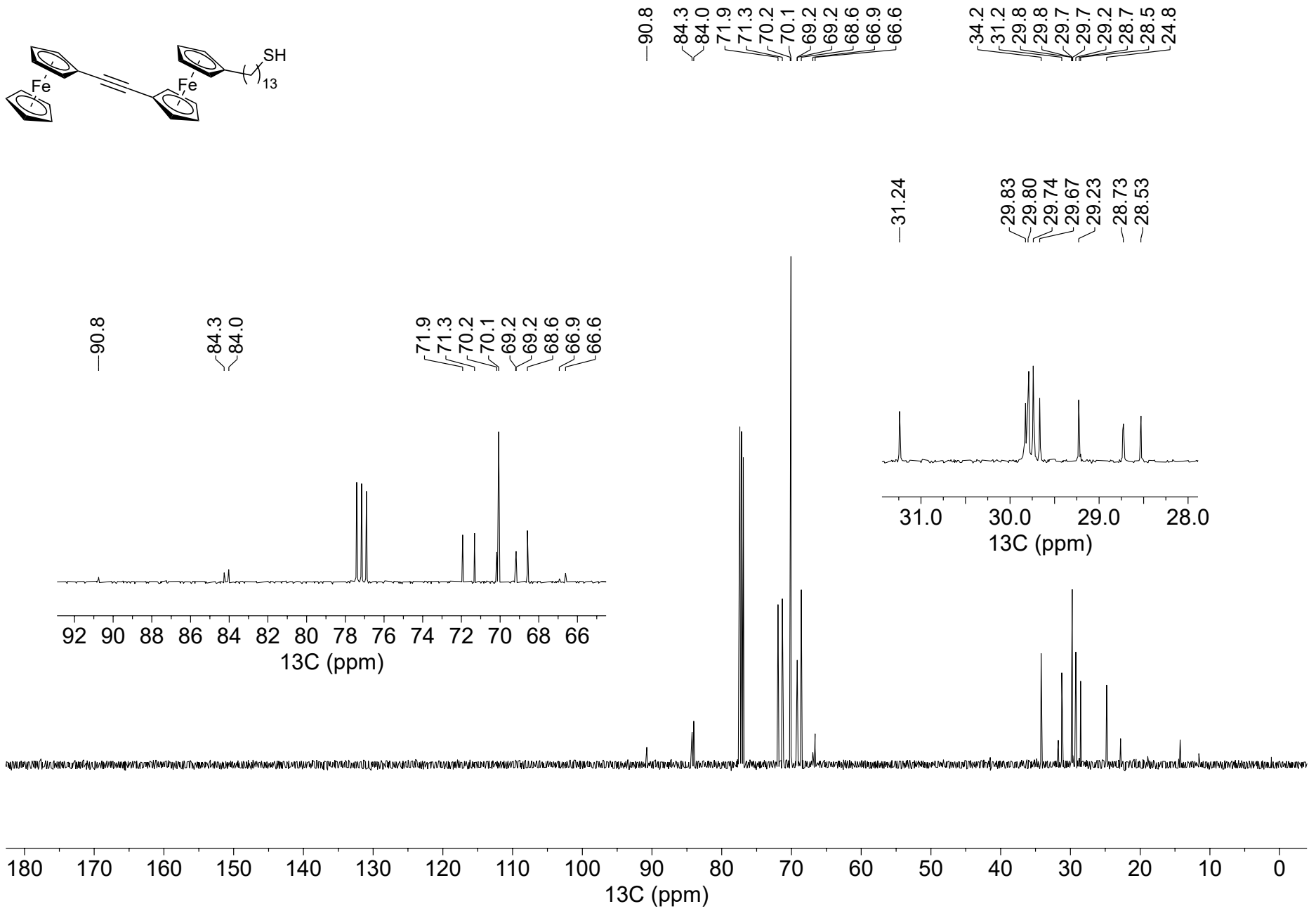
Fe
Fe
SH
13
90.8
84.3
84.0
71.9
71.3
70.2
70.1
69.2
69.2
68.6
66.9
66.6
34.2
31.2
29.8
29.8
29.7
29.7
29.2
28.7
28.5
24.8
31.24
29.83
29.80
29.74
29.67
29.23
28.73
28.53
92 90 88 86 84 82 80 78 76 74 72 70 68 66
13C (ppm)
31.0 30.0 29.0 28.0
13C (ppm)
180 170 160 150 140 130 120 110 100 90 80 70 60 50 40 30 20 10 0
13C (ppm)

Acquisition Parameter

Source Type	ESI	Ion Polarity	Positive	Set Nebulizer	2.0 Bar
Focus	Not active	Set Capillary	4500 V	Set Dry Heater	200 °C
Scan Begin	50 m/z	Set End Plate Offset	-500 V	Set Dry Gas	6.0 l/min
Scan End	1800 m/z	Set Collision Cell RF	200.0 Vpp	Set Divert Valve	Source

Meas. m/z	#	Formula	m/z	err [ppm]	rdb	e⁻ Conf	N-Rule
609.1928	1	C 35 H 45 Fe 2 S	609.1936	1.4	13.5	even	ok

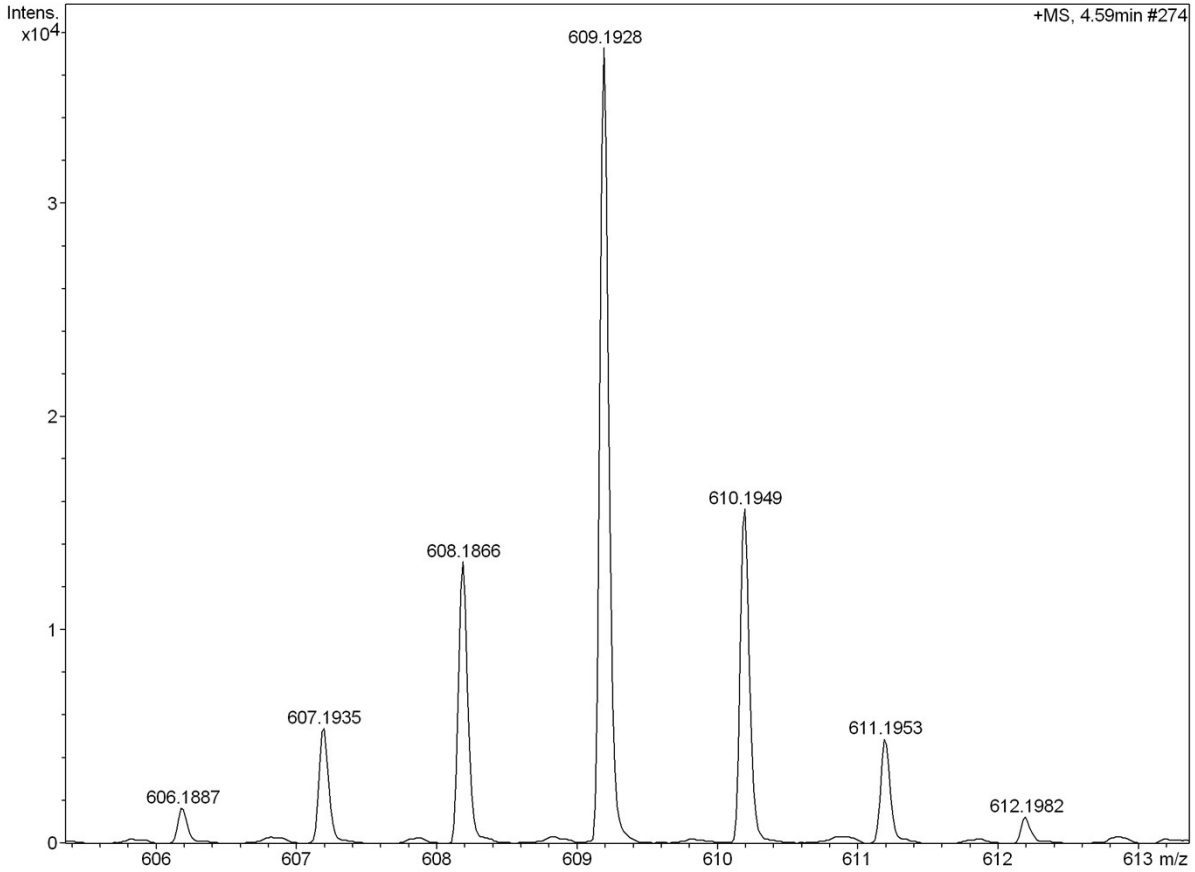

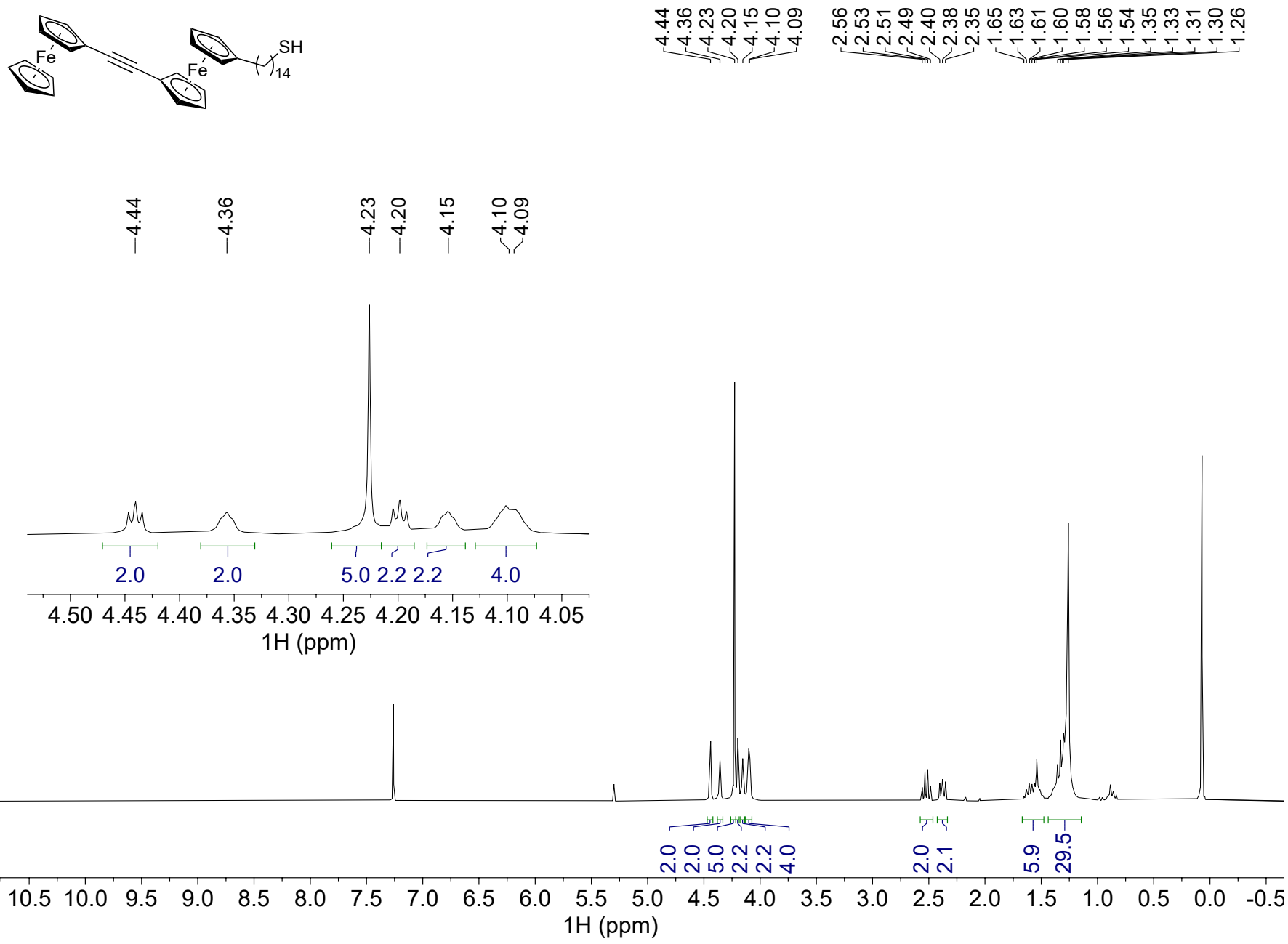
Fe
Fe
SH
14
4.44
4.36
4.23
4.20
4.15
4.10
4.09
2.56
2.53
2.51
2.49
2.40
2.38
2.35
1.65
1.63
1.61
1.60
1.58
1.56
1.54
1.35
1.33
1.31
1.30
1.26
2.0
2.0
5.0
2.2
2.2
4.0
2.0
2.1
5.9
29.5
11.0 10.5 10.0 9.5 9.0 8.5 8.0 7.5 7.0 6.5 6.0 5.5 5.0 4.5 4.0 3.5 3.0 2.5 2.0 1.5 1.0 0.5 0.0 -0.5
1H (ppm)
4.50 4.45 4.40 4.35 4.30 4.25 4.20 4.15 4.10 4.05
1H (ppm)

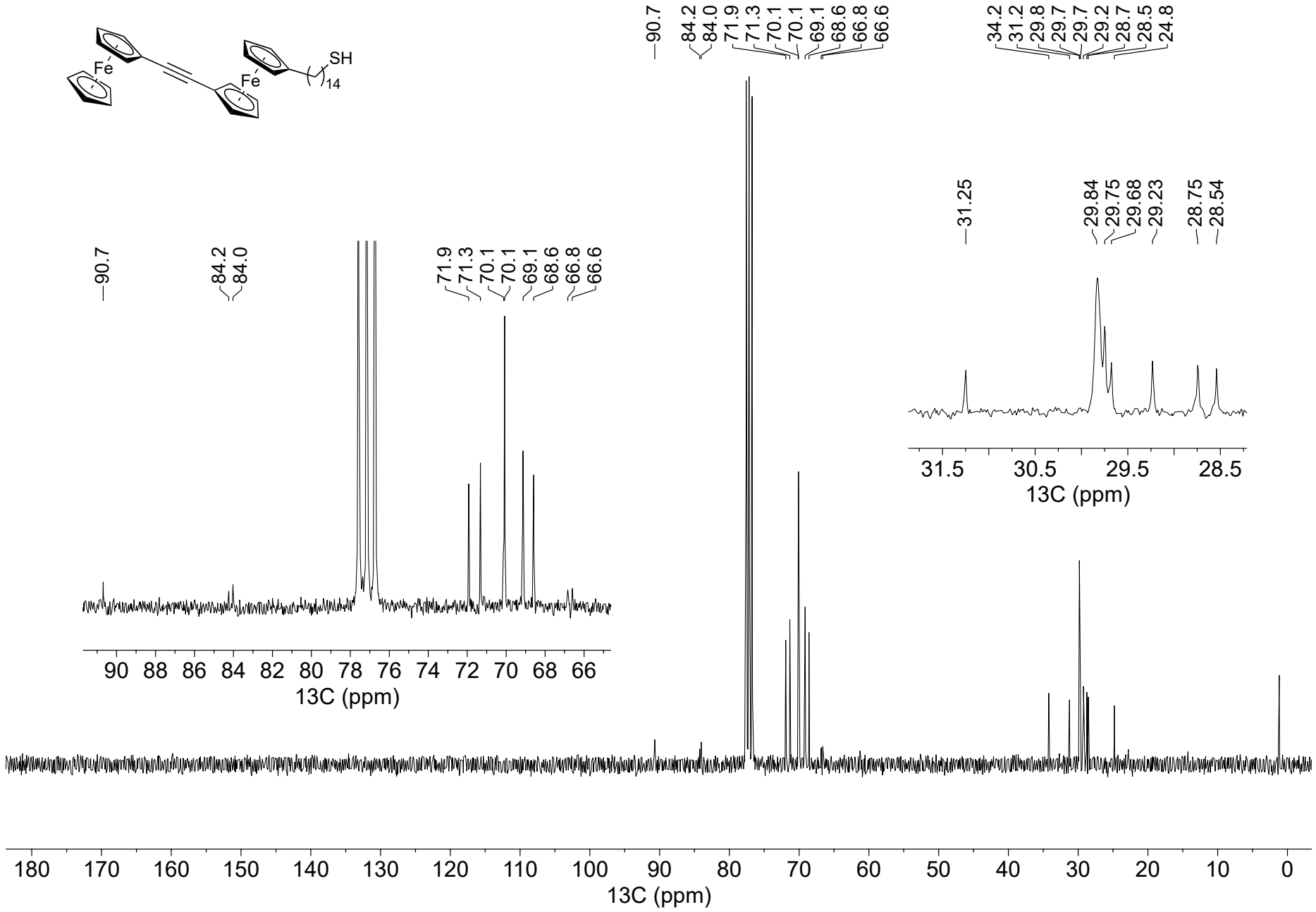
Fe
Fe
SH
14
90.7
84.2
84.0
71.9
71.3
70.1
70.1
69.1
68.6
66.8
66.6
34.2
31.2
29.8
29.7
29.7
29.2
28.7
28.5
24.8
31.25
29.84
29.75
29.68
29.23
28.75
28.54
31.5
30.5
29.5
28.5
13C (ppm)
90 88 86 84 82 80 78 76 74 72 70 68 66
13C (ppm)
180 170 160 150 140 130 120 110 100 90 80 70 60 50 40 30 20 10 0
13C (ppm)

Acquisition Parameter

Source Type	ESI	Ion Polarity	Positive	Set Nebulizer	2.0 Bar
Focus	Not active	Set Capillary	4500 V	Set Dry Heater	200 °C
Scan Begin	50 m/z	Set End Plate Offset	-500 V	Set Dry Gas	6.0 l/min
Scan End	1800 m/z	Set Collision Cell RF	200.0 Vpp	Set Divert Valve	Source

Meas. m/z	#	Formula	m/z	err [ppm]	rdb	e^- Conf	N-Rule
623.2096	1	C 36 H 47 Fe 2 S	623.2093	-0.5	13.5	even	ok

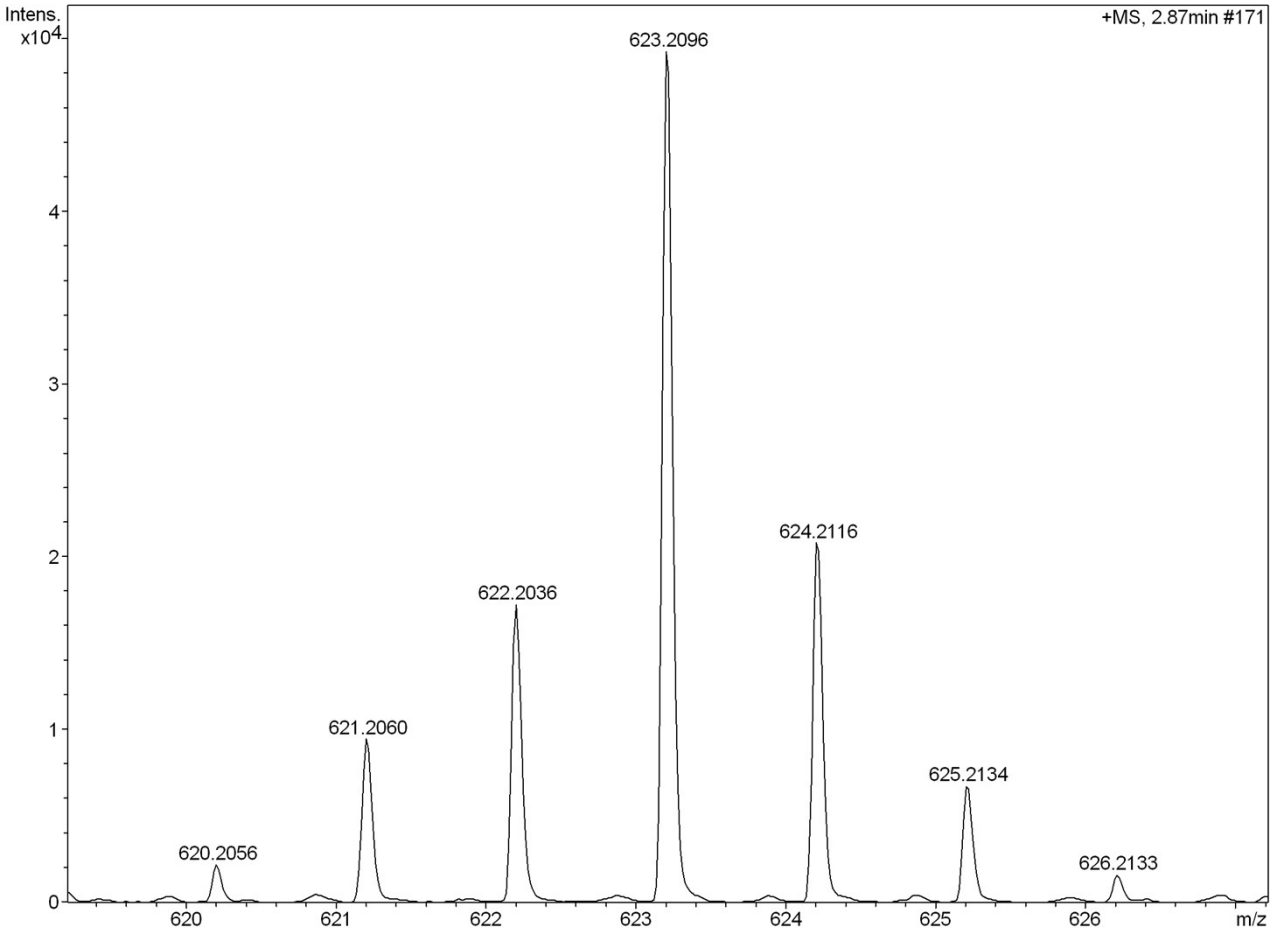

The Odd-even Effect of the Melting Points

The melting points of the SAM precursors $HS(CH_2)_nFc–C\equiv C–Fc$ (n_c = 9 – 15) show an odd-even effect with odd numbered homologues melting at lower temperatures compared to the even numbered homologues (Figure S1).

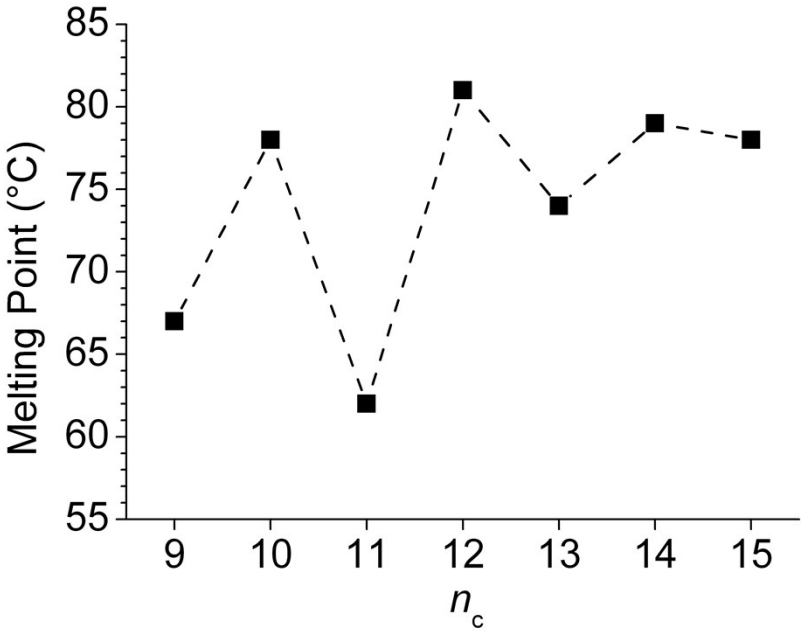

Figure S1. Melting points of the series of molecules $HSC_nFc–C\equiv C–Fc$ (n_c = 9 – 15). The line serves as a guide for the eye only.

3. SAM Formation and Characterisation

The SAM formation for each compound of the $HSC_nFc–C≡C–Fc$ series was conducted according to the procedure we reported previously for the SAMs of $M\text{-}SC_{15}Fc–C≡C–Fc$.[5] Briefly, we first deposited Pt, Ag, and Au metals of 200 nm thickness on clean Si(100) wafers under a high vacuum of ~2×10^{-6} mbar using a thermal evaporator (ShenYang KeYi, China) for Au and Ag, and an electron beam evaporator (Denton Vacuum Explorer, NJ USA) for Pt.

The metal substrates were then prepared by template stripping as described in the following. Glass slides, thoroughly cleaned by piranha solution, were attached to the metal layer using a thermocurable adhesive (EPOTEK 353ND) as adhesion layer, and cured at 80 °C for 16 h. The as-prepared substrates were removed carefully from the wafer directly prior to SAM formation using a scalpel and tweezer. We prepared the SAMs, $M\text{-}SC_nFc–C≡C–Fc$, by immersing template-stripped metal substrates in a binary THF/ethanol solution (1:9; 5 mL; degassed) with 1 mM of precursor $HSC_nFc\text{-}C≡C\text{-}Fc$ for 3h under an atmosphere of N_2. The substrates were then taken out and rinsed thoroughly with first THF and then ethanol, and finally dried under a stream of N_2.

Cyclic Voltammetry

The SAMs on Au and Pt were characterised by cyclic voltammetry. An Autolab PGSTAT302T equipped with NOVA 1.10 software was applied to record the cyclic voltammograms (CVs). The CV curves were recorded using a three-electrode system: Pt as counter electrode, Ag/AgCl as reference electrode, and the SAM on Au or Pt as working electrode. The potential range applied was -0.1-0.9 V at a scan rate of 1.00 V/s. The surface coverages of the SAMs (Γ_{CV}, in mol/cm^2) were calculated using Faraday's equation S1, and the HOMO level (E_{HOMO}, in eV) was calculated using equation S2:

$$\Gamma_{CV} = Q_{tot}/nFA \quad \text{(S1)}$$

$$E_{HOMO} = E_{abs,\,NHE} - e\,E_{1/2,NHE} \quad \text{(S2)}$$

wherein Q_{tot} is the total charge transferred during the reduction or oxidation process, n is the number of electron transfer during reduction or oxidation per mole of reaction (here n = 2), F is the Faraday constant, and A represents surface area of the working electrode (here A = 0.50 cm^2), $E_{abs,\,NHE}$ is the absolute potential energy of the normal hydrogen electrode (-4.5 eV), e is the charge of one electron (1.602×10^{-19} C), and $E_{1/2,NHE}$ is the formal half-wave potential versus normal hydrogen electrode (NHE). We also calibrated the absolute potential of Ag/AgCl vs. NHE, which is +0.197 V. Cyclic voltammograms of Au-SC_nFc–C≡C–Fc and Pt-SC_nFc–C≡C–Fc are shown in Figure S2 and Figure S3, respectively. Summaries of determined surface coverages and electrochemical properties of the SAMs on Au and Pt surfaces are reported in Table S1 and Table S2.

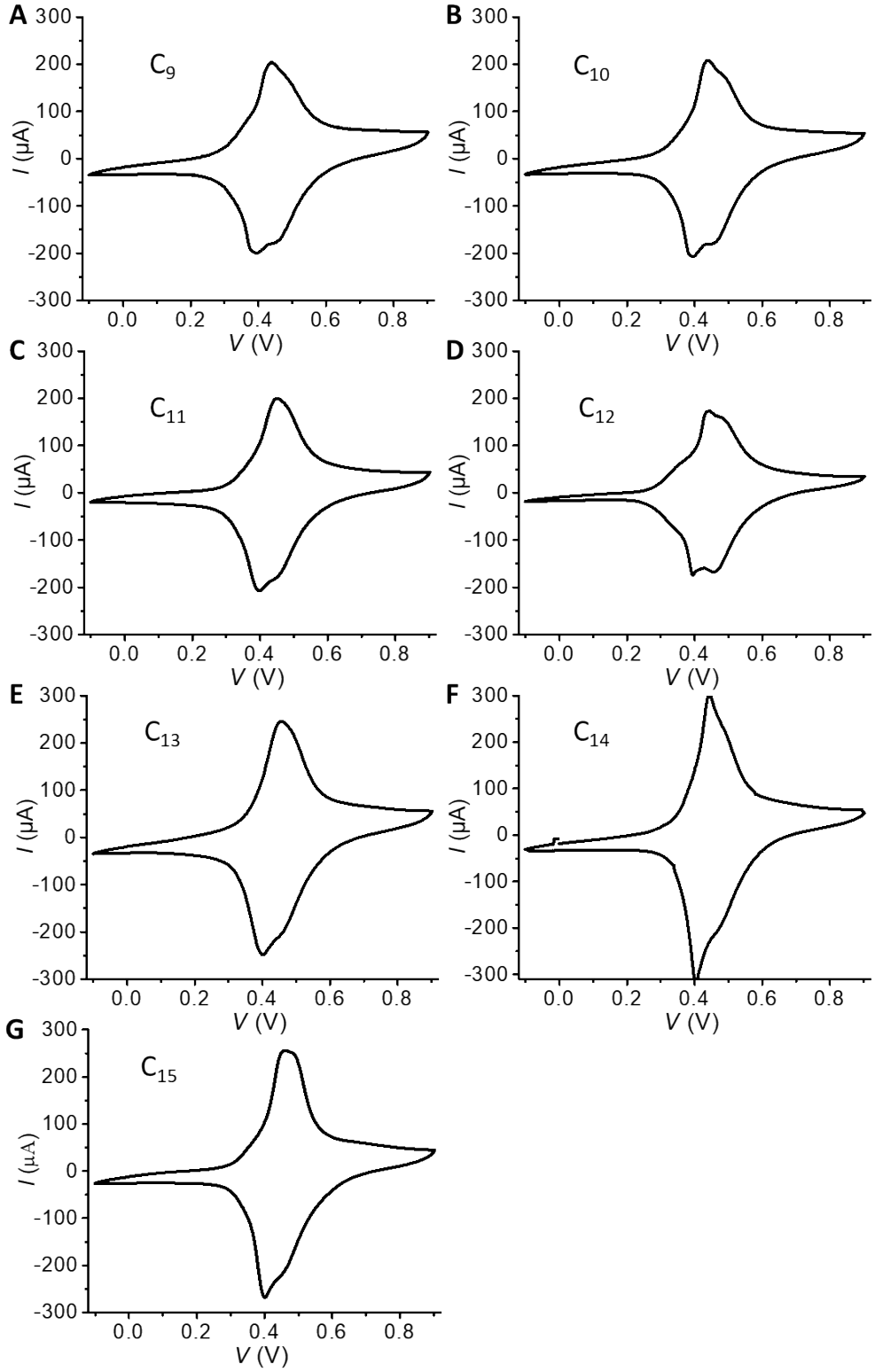

Figure S2. CV curves of Au-SC$_n$Fc–C≡C–Fc. Platinum plate was used as counter electrode, Ag/AgCl as reference electrode and Au as working electrode in 1.0 M $HClO_4$ aqueous solution as electrolyte, the scan rate was 1.00 V/s. The data of panel G was taken from our previous manuscript for the sake of completion.[5]

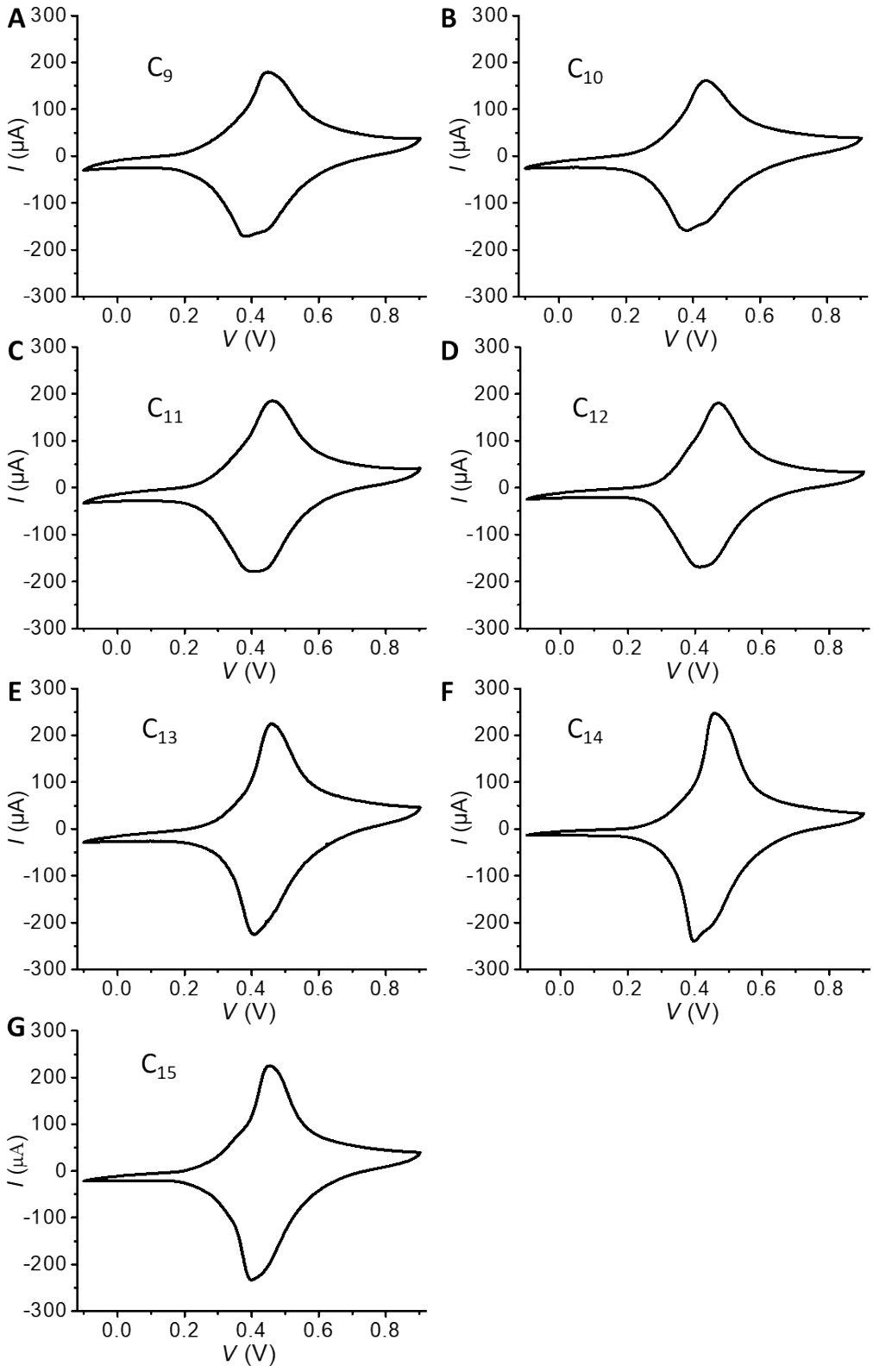

Figure S3. CV curves of Pt-SC$_n$Fc–C≡C–Fc. Platinum plate was used as counter electrode, Ag/AgCl as reference electrode and Au as working electrode in 1.0 M $HClO_4$ aqueous solution as electrolyte, the scan rate was 1.00 V/s. The data of panel G was taken from our previous manuscript for the sake of competion.[5]

Table S1. Details from the SAM characterisation of Au-SC$_n$Fc–C≡C–Fc (n_c = 9–15).[a]

n_c	Γ_{CV} (× 10^{-10} mol/cm^2)	E_{pa} (mV)	E_{pc} (mV)	ΔE_p (mV)	I_{pa}/I_{pc}	FWHM$_{pa}$ (mV)	FWHM$_{pc}$ (mV)	E_{HOMO} (eV)
9	3.14 ± 0.05	441 ± 2	395 ± 1	46 ± 1	0.98±0.01	130±3	162±4	-5.12 ± 0.01
10	3.12 ± 0.09	442 ± 3	397 ± 4	45 ± 1	0.96±0.02	133±5	159±4	-5.12 ± 0.01
11	3.18 ± 0.11	449 ± 2	401 ± 2	49 ± 4	0.95±0.03	130±7	152±3	-5.12 ± 0.01
12	3.08 ± 0.02	452 ± 9	411 ± 6	41 ± 4	0.98±0.09	130±13	154±12	-5.11 ± 0.01
13	3.28 ± 0.06	451 ± 3	402 ± 2	49 ± 2	0.94±0.02	121±1	142±3	-5.12 ± 0.01
14	3.24 ± 0.13	459 ± 5	424 ± 11	35 ± 2	0.94±0.08	145±10	160±12	-5.13 ± 0.01
15	3.40 ± 0.02	458 ± 7	421 ± 8	37 ± 2	1.00±0.02	115±5	141±2	-5.13 ± 0.01

[a]E_{pa} = anodic peak potential; E_{pc} = cathodic peak potential; ΔE_p = difference between anodic and cathodic peak potential, $\Delta E_p = | E_{pa} - E_{pc} |$; E_{HOMO} = the energy of the highest occupied molecular orbital. All data were determined at a scan rate of 1.00 V/s.

Table S2. Details from the SAM characterisation of Pt-SC$_n$Fc–C≡C–Fc (n_c = 9–15).

n_c	Γ_{CV} (× 10^{-10} mol/cm^2)	E_{pa} (mV)	E_{pc} (mV)	ΔE_p (mV)	I_{pa}/I_{pc}	FWHM$_{pa}$ (mV)	FWHM$_{pc}$ (mV)	E_{HOMO} (eV)
9	3.45 ± 0.10	452 ± 4	384 ± 10	68 ± 7	1.08±0.03	169±9	200±8	-5.12 ± 0.01
10	3.26 ± 0.12	447 ± 8	387 ± 4	60 ± 5	1.06±0.01	176±12	199±7	-5.11 ± 0.01
11	3.49 ± 0.10	461 ± 1	399 ± 3	53 ± 2	1.01±0.01	147±28	170±23	-5.13 ± 0.01
12	3.36 ± 0.07	462 ± 13	406 ± 17	56 ± 9	1.01±0.05	149±26	176±23	-5.14 ± 0.01
13	3.57 ± 0.10	457 ± 10	405 ± 11	52 ± 1	1.02±0.03	130±13	150±10	-5.13 ± 0.01
14	3.53 ± 0.10	444 ± 11	393 ± 9	51 ±6	1.03±0.04	120±9	145±6	-5.11 ± 0.01
15	3.61 ± 0.10	453 ± 4	407 ± 7	46 ± 4	1.02±0.02	122±8	142±6	-5.13 ± 0.01

Surface Characterisation by XPS, UPS and NEXAFS

We used synchrotron-based angle-resolved X-ray photoelectron spectroscopy (AR-XPS), ultraviolet photoelectron spectroscopy (UPS), and near edge X-ray absorption fine structure (NEXAFS) spectroscopy to characterise the packing structure and energy levels of the SAMs on metals. The XPS, UPS and NEXAFS were carried out at the SINS (Surface, Interface and Nanostructure Science) beamline of Singapore Synchrotron Light Source (SSLS) in an ultrahigh vacuum (UHV) chamber with a base pressure of 1×10^{-10} mbar.[7, 8] For XPS, we used photon energy of 850 eV for Fe 2*p* and Ag 3*d* orbitals, and 350 eV for C 1*s*, S 2*p*, Au 4*f* , and Pt 3*d* orbitals. A sputter-cleaned Au foil was used to calibrate the photon energy of spectra. Two emission angles (θ, the angle between the emission electrons and the surface, 90° and 40°) were recorded from the AR-XPS. The XPS narrow band scans of M-SC_{14}Fc–C≡C–Fc and M-SC_{13}Fc–C≡C–Fc for the three different metals (M = Ag, Au and Pt) are shown in Figures S4 – S7; Ag 3d, Au 4f, and Pt 3d signals (Figure S4), C1s signals (Figure S5); S2p signals (Figure S6); Fe2p signal (Figure S7).

For UPS measurements, we applied 60 eV to probe the valence band and -10.0 V to overcome the work function of the analyser. The Fermi edges and work function values were calibrated against a reference, clean Au surface (Φ = 5.30 eV). We analysed the data following the previous method.[9] Briefly, the secondary cutoff edge (Φ_{SAM}, in eV) was determined from the intercept between the linear extrapolation of the baseline and the linear extrapolation of the lower kinetic energy; the valance band edges, HOMO onset (δE_{ME}, in eV), was determined using a similar method of taking the intercept between the baseline and the lower binding energy. The secondary cutoff edges and valance band edges are shown in Figure S8.

As for NEXAFS, the spectra were recorded using an Auger electron yield (AEY) mode with a Scienta R4000 electron energy analyzer at incident angles of 90° (NI) and 40°

(GI). The tilt angle (α, in °) of the head group Fc–C≡C–Fc with respect to the surface normal was determined using equation S3 with the liner polarisation factor P of 0.90.

$$\frac{I_{90}}{I_{40}} = \frac{P[sin^2(90°)sin^2(\alpha) + 2cos^2(90°)cos^2(\alpha)] + (1-P)[sin^2(\alpha)]}{P[sin^2(40°)sin^2(\alpha) + 2cos^2(40°)cos^2(\alpha)] + (1-P)[sin^2(\alpha)]} \quad \text{(S3)}$$

The recorded NEXAFS spectra shown in Figure S9. The results of the UPS and NEXAFS measurements are summarised in Table S3.

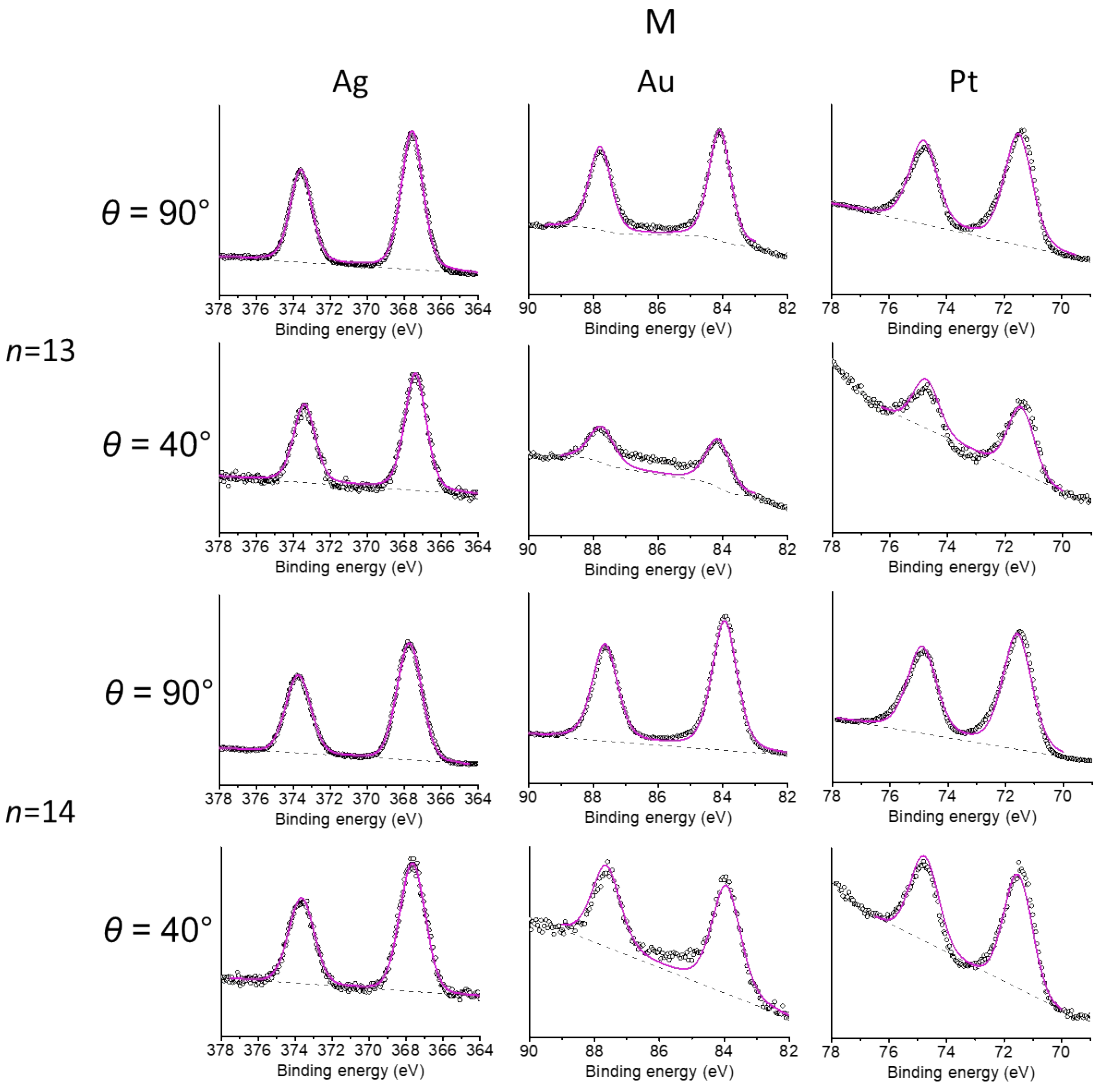

Figure S4. XPS narrow band scans for Ag 3d, Au 4f, and Pt 3d of SAMs of M-SC_{13}Fc–C≡C–Fc and M-SC_{14}Fc–C≡C–Fc.

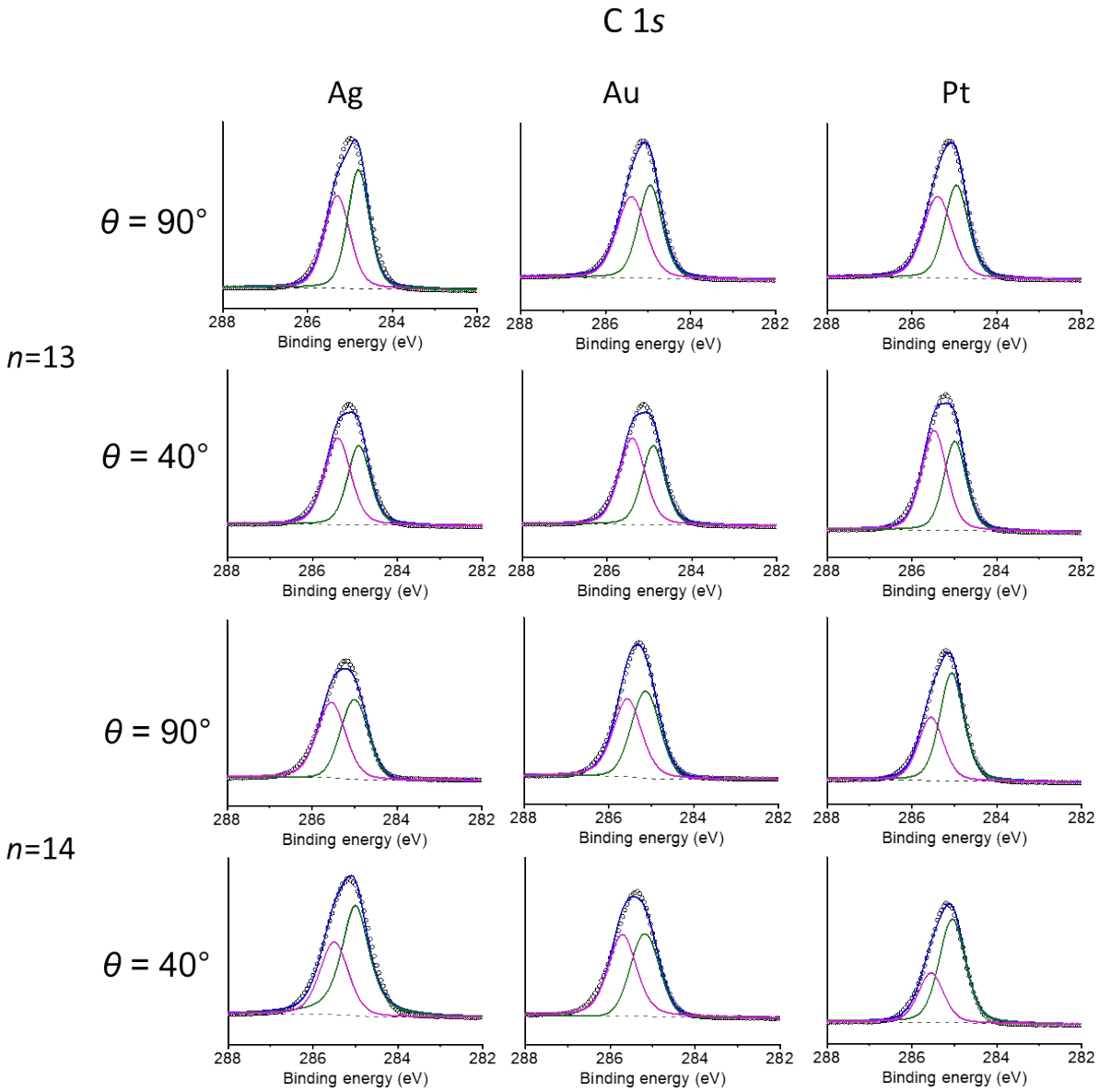

Figure S5. XPS narrow band scans for the C1s signal of SAMs of M-SC_{13}Fc–C≡C–Fc and M-SC_{14}Fc–C≡C–Fc.

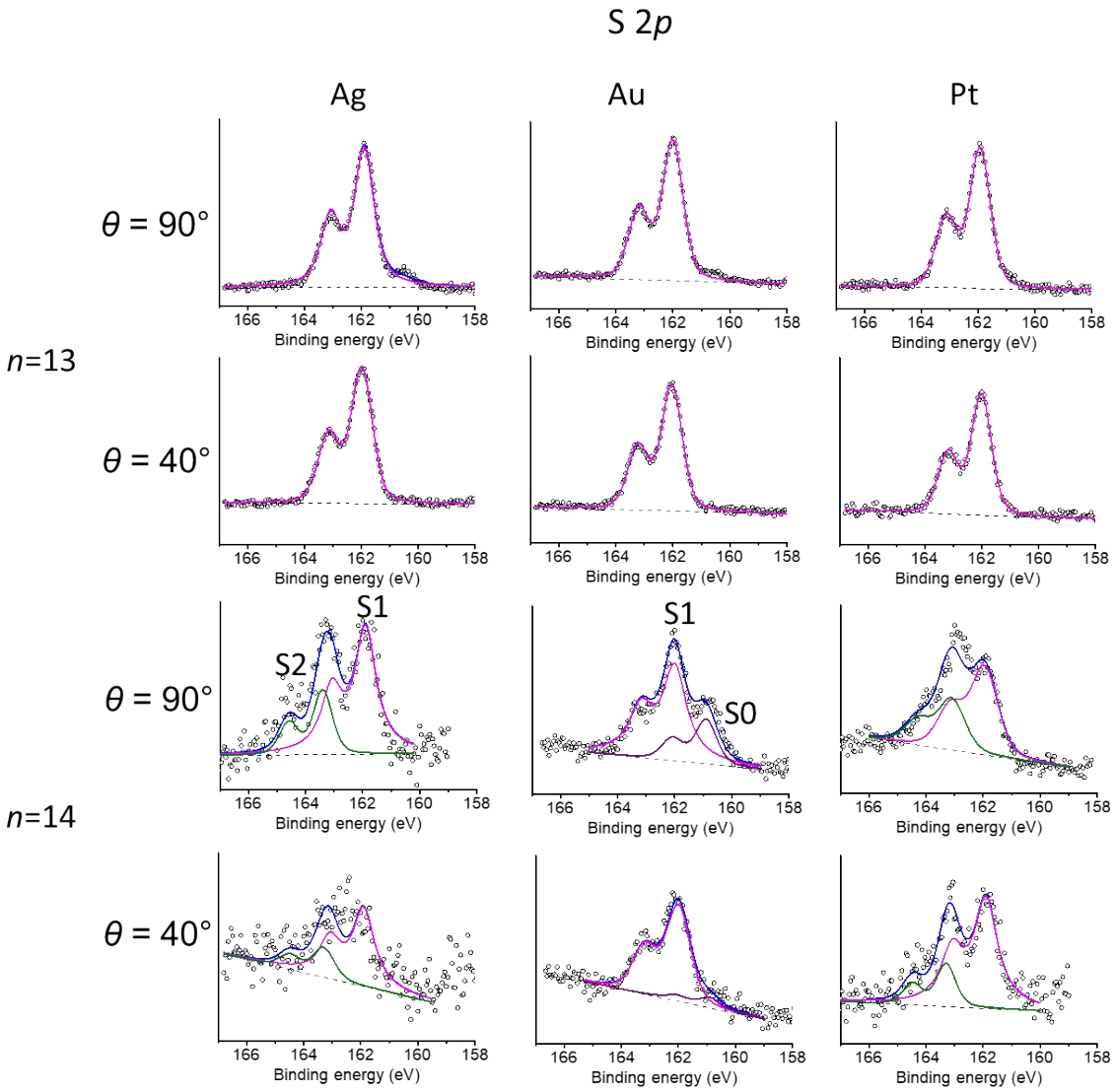

Figure S6. XPS narrow band scans for the S2p signal of SAMs of M-SC_{13}Fc–C≡C–Fc and M-SC_{14}Fc–C≡C–Fc.

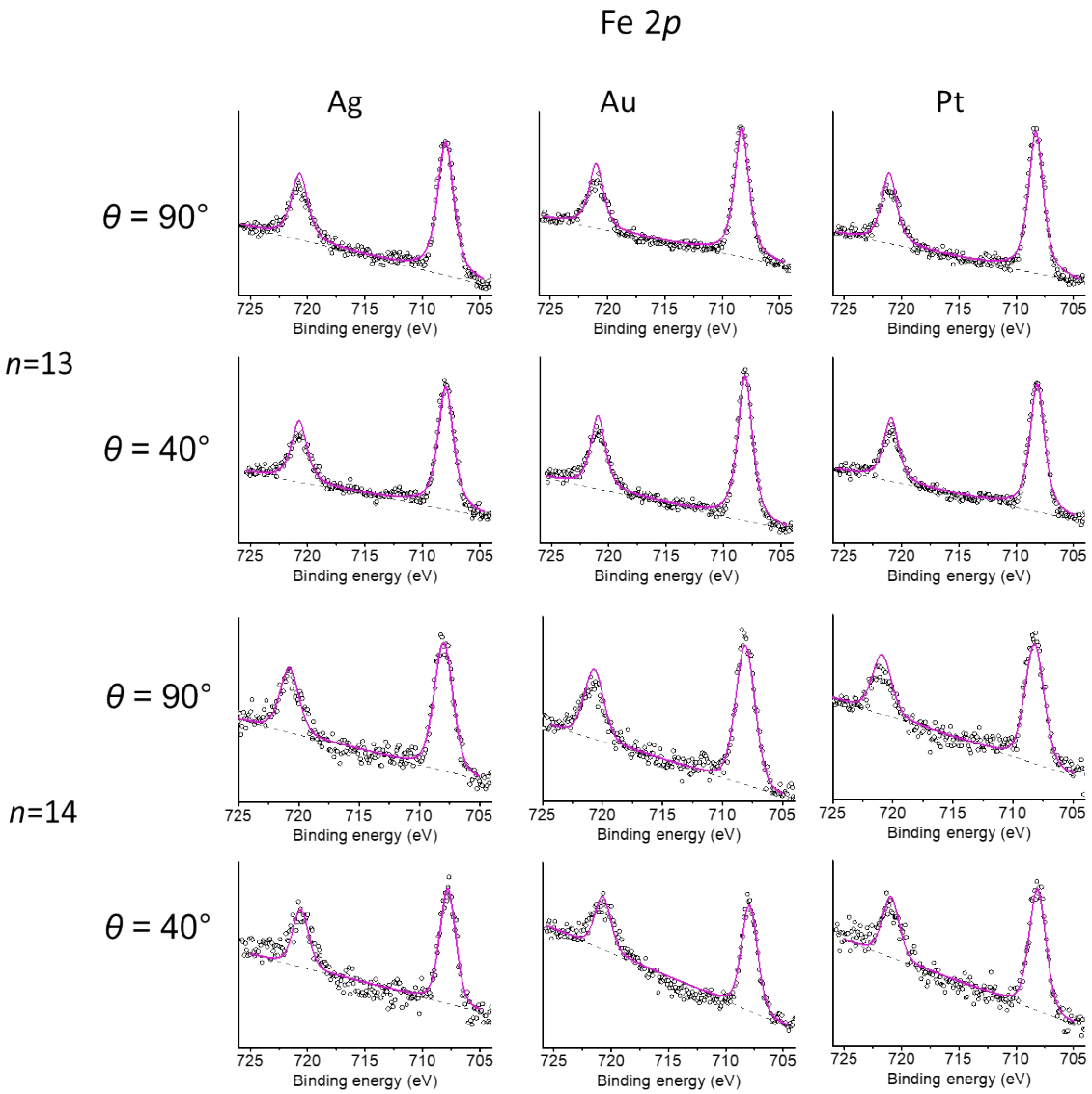

Figure S7. XPS narrow band scans for the Fe2p signal of SAMs of M-SC_{13}Fc–C≡C–Fc and M-SC_{14}Fc–C≡C–Fc.

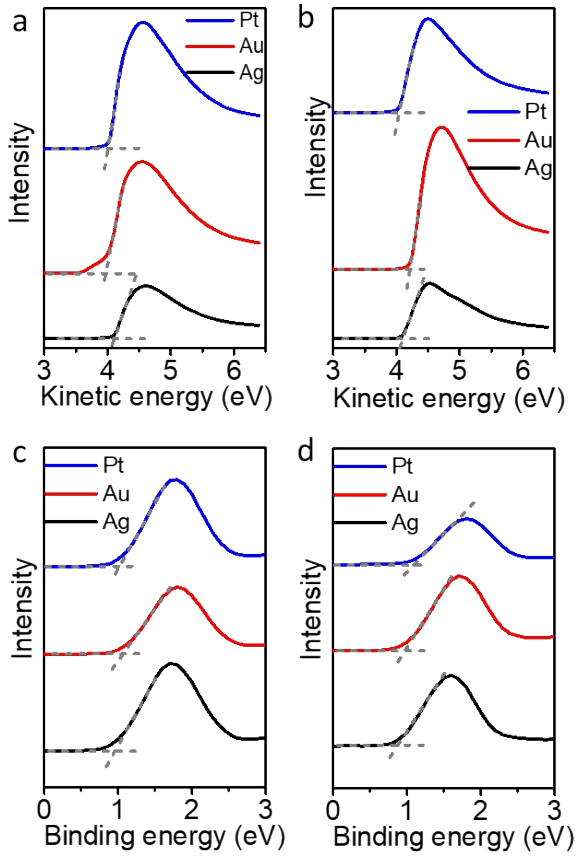

Figure S8. The secondary cutoff edges (a and b) and valance band edges (c and d) of SAMs of M-$SC_{13}Fc–C{\equiv}C–Fc$ and M-$SC_{14}Fc–C{\equiv}C–Fc$, respectively.

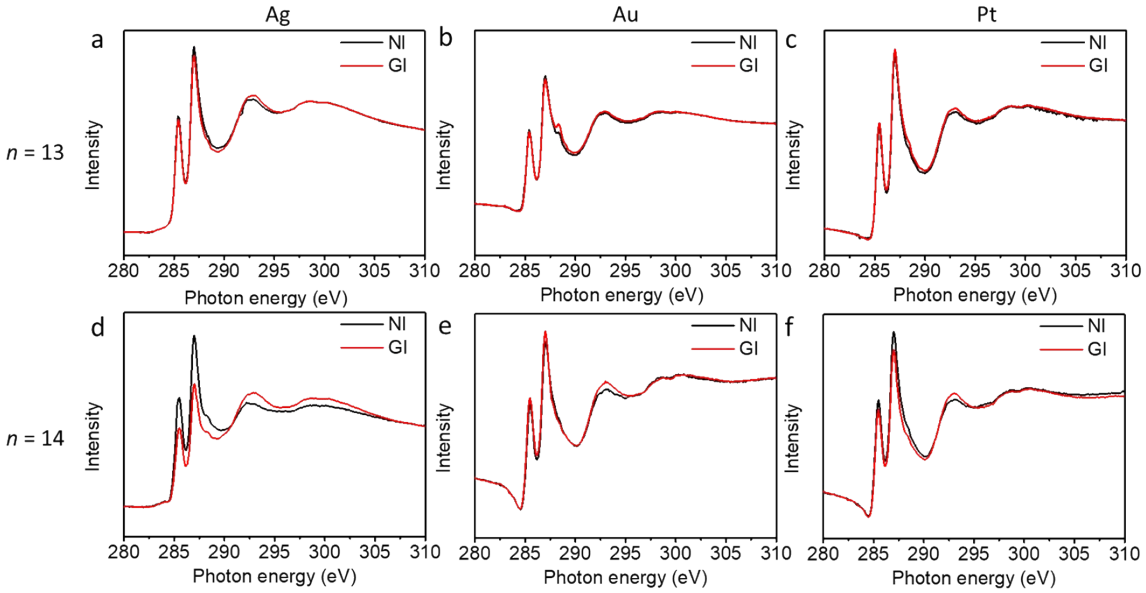

Figure S9. NEXAFS of SAMs of M-$SC_{13}Fc–C{\equiv}C–Fc$ (M = Ag (a), Au (b), Pt (c)) and M-$SC_{14}Fc$-C≡C-Fc (M = Ag (d), Au (e), Pt (f)).

Table S3. Summary of the UPS and NEXAFS results of the SAMs.

SAM	Φ_{SAM} (eV)	HOMO (eV)	δE_{ME} (eV)	α (°)
n_c=13, M=Ag	-4.15	-5.10	0.95	55
n_c=13, M=Au	-4.10	-5.14	1.04	55
n_c=13, M=Pt	-4.05	-5.03	0.98	54
n_c=14, M=Ag	-4.15	-5.04	0.89	63
n_c=14, M=Au	-4.20	-5.18	0.98	54
n_c=14, M=Pt	-4.10	-5.15	1.05	55

4. Molecular Dynamics (MD) Calculations

For each system, a three-layer slab of (111) of metal is used as substrate. For gold and silver, the surface area is 12.69 nm × 12.50 nm and the substrate was placed in a unit cell measuring 12.69 nm × 12.50 nm × 5.2 nm. For platinum, the surface area is 12.21 nm × 12.01 nm and the substrate was placed in a unit cell measuring 12.21 nm × 12.01 nm × 5.2 nm. 324 and 319 molecules are placed in the cell to mimic the estimated experimental surface coverage Γ_{SAM} of Au-SC_{15}-Fc-C≡C-Fc of 3.4×10^{-10} mol/cm^2 and the estimated experimental surface coverage Γ_{SAM} of Pt-SC_{15}-Fc-C≡C-Fc of 3.6×10^{-10} mol/cm^2, respectively. The Fc–C≡C–Fc head groups are parametrised with ParamChem[10, 11], which provides the CHARMM General Force Field (CGenFF)[12] parameters, based on a model we used previously[5, 6, 13]. Metal parameters are the standard parameters available in CHARMM. MD simulations are carried out using the Gromacs 2018.4[14] package with a time step of 2 fs using the Leapfrog integrator[15]. Bond lengths to hydrogen are constrained using the LINCS[16, 17] algorithm. Long-range electrostatics are treated by the Particle mesh Ewald (PME) method[18]. The SAM molecule chains and gold atoms are coupled separately to an external heat bath (300 K) with a coupling time constant of 2 ps using the velocity rescaling method[19]. The system is minimised for 100 ps, and equilibrated for 1 ns in the constant volume NVT ensemble. The production runs are split into two phases. Initially, the chains are not bound to individual metal atoms on the electrode surface but are only constrained to keep their sulphur anchoring groups within bonding distance of the metal surface. This allows the molecules to self-assemble into a uniform film on the surface. This initial physisorption step was carried out for 1 μs, after which each molecule is chemisorbed by bonding its sulphur atom to the closest available metal site. A production phase of 1 μs is then carried out with structures saved every 2 ps. For all the simulations presented here, the metal atoms are constrained to their starting positions. Future models could include local metal substrate restructuring in response to

mechanical or optical perturbation, requiring large-scale electronic structure calculations that are becoming feasible with advances in supercomputing[20-22].

On Pt, α for the odd numbered derivatives (α_{odd}) is on average smaller (ca. 5°) than the even numbered derivatives (α_{even}), confirming that the odd numbered derivatives are less tilted and therefore form more tightly packed SAMs. Interestingly, when comparing these results to the previous work involving SC$_n$Fc SAMs,[23, 24] the α of the Fc–C≡C–Fc is increased by several degrees (3 – 5°) for each member of the series, which may reflect how the second Fc increases the bulkiness of the head group.

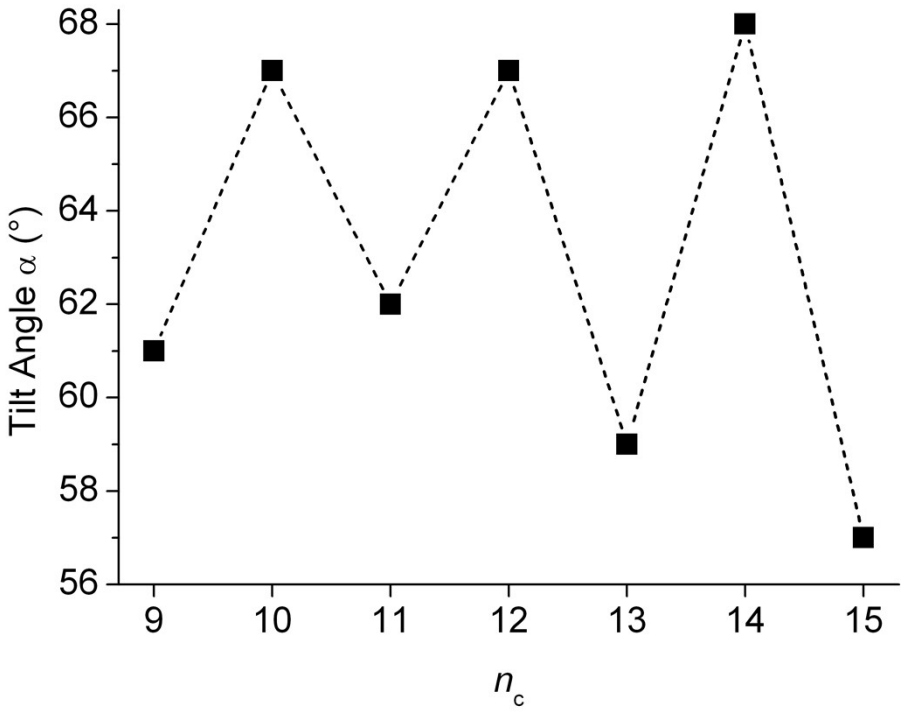

Figure S10. Computed head group tilt angles (α) of the Pt-SC$_n$Fc–C≡C–Fc SAMs.

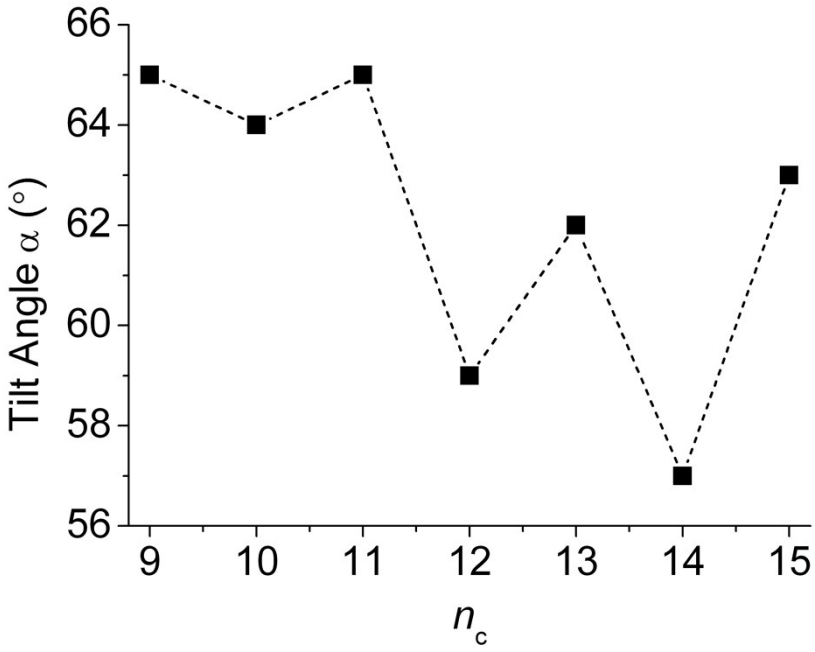

Figure S11. Computed head group tilt angles (α) of the Au-SC$_n$Fc–C≡C–Fc SAMs.

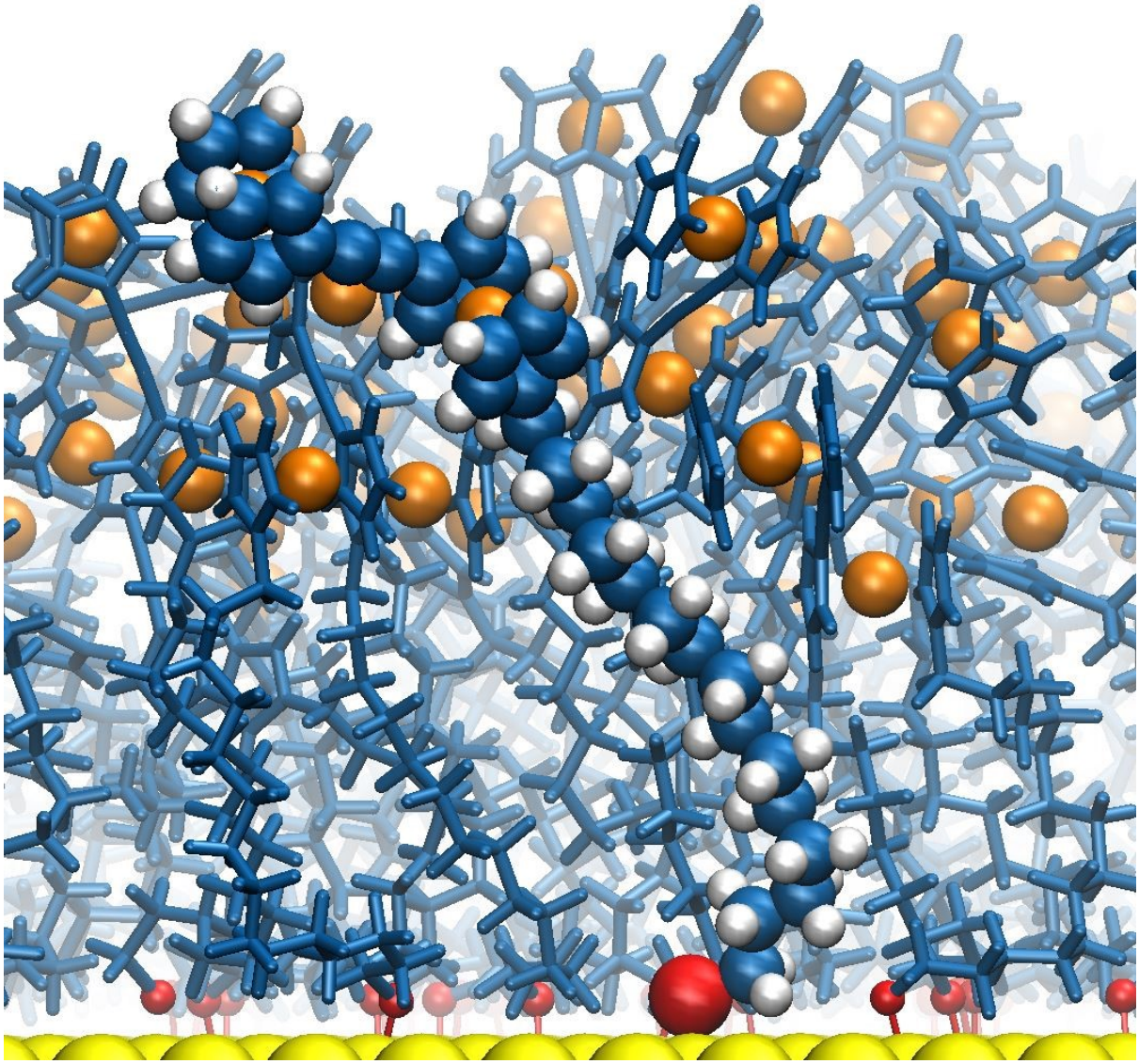

Figure S12. Side-on view of representative SAM supramolecular packing modes following 1 ns of fully equilibrated room temperature molecular dynamics. Gold substrate atoms are yellow, sulphur atoms are red, carbon atoms are blue, hydrogen atoms are white and iron atoms are orange. The modelling unit cell area of 12.7 x 12.5 sq. nm contains 325 molecules matching the experimentally measured surface coverage of 0.34 nmol/cm^2.

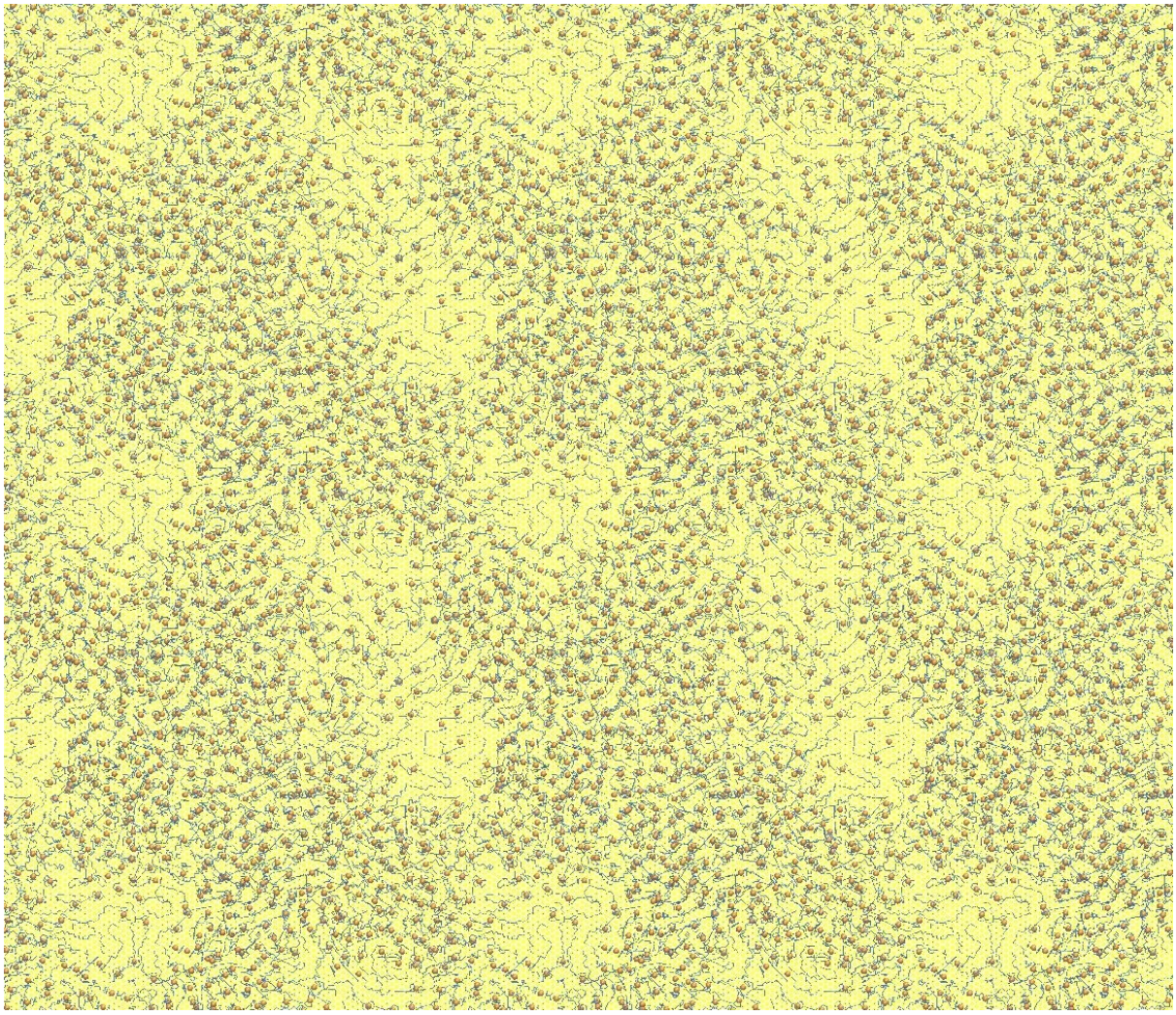

Figure S13. Plan view of the SAM from a large-area 3x3 supercell. The early stage assembly shows clusters of well-packed upright molecules and also some lower density regions with more flat-lying molecules, typical of orientations found at metal grain boundaries or defect features such as step edges and SAM domain boundaries.

5. Electrical Characterisation of the SAMs

The electrical *J*(V) characterisation of the molecular junctions was carried out following the same methodology as described before.[25] A freshly made cone-shaped GaO_x/EGaIn tip served as the top electrode, the SAM substrate served as the bottom electrode. A Keithley 6430 source meter was used to apply voltage to the junction and the LabView 2010 software was used to control the Keithley and to record the data. For each type of molecular junctions, we recorded ~400 *J*(V) curves from ~20 junctions (20 traces *J*(V) traces per junction) following the bias cycle of 0 V → X V → 0 V → -X V → 0 V (X is the maximum applied bias). The obtained *J*(V) data were analysed as follows: we plotted the $\log_{10}|J|$ at each bias V for all the curves and determined the Gaussian log-average values of the current densities, $\langle\log_{10}|J|\rangle_G$, and the Gaussian log-standard deviation $\sigma_{\log,G}$. The same method was used to determine the Gaussian log-average values of the rectification ratio R at ±1.0 V, $\langle\log_{10}R\rangle_G$ and $\sigma_{\log,G}$.

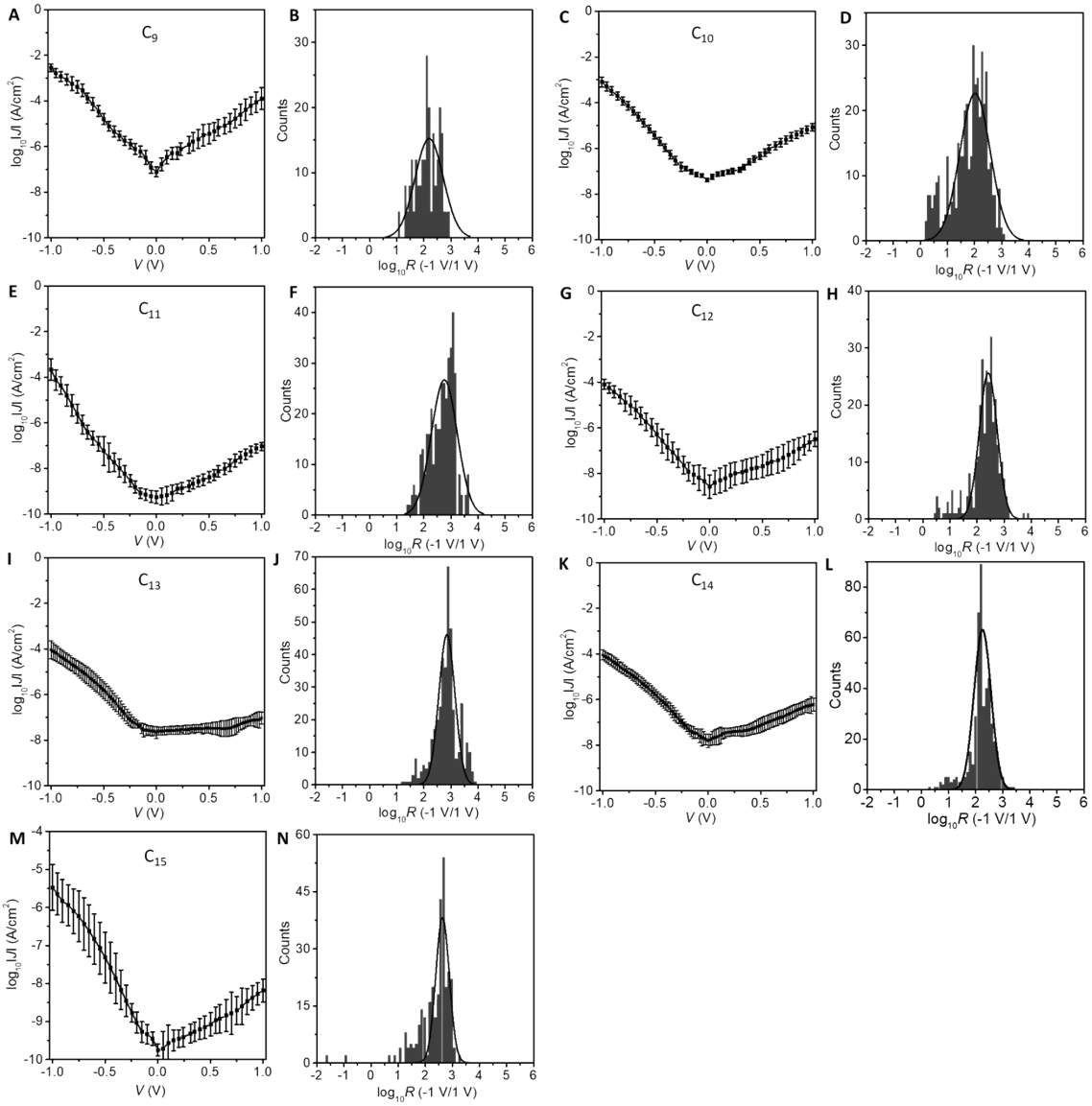

Figure S14. $\langle \log_{10}|J| \rangle_G$ vs V for Ag-SC$_n$Fc–C≡C–Fc//GaO$_x$/EGaIn junctions at ±1.0 V and the corresponding histogram distributions of $\log_{10}R$ with a Gaussian fit (black line) to obtain $\langle \log_{10}R \rangle_G$ and Gaussian log-standard deviations ($\sigma_{\log,G}$). The error bars represent the $\sigma_{\log,G}$ from J(V) analysis. The data of panels M and N was taken from our previous manuscript for the sake of completion.[5]

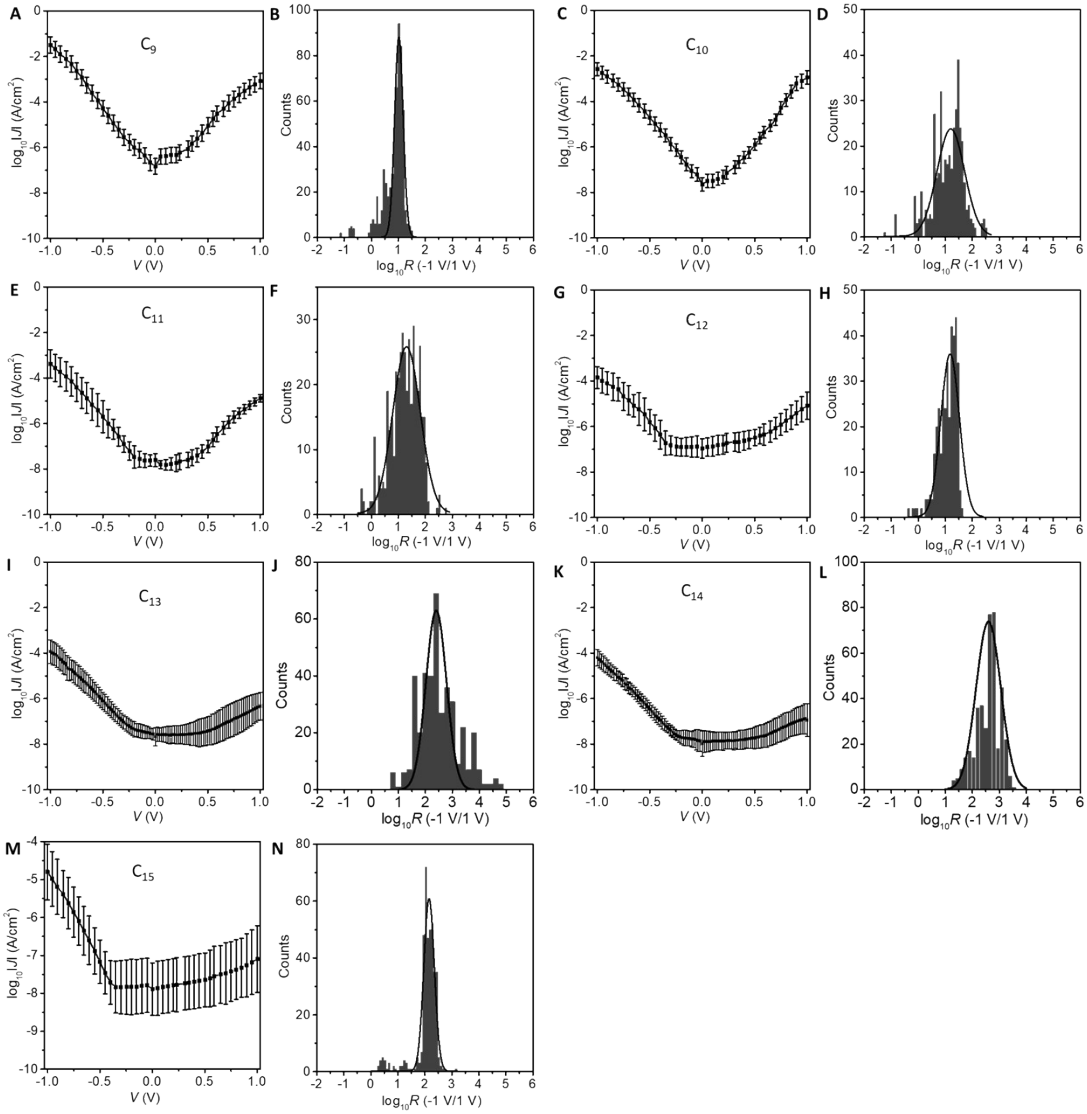

Figure S15. $\langle \log_{10}|J| \rangle_G$ vs V for Au-SC$_n$Fc–C≡C–Fc//GaO$_x$/EGaIn junctions at ±1.0 V and the corresponding histogram distributions of $\log_{10}R$ with a Gaussian fit (black line) to obtain $\langle \log_{10}R \rangle_G$ and Gaussian log-standard deviations ($\sigma_{\log,G}$). The error bars represent the $\sigma_{\log,G}$ from J(V) analysis. The data of panels M and N was taken from our previous manuscript for the sake of completion.[5]

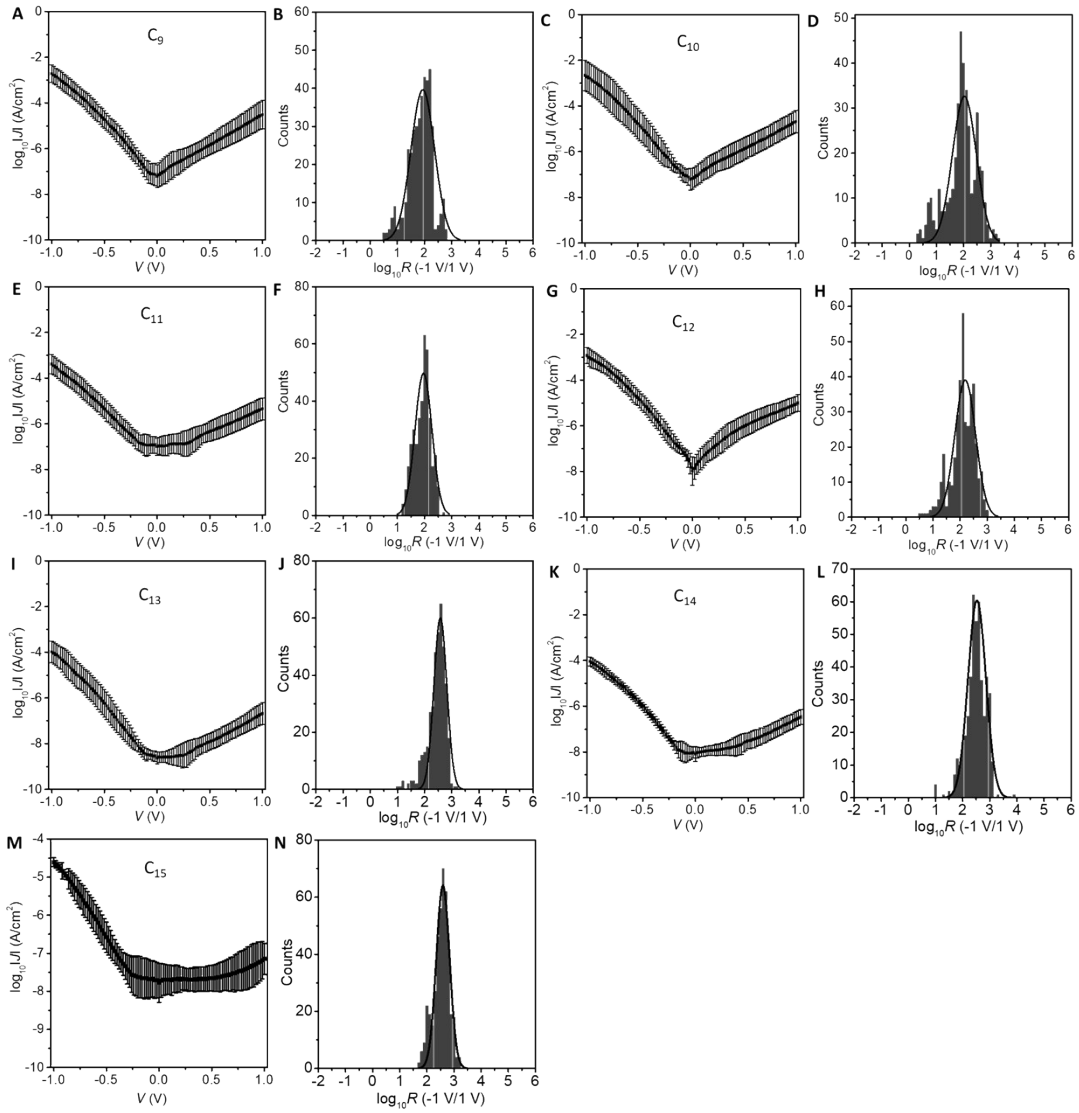

Figure S16. $\langle \log_{10}|J| \rangle_G$ vs V for Pt-SC$_n$Fc–C≡C–Fc//GaO$_x$/EGaIn junctions at ±1.0 V and the corresponding histogram distributions of $\log_{10}R$ with a Gaussian fit (black line) to obtain $\langle \log_{10}R \rangle_G$ and Gaussian log-standard deviations ($\sigma_{\log,G}$). The error bars represent the $\sigma_{\log,G}$ from J(V) analysis. The data of panels M and N was taken from our previous manuscript for the sake of completion.[5]

Table S4. Summary of the measured junctions of Ag-SC$_n$Fc–C≡C–Fc//GaO$_x$/EGaIn at a bias range of ±1.0 V.

n_c	No. of Shorts/Unstable Junctions [a]	No. of Junctions [b]	No. of Traces [c]	Yield (%) [d]	$\langle \log_{10}R \rangle_G$ ($\sigma_{log,G}$)
9	2	17	248	86	2.2 (0.5)
10	5	28	424	78	2.0 (0.6)
11	4	24	397	80	2.8 (0.5)
12	3	19	297	81	2.4 (0.3)
13	4	25	403	81	2.9 (0.3)
14	3	26	457	87	2.6 (0.3)
15[e]	2	19	313	88	3.0 (0.3)

[a] A short junction is defined when the value of *J* overflow the detection limit of our instrument (100 A/cm^2) during recording the *J*(V) scans; an unstable junction is defined when the value of *J* increased suddenly by three orders of magnitude compared to the average *J*.
[b] All the junctions used in one type of measurement.
[c] Number of traces is defined by the total non-shorting traces of the Ag-SC$_n$Fc–C≡C–Fc //GaO$_x$/EGaIn junctions.
[d] Yield of non-shorting junctions is the percentage of non-shorting junctions out of the total number of junctions.
[e] The data is was taken from our previous manuscript.[5]

Table S5. Summary of the measured junctions of Au-SC$_n$Fc–C≡C–Fc//GaO$_x$/EGaIn at a bias range of ±1.0 V.

n_c	No. of Shorts/ Unstable Junctions	No. of Junctions	No. of Traces	Yield (%)	$\langle \log_{10}R \rangle_G$ ($\sigma_{log,G}$)
9	5	32	575	81	1.0 (0.2)
10	3	23	394	85	1.2 (0.5)
11	3	24	422	86	1.3 (0.5)
12	3	22	382	84	1.2 (0.4)
13	3	23	399	85	2.4 (0.4)
14	4	25	411	81	2.6 (0.5)
15	3	23	400	85	2.4 (0.2)

Table S6. Summary of the measured junctions of Pt-SC$_n$Fc–C≡C–Fc//GaO$_x$/EGaIn at a bias range of ±1.0 V.

n_c	No. of Shorts/ Unstable Junctions	No. of Junctions	No. of Traces	Yield (%)	$\langle \log_{10}R \rangle_G$ ($\sigma_{log,G}$)
9	5	25	388	75	1.9 (0.4)
10	4	24	398	80	2.0 (0.4)
11	4	25	411	81	2.0 (0.3)
12	3	23	388	85	2.2 (0.4)
13	4	24	398	80	2.6 (0.2)
14	5	28	454	78	2.5 (0.3)
15	3	24	424	88	2.6 (0.2)

Determination of the Breakdown Voltages

Figure S17 shows the results of the breakdown voltage determination for Pt-SC$_n$Fc–C≡C–Fc //GaO$_x$/EGaIn (n_c = 9, 11, 13, 15).

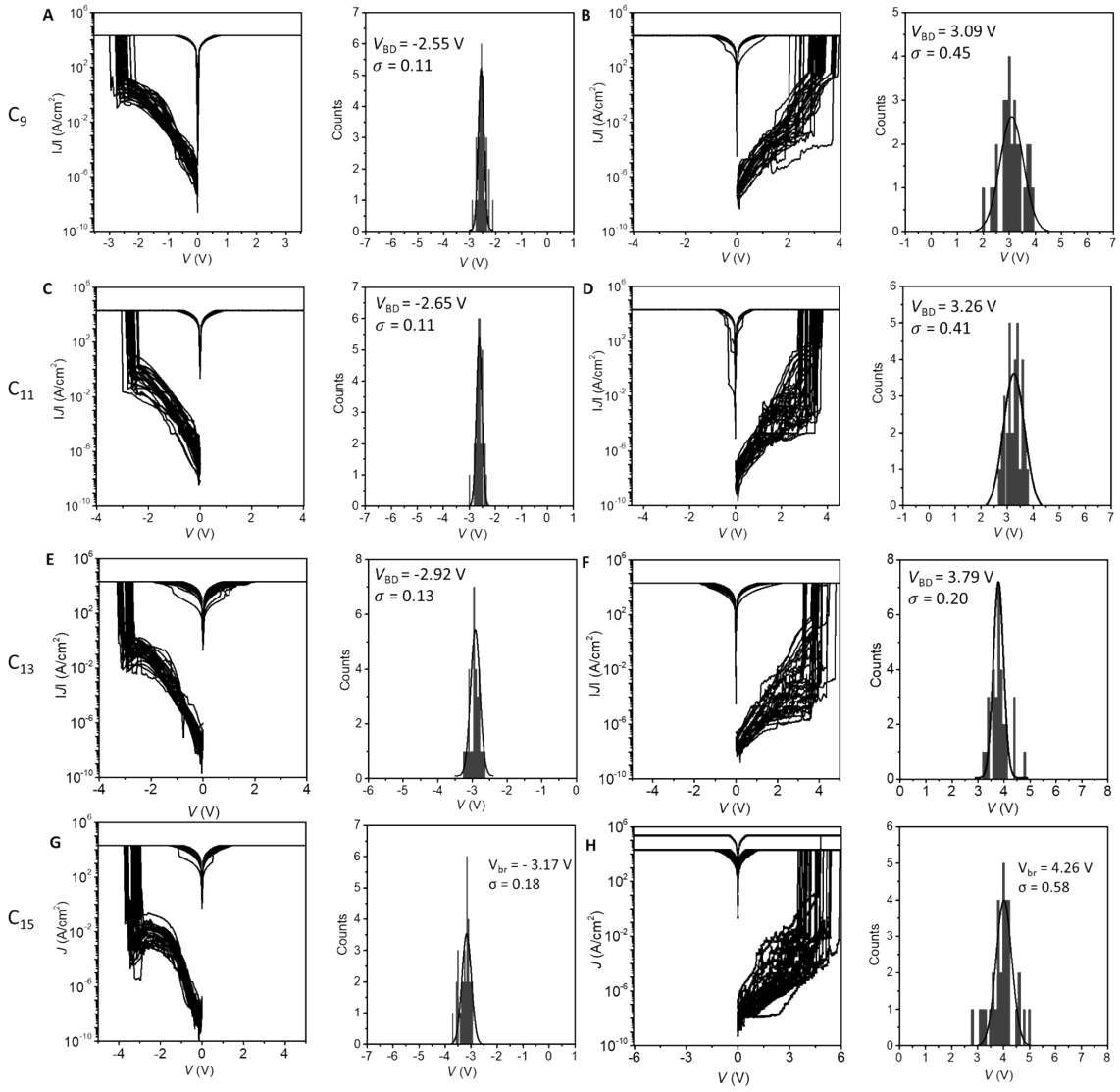

Figure S17. *J*(V) and histograms of the breakdown voltages for junctions of Pt-SC$_9$Fc–C≡C–Fc //GaO$_x$/EGaIn (A, negative bias; B, positive bias), Pt-SC$_{11}$Fc–C≡C–Fc //GaO$_x$/EGaIn (C, negative bias; D, positive bias), Pt-SC$_{13}$Fc–C≡C–Fc//GaO$_x$/EGaIn (E, negative bias; F, positive bias), Pt-SC$_{15}$Fc–C≡C–Fc//GaO$_x$/EGaIn (G, negative bias; H, positive bias). V_{BD} represents the breakdown voltage, σ indicates the standard deviation from the Gaussian fit. The data of panels G and H was taken from our previous manuscript for the sake of completion.[5]

6. Theoretical Modelling

Single Level Tunnelling Model

We model the behavior of the junctions using a theoretical model for the Landauer formalism developed previously.[26] Equation 1 below describes a modified version of the Landauer single-level model that accounts for the multiple junctions present in a SAM junction. Further, a function was used to describe the number of molecules contributing to conduction as a function of the bias voltage. Our previous work showed that at high negative bias voltages, the number of molecules which contribute to conduction increases exponentially.[5]

$$I = \frac{n(V)q}{\hbar}\int_{-\infty}^{\infty} dE dE' D_{E'}(E) G_{\epsilon}\Gamma(E')\left[f_L(E) - f_R(E)\right] \quad \#(Eq.\,1)$$

here, q is the electron charge, and $\hbar$ is the reduced Plank's constant. Γ is the coupling strength between the molecule and electrodes which is dependent on the coupling strength between the left (γ_L) and right (γ_R) electrodes by $\Gamma = \gamma_L\gamma_R/(\gamma_L + \gamma_R)$.

$D_{E'}(E)$ represents the density of states given by a Lorentzian function as shown in equation 2:

$$D_{E'}(E) = \frac{\frac{\gamma_L + \gamma_R}{2\pi}}{\left(E - \left(E' + \left(\eta - \frac{1}{2}\right)V\right)\right)^2 + \left(\frac{\gamma_L + \gamma_R}{2}\right)^2} \quad \#(Eq.2)$$

where V is the bias voltage applied to the junction. The voltage division parameter η accounts for the asymmetry of the junction and the associated voltage drop between the HATNA moiety and the electrodes.

$G_{\epsilon}(E^{'})$ is a Gaussian distribution used to describe the dispersion of the molecular orbital energy of the on and off states in the large-area HATNA molecular tunneling junctions, as shown in equation 3:

$$G_{\epsilon}(E^{'}) = A\ exp\left(\frac{(E^{'} - \varepsilon)^2}{2\sigma^2}\right) \#(Eq.3)$$

where, ε is the zero-bias energy offset of the molecular orbitals with respect to the electrochemical potential of the electrodes, and σ^o represents its energy dispersion (width of the distribution).

$f_{L/R}(E)$ expresses the Fermi occupation distributions for each of the electrodes, which is generated from the thermal broadening of the electrodes and ultimately affects the conductance of the junction, as shown in equation 4:

$$f_{L/R}(E) = \frac{1}{1 + e^{\frac{(E \pm V/2)}{k_B T}}} \#(Eq.4)$$

Finally, the number of molecules contributing to conduction was modeled as an exponential which agrees with previous work. Eq. S5 is the function used.

$$n(V) = e^{-\frac{V_o - V}{s}} + n_0 \#(Eq.4)$$

Here, V_0 represents the voltage at which we start to see an increase in the number of molecules contributing to conduction. s is a shaping parameter which describes the rate of increase and n_0 is the baseline number of molecules contributing to conduction. For this work, n_0 was fixed to be 75.

Fitting of the Data

Figure S18 shows the fitting results for all junctions. We can see that there is strong agreement between the theoretical calculations and the experimental data. For this work, several parameters were held to be constant across the various junctions. For all junctions, the temperature which was experimentally obtained was held at 300 K. The number of molecules contributing to conduction was held at 75 and the width of the gaussian distribution was held at 0.09 eV.

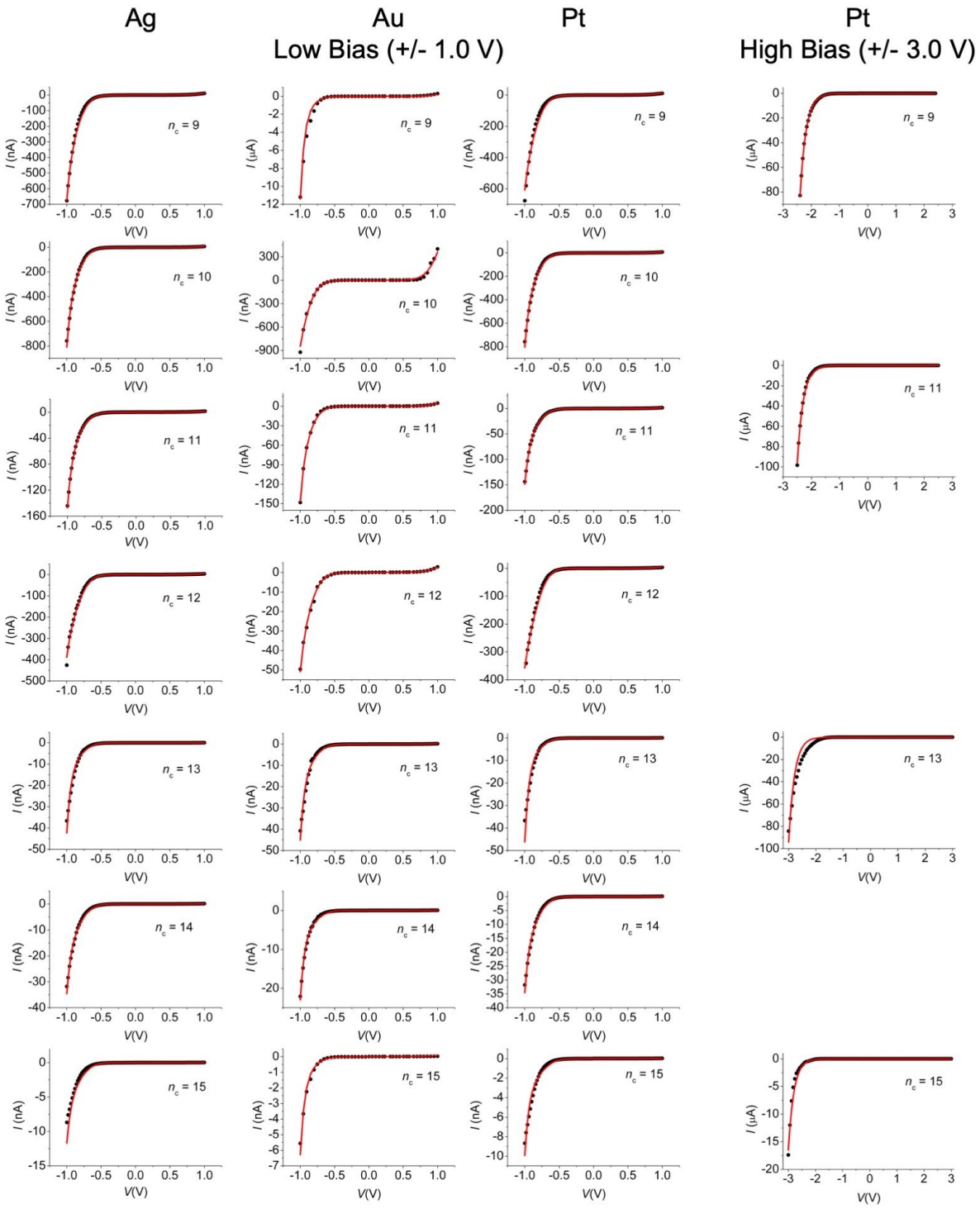

Figure S18. Fits for all studied junctions. The black dots represent the experimental results while the red lines represent the Landauer theoretical fits.

Further, there were a couple of differences between the low voltage and high voltage data. All of the data taken at low voltage had the energy fixed at $\epsilon = 0.55\ eV$ and the high voltage data was fixed at $\epsilon = 0.90\ eV$. Further, we see that the data taken at lower voltages sees an earlier

onset voltage of $V_0 = 0.40\,V$ while the higher voltage data doesn't see contributions from other molecules until $0.6\,V$. Table S7 shows the complete list of all parameters that were not fixed across all junctions.

Table S7. Fitting parameters for all junctions modeled.

	n_c	s (V)	η	Γ (eV)	ϵ (eV)	V_0(V)
Ag Substrate Fig S18, Au	9	0.088	0.64	2.2×10^{-5}	0.55	-0.6
	10	0.083	0.65	2.0×10^{-5}		
	11	0.079	0.66	3.3×10^{-6}		
	12	0.096	0.66	1.4×10^{-5}		
	13	0.068	0.71	4.8×10^{-7}		
	14	0.078	0.70	6.4×10^{-7}		
	15	0.078	0.70	2.1×10^{-7}		
Au Substrate Fig S18, Ag	9	0.069	0.60	1.7×10^{-4}		
	10	0.15	0.53	9.2×10^{-5}		
	11	0.084	0.61	4.6×10^{-6}		
	12	0.099	0.61	2.2×10^{-6}		
	13	0.071	0.69	6.4×10^{-7}		
	14	0.068	0.71	2.7×10^{-7}		
	15	0.070	0.64	8.7×10^{-8}		
Pt Substrate Fig S18, Pt	9	0.099	0.64	2.4×10^{-5}		
	10	0.081	0.65	2.0×10^{-5}		
	11	0.078	0.66	3.3×10^{-6}		
	12	0.11	0.66	1.5×10^{-5}		
	13	0.067	0.71	4.2×10^{-7}		
	14	0.076	0.70	6.4×10^{-7}		
	15	0.070	0.75	1.3×10^{-7}		
Pt Substrate (high bias) Fig S18, hPt	9	0.21	0.65	2.5×10^{-5}	0.9	-0.4
	11	0.21	0.62	1.8×10^{-5}		
	13	0.22	0.75	2.2×10^{-6}		
	15	0.21	0.75	2.1×10^{-7}		

Discussion of the Fits

$We\ can$ see from Table S7 that essentially three parameters were allowed to vary while fitting; the shape parameter, s, which determines the rate of increase in the number of molecules across the junction,η which describes the asymmetry of the junction and the coupling parameter Γ which describes the coupling between the molecule and the electrodes. Essentially two parameters were used to describe the increase in molecular junctions, V_0 and s. With V_0 fixed, s was allowed to vary as each junction understandably will have some variation. The parameter η, increased as the molecular length increased, as shown in Fig S19b. This increase was seen

across all junctions and has been shown in previous works where the molecular structure had been systematically varied.[27] The coupling with the electrodes also changed as a function of molecular length, this shows that as the active elements of the molecular species are further isolated from the electrodes, the coupling and therefore conduction through the molecule decreases. This agrees with findings of Baranger et al. who studied an asymmetric metal-molecule-metal junction consisting of an asymmetrical cobaltocene rectifier bearing a four carbon atom alkyl chain,[28] and Kornilovitch et al. who investigated the charge transport through asymmetrical aryl based rectifiers bearing two alkyl chains of varying length.[29]

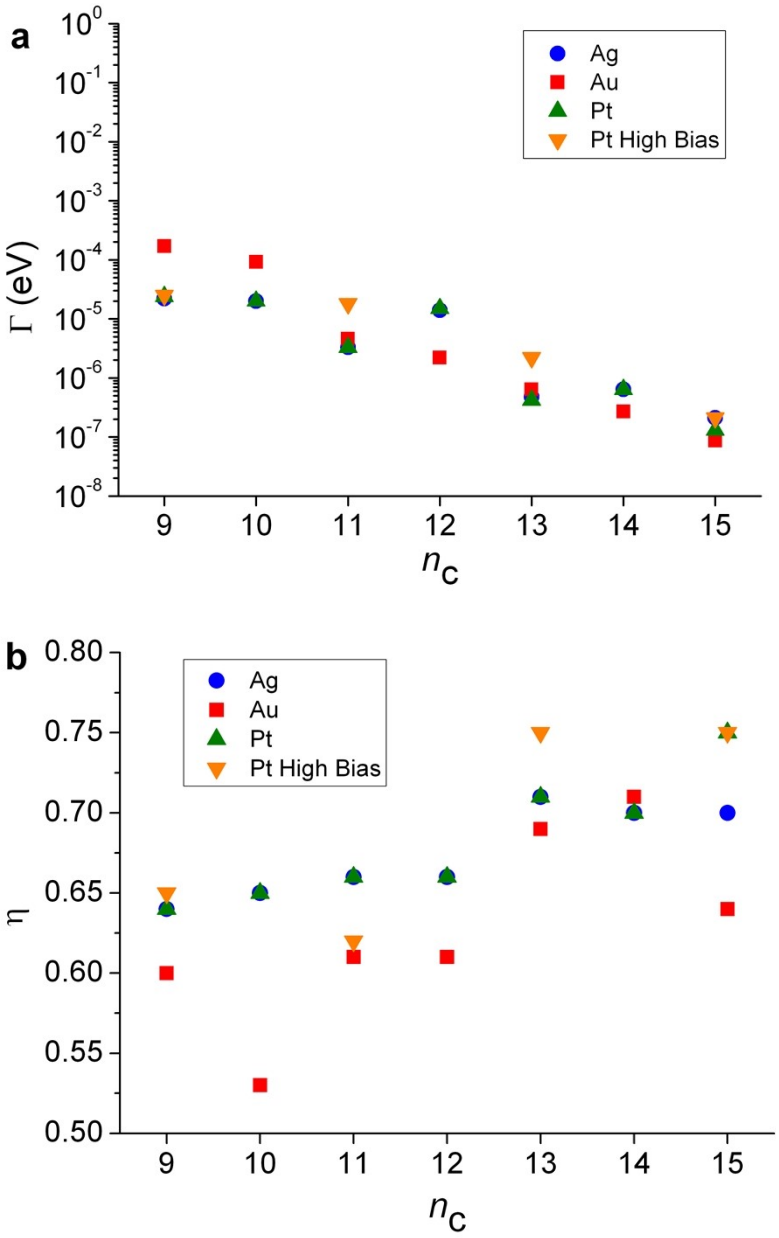

Figure S19. (a) Shows the coupling parameter (Γ) as a function of the length of the molecular chain. We can see that as the length increase, the coupling between the molecule and the electrodes decreases. (b) Shows the asymmetry of the junction described by, η. As the molecular length increases, we also see an increase in the asymmetry of the conduction through the molecular junction.

6. References

1. M. Roemer and C. A. Nijhuis, *Dalton Trans.*, 2014, **43**, 11815-11818.
2. M. Roemer, Y. K. Kang, Y. K. Chung and D. Lentz, *Chem. Eur. J.*, 2012, **18**, 3371-3389.
3. M. Roemer, B. Donnadieu and C. A. Nijhuis, *Eur. J. Inorg. Chem.*, 2016, 1314-1318.
4. G. R. Fulmer, A. J. M. Miller, N. H. Sherden, H. E. Gottlieb, A. Nudelman, B. M. Stoltz, J. E. Bercaw and K. I. Goldberg, *Organometallics*, 2010, **29**, 2176-2179.
5. X. Chen, M. Roemer, L. Yuan, W. Du, D. Thompson, E. del Barco and C. A. Nijhuis, *Nat. Nanotechnol.*, 2017, **12**, 797-803.
6. N. Nerngchamnong, L. Yuan, D. C. Qi, J. Li, D. Thompson and C. A. Nijhuis, *Nat. Nanotechnol.*, 2013, **8**, 113-118.
7. L. Yuan, R. Breuer, L. Jiang, M. Schmittel and C. A. Nijhuis, *Nano Lett.*, 2015, **15**, 5506-5512.
8. X. Yu, O. Wilhelmi, H. O. Moser, S. V. Vidyaraj, X. Gao, A. T. S. Wee, T. Nyunt, H. Qian and H. Zheng, *J. Electron Spectrosc. Relat. Phenom.*, 2005, **144-147**, 1031-1034.
9. Y. Qi, O. Yaffe, E. Tirosh, A. Vilan, D. Cahen and A. Kahn, *Chem. Phys. Lett.*, 2011, **511**, 344-347.
10. K. Vanommeslaeghe and A. D. MacKerell, *J. Chem. Inf. Model.*, 2012, **52**, 3144-3154.
11. K. Vanommeslaeghe, E. P. Raman and A. D. MacKerell, *J. Chem. Inf. Model.*, 2012, **52**, 3155-3168.
12. K. Vanommeslaeghe, E. Hatcher, C. Acharya, S. Kundu, S. Zhong, J. Shim, E. Darian, O. Guvench, P. Lopes, I. Vorobyov and A. D. MacKerell, *J. Comput. Chem.*, 2010, **31**, 671-690.
13. N. Nerngchamnong, D. Thompson, L. Cao, L. Yuan, L. Jiang, M. Roemer and C. A. Nijhuis, *J. Phys. Chem. C*, 2015, **119**, 21978-21991.

14. D. Van der Spoel, E. Lindahl, B. Hess, G. Groenhof, A. E. Mark and H. J. C. Berendsen, *J. Comput. Chem.*, 2005, **26**, 1701-1718.

15. R. W. Hockney, S. P. Goel and J. W. Eastwood, *J. Comput. Phys.*, 1974, **14**, 148-158.

16. B. Hess, *J. Chem. Theory Comput.*, 2008, **4**, 116-122.

17. B. Hess, H. Bekker, H. J. C. Berendsen and J. Fraaije, *J. Comput. Chem.*, 1997, **18**, 1463-1472.

18. T. Darden, D. York and L. Pedersen, *J. Chem. Phys.*, 1993, **98**, 10089-10092.

19. G. Bussi, D. Donadio and M. Parrinello, *J. Chem. Phys.*, 2007, **126**.

20. D. Thompson, J. Liao, M. Nolan, A. J. Quinn, C. A. Nijhuis, C. O'Dwyer, P. N. Nirmalraj, C. Schönenberger and M. Calame, *J. Phys. Chem. C*, 2015, **119**, 19438-19451.

21. J. Griffiths, T. Földes, B. de Nijs, R. Chikkaraddy, D. Wright, W. M. Deacon, D. Berta, C. Readman, D.-B. Grys, E. Rosta and J. J. Baumberg, *Nat. Commun.*, 2021, **12**, 6759.

22. C. Carnegie, M. Urbieta, R. Chikkaraddy, B. de Nijs, J. Griffiths, W. M. Deacon, M. Kamp, N. Zabala, J. Aizpurua and J. J. Baumberg, *Nat. Commun.*, 2020, **11**, 682.

23. N. Nerngchamnong, L. Yuan, D.-C. Qi, J. Li, D. Thompson and C. A. Nijhuis, *Nat. Nanotechnol.*, 2013, **8**, 113-118.

24. N. Nerngchamnong, D. Thompson, L. Cao, L. Yuan, L. Jiang, M. Roemer and C. A. Nijhuis, *J. Phys. Chem. C*, 2015, **119**, 21978-21991.

25. R. C. Chiechi, E. A. Weiss, M. D. Dickey and G. M. Whitesides, *Angew. Chem. Int. Ed. Engl.*, 2008, **47**, 142-144.

26. A. R. Garrigues, L. Yuan, L. Wang, E. R. Mucciolo, D. Thompon, E. del Barco and C. A. Nijhuis, *Sci. Rep.*, 2016, **6**, 26517.

27. L. Yuan, N. Nerngchamnong, L. Cao, H. Hamoudi, E. del Barco, M. Roemer, R. K. Sriramula, D. Thompson and C. A. Nijhuis, *Nat. Commun.*, 2015, **6**, 6324.

28. R. Liu, S. H. Ke, W. Yang and H. U. Baranger, *J. Chem. Phys.*, 2006, **124**, 024718.

29. P. E. Kornilovitch, A. M. Bratkovsky and R. Stanley Williams, *Phys. Rev. B.*, 2002, **66**.